I. Literature Review

1-1 Gold nanoparticles

Nanoparticles, especially gold nanoparticles (AuNPs), have received great interests due to their attractive electronic, unique optical, thermal, and physical properties as well as catalytic properties and its bio-complementary [Guo and Wang, 2007; Wang *et al*., 2008; Patra *et al*., 2010].

Recently, AuNPs-based platforms have been applied in clinical diagnosis and drug delivery due to their characteristics that could be separated in main three parts. First, the aggregation of AuNPs could make detecting solution change its color (usually from red to purple or blue). The most usual example is ssDNA-functionalized AuNPs that could specifically hybridize the complementary target for detecting specific nucleic acid sequences. These modified AuNPs are widely used in biological samples identification [Mirkin *et al*., 1996; Baptista *et al*., 2008; Nguyen *et al*., 2011]. Second, using AuNPs as the core/seed could be tailored with various surface functionalities (such as antibodies and ligands) to provide highly selective nanoprobes for *in vivo* drug delivery and *in vitro* diagnosis [You *et al*., 2007; Baptista *et al*., 2008; Eck *et al*., 2010]. Third, AuNPs are used as the strong enhancer or a quencher because of their surface plasmon characteristic. This property could be applied in surface enhance Raman and fluorescence resonance energy transfer [Kneipp *et al*., 2008; Allgeyer *et al*., 2009; Yi *et al*., 2010]. Therefore, the synthesis and characterization of AuNPs have attracted considerable attention. Furthermore, AuNPs have been proposed as future building blocks in nanotechnology [Persoons and Verbiest, 2006; Song *et al*., 2010]. **Table 1-1** and **Figure 1-1** show the properties and applications of AuNPs.

Since the first report of AuNPs synthesis appeared in 1950s, numerous methods of monodispersed particles with size and shape tunability have been developed. The common

method of AuNPs synthesis is wet chemical synthesis. Another method of monodispersed AuNPs generation is sonolysis. The details of synthesis methods, characteristics, and applications of AuNPs are shown below:

1-1-1 Wet chemical synthesis techniques for small spherical particles

The most common method of AuNPs synthesis is wet chemical synthesis. Typically, gold salt such as $HAuCl_4$ is reduced by adding reducing agent. The reduction leads to the nucleation of Au ions to nanoparticles. Furthermore, a stabilizing agent is also required for the stabilization of AuNPs. The size and shape of nanoparticles greatly influence their properties [Rao and Cheethama, 2001; Nguyen *et al*., 2011]. For example, spherical AuNPs exhibit a single plasmon resonance in the visible region of the spectrum, while rod-like particles exhibit a longitudinal and transversal plasmon resonance [Hutter and Fendler, 2002]. Additionally, different sizes of AuNPs display various optical properties because of the surface plasmon resonance [Ray, 2010], and have distinct electrical properties [Chirea *et al*., 2009]. The common wet chemical synthesis methods of AuNPs include the citrate reduction method and the Brust method.

The citrate reduction method: The citrate reduction method was proposed by Turkevich in 1951 [Turkevich *et al*., 1951], and this is the most well-known and simplest method for synthesizing AuNPs. This method is used to produce modestly monodispersed spherical AuNPs involving the reduction of $HAuCl_4$ by sodium citrate in water. A typical standard citrate reduction procedure to fabricate 20 nm AuNPs is described as follow [Frens 1973; Grabar *et al*., 1997; Glomm, 2005]:

Initially, a solution of 100 mL 1 mM hydrogen tetrachloroaurate ($HAuCl_4$) in water was boiled in reflux conditions under vigorous stirring, and then 10 mL of 38.8 mM aqueous sodium citrate was quickly added to the $HAuCl_4$ solution. This reaction resulted in color changed of the originally yellow solution to dark blue/grey. After 2 min, the color of

solution became wine-red, indicating the end of the reaction. This mixture was further stirred and boiled for 15 min and subsequently cooled to room temperature while stirring continuously. The resulted colloidal AuNPs were approximately spherical and had an overall negative surface charge due to the citrate coverage. In the reaction, the citrate ions reduced the gold salt $HAuCl_4$ according to

$$3\ (H_2CCOOH)_2C(OH)COO^- + 2AuCl^-_4 \leftrightarrow 3\ (H_2CCOOH)_2C{=}O + 2Au + 8Cl^- + 3CO_2 + 3H^+$$

Moreover, AuNPs were stabilized by negatively charged citrate ions and chloride ions that were still present in the solution. The citrate was not only as a reductant but also as a kinetic stabilizer. Irreversible aggregation or coagulation was easily induced by adding electrolytes (e.g., KI, NaCl, and KNO_3) to the solution. AuNPs size could be control by changing the concentration of the added sodium citrate [Frens, 1973]. To synthesis larger particles, less sodium citrate should be added. However, the results were less reproducible, the larger particles were less monodispersed and the color of the solution was violet. This result indicates the importance of the citrate ions stabilizing the AuNPs [Glomm, 2005; Persoons and Verbiest, 2006; Kumar *et al*., 2007]. Therefore, AuNPs were stabilized by electrostatic repulsion effect due to adsorbed citrate ions on their surface that imparted negative charge to the nanoparticles [Turkevich, 1985; Nath and Chilkoti, 2004].

The Brust method: This two-phase synthesis method was described by Brust and Schiffrin in 1994, and could be used to synthesize AuNPs in organic liquids that were normally not miscible with water [Brust *et al*., 1994].

In the Brust method, the AuNPs were sterically stabilized by organic molecules having thiol, amide, or acid groups in the solutions. The stabilization by organic molecules with thiol groups was due to the covalent bond that gold bound specifically to the sulfur atom of the thiol group [Rodriguez *et al*., 2003; Nguyen *et al*., 2011], while the organic molecules formed the actual stabilization preventing the particles to aggregate. The main advantage of

the Brust method is that AuNPs behave like chemical compounds [Whyman, 1996]. The AuNPs could be precipitated, filtered off, and redissolved in organic solutions. Furthermore, several stabilization agents with thiol, amide, or acid groups could be used to sterically stabilize the AuNPs. The preparation processes are discribed as follow [Brust *et al*., 1994]:

First, 30 mL of a 30 mM aqueous solution of $HAuCl_4$ was mixed with a solution of tetraoctylammonium bromide (TOAB or TOABr) in 80 mL of 50 mM toluene ($C_6H_5CH_3$) and stirred vigorously. After the tetrachloroaurate was transferred into the organic layer, the l70 mg dodecanethiol was then added to the organic phase. Second, 25 mL of a freshly prepared 0.4 M aqueous solution of sodium borohydride ($NaBH_4$) was slowly added with vigorous stirring. After further stirring for 3 hr, the organic phase was separated, and evaporated to 10 mL in a rotary evaporator. To remove the excess of thiocholesterol, the organic phase was mixed with 400 mL ethanol. The mixture was then kept at -18°C for 4 hr, and the dark brown precipitate was filtered off and washed with ethanol. The crude product was dissolved in 10 mL toluene and again precipitated with 400 mL ethanol. The overall reaction shows as follow [Brust *et al*., 1994]:

$$AuCl_4^- (aq) + N(C_8H_{17})_4^+ (toluene) \rightarrow N(C_8H_{17})_4^+ AuCl_4^- (toluene)$$

$$mAuCl_4^- (toluene) + nC_{27}H_{45}SH (toluene) + 3me^- \rightarrow 4mCl^- (aq) + (Au_m) (C_{27}H_{45}SH)_n (toluene)$$

1-1-2 Synthesis of AuNPs by ultrasound

An alternative method for the fabrication of AuNPs is ultrasound method. This method could effectively form gold complexes, and only after adding suitable reducing agent to the ultrasonic solution will the formation of AuNPs be observed. The mechanism of the AuNPs fabrication depends on the pyrolysis of water and other organic compounds present in the aqueous solution that results in the formation of free radicals at high temperatures and pressures. When water is ultrasonic in the presence of ethanol, the following reactions proceed [Okitsu *et al*., 2001; Caruso *et al*., 2002]:

$$H_2O \rightarrow \cdot H + \cdot OH$$

$$CH_3CH_2OH + \cdot H(\cdot OH) \rightarrow CH_3CH\cdot OH + H_2\ (H_2O)$$

$$CH_3CH_2OH \rightarrow \text{pyrolysis radicals}$$

These radicals could reduce gold(III) ions into gold(II), gold(I), and finally gold(0). When $AuCl_4^-$ was ultrasonic in water without adding ethanol, some AuNPs were produced due to three separate near diffusion-controlled one-electron transfer steps with H• as the primary reducing species [Caruso *et al.*, 2002]:

$$AuCl^-_4 + 3\cdot H \rightarrow Au(0) + 4Cl^- + 3H^+$$

In the presence of ethanol, more complex sequence of three separate one-electron transfer reactions might be summarized [Okitsu *et al.*, 2001; Caruso *et al.*, 2002]:

$$3CH_3CH\cdot OH + AuCl_4^- \rightarrow 3CH_3CHO + Au(0) + 4Cl^- + 3H^+$$

The reduction of $AuCl_4^-$ to colloidal AuNPs according to the above two reactions was simplified, and the particle growth was much more complex in the real sample solution. The rate of gold(III) reduction could be controlled by the ultrasound irradiation conditions, such as the temperature and the ultrasound intensity. The size of AuNPs was controlled by changing the alcohol concentration and alkyl chain length [Caruso *et al*, 2002]. This method is useful in the rapid fabrication of AuNPs, but the particles are poly-disperse which is a problem for applications when monodispersed solutions are required [Persoons and Verbiest, 2006].

1-1-3 Synthesis process of AuNPs

The synthesis process of AuNPs involves three distinct stages: nucleation, growth, and coagulation [Turkevich, 1985; Goia and Matijevic, 1998; Goia and Matijevic, 1999; Sperling and Parak, 2010].

In the first stage, nucleation, metal ions are reduced to metal atoms and form stable icosahedral nuclei of 1-2 nm in size due to rapid collision. The factors that affect the initial concentration of nuclei include the concentration of the reducing agent, the solvent,

temperature, and reduction potential of the reaction. Increasing the molar ratio of reducing agent to metal salt causes rapid formation of a number of nuclei and leads to smaller, monodispersed AuNPs. In contrast, decreasing the molar ratio of reducing agent leads slow formation of few nuclei and results in larger diameter of AuNPs with a greater heterogeneity in size. This stage is important for controlling the shape, size, and structure distribution of AuNPs and is typically complete in a few seconds. In the growth stage, the metal ions are reduced on the surface of the nuclei, until all the metal ions are consumed. The final stage for synthesis of AuNPs is coagulation that involves prevention of AuNPs aggregation by adding stabilizing agents. It is either adsorbed or chemically bound to the surface of AuNPs with charge. The equally charged AuNPs repel each other, so they are colloidally stable [Sperling *et al*., 2008; Sardar, 2009; Nguyen *et al*., 2010]. The **Table 1-2** shows different sizes of AuNPs and their synthesis methods.

1-2 Surface modification and bioconjugation of AuNPs

AuNPs are surrounded by a shell of stabilizing molecules, which usually have thiol groups in the terminal. One end of these stabilizing molecules are either adsorbed or chemically linked to the gold surface, while the other end points exposed in the solution. The stabilizing molecules provide colloidal stability and form as monolayer protected clusters (MPCs) [Sperling *et al*., 2008; Chandra, 2010]. After synthezing AuNPs, the stabilizing molecules could be replaced by other molecules in the ligand exchange reaction [Pellegrino *et al*., 2005; Ghosh *et al*., 2008; Sperling and Parak, 2010].

Biological molecules could attach to AuNPs in several ways. When the biological molecules have the functional groups that could bind to the AuNPs surface (e.g., -SH, -CN, $-NH_2$, -COOH, and -OH), the biological molecules could replace some of the original stabilizing molecules after biological molecules are added directly to the AuNPs solution [Grabar *et al*., 1995; Kumar *et al*., 2004; Giljohann *et al*., 2010]. By choosing the suitable

molecules, it is possible to adjust the surface properties of the particles and attach different kinds of molecules to AuNPs.

Using AuNPs as versatile and efficient templates for the immobilization of biomolecules has been recognized since the early 1980s [Rembaum and Dreyer, 1980]. Examples of AuNPs-biomolecule conjugation include immuno-microspheres, which could react in a very specific way with antibodies, target cells or viruses, depending on the type of antigen adsorbed on the microspheres. Since AuNPs have very large surface-area-to-volume ratio and good biocompatibility, biosensors based on enzyme-covered AuNPs have been reported by many groups [Xiao *et al*., 1999; Zhang *et al*., 2008; Chuang *et al*., 2010]. The interaction between proteins and AuNPs depends upon three separate but dependent phenomena: (a) the ionic attraction between the negative-charged AuNPs and the positive-charged protein; (b) the hydrophobic attraction between the antibody and the AuNPs surface; (c) the dative covalent binding between the AuNPs conducting electrons and sulfur atoms which may occur with amino acids of the protein.

1-3 Surface plasmon resonance of AuNPs

AuNPs have emerged as the important colorimetric reporters because of their high extinction coefficients and strongly distance-dependent optical properties [Kim *et al*., 2001; Huang *et al*., 2005; Pissuwan *et al*., 2010]. The interesting optical and electronic properties have served as a versatile platform for exploring many facets of basic science. AuNPs could strongly absorb and scatter visible light. When the visible light shines on AuNPs, the light of a resonant wavelength is absorbed by AuNPs, and the energy of visible light excites the bounded electron of AuNPs to free. The phenomenon induces the surface electron oscillation of AuNPs and is responsible for the intense colors exhibited of AuNPs, the so-called surface plasmon resonance (SPR) [Sönnichsen *et al*., 2002; Nath and Chilkoti, 2004; Zhao *et al*., 2008]. The schematic presentation of the SPR is shown in **Figure 1-2**.

Moreover, the SPR depends strongly on the size, shape, medium, and the relative distance of the AuNPs [Schultz, 2003; Su *et al*., 2003; Sun and Xia, 2003; Sardar *et al*., 2009].

Small AuNPs (e.g., 13 nm in diameter) absorb green light, which corresponds to a strong absorption band (surface plasmon band) at about 520 nm in the visible light spectrum and results in AuNPs displaying red in color. When AuNPs are small, the surface electrons are oscillated by the incoming light in a dipole mode. As the size of AuNPs increases, the light could no longer polarize the nanoparticles homogeneously. Hence, the higher order modes dominate at lower energy. This causes a red-shift and broadening of the SPR. Therefore, the surface plasmon band red-shift with the increasing size of AuNPs [Ghosh and Pal, 2007; Cobley *et al*., 2011]. The red-shift and color change also could be observed by the aggregation of small AuNPs. When the interparticle distance among spherical AuNPs is higher than the average of particle diameter, AuNPs would appear red in color. However, when the interparticle distance become smaller than the average particle diameter, the surface plasmons of AuNPs combine (interparticle plasmon coupling), and the aggregated AuNPs could be considered as a single large particle. This AuNPs aggregation results in color changing from red to blue [Link and El-Sayed, 1999; Jena and Raj, 2008; Azzazy and Mansour, 2009]. The interparticle plasmon coupling could generate a huge absorption band shift (up to 300 nm), and the color change could be observed by the naked eye. Therefore, complicated instruments are not required for analysis.

This unique optical property of AuNPs provides an elegant colorimetric platform for detecting biological molecular interactions. When the target analyte or biological molecule directly or indirectly triggers AuNPs aggregation (or redispersion from aggregation), this process is detected by the color change of AuNPs solution. Thus, the ratio of the absorbance at 520 nm (for 13 nm AuNPs) that corresponds to dispersed particles and a longer wavelength (e.g., 600 nm) that corresponds to aggregated particles, is often used to quantify the

aggregation process or color change [Zhao *et al.*, 2008].

Since AuNPs have high SPR, AuNPs are promising fluorescence quenchers [Wang *et al.*, 2010; Kang *et al.*, 2011]. Through Föster resonance energy transfer (FRET) effect, AuNPs (acceptors) could transfer the energy from excited donors (fluorophores) due to their overlapped emission or excitation spectrum, which also changes the fluorophore emission level and causes quench [Iosin *et al.*, 2009]. Additionally, the efficiency of FRET relates to the relative distance and orientation (parallel) of the donor and acceptor dipole, which is usually limited to donor-acceptor distances smaller than 5-7 nm [Mayilo *et al.*, 2009]. However, AuNPs are highly efficient fluorescence quenchers over longer distances (>10 nm) [Swierczewska *et al.*, 2011] because the spherical AuNPs could take place energy transferring for any orientation of the donor relative to the surface of AuNPs [Gersten, 2005; Swierczewska *et al.*, 2011]. Moreover, due to the size of the AuNPs, the energy transferring efficiency from the donors to AuNP acceptors decay slower with distance as compares to the case of a molecular acceptors [Anger *et al.*, 2006; Mayilo *et al.*, 2009]. Therefore, in contrast to molecular acceptors, AuNPs act as good acceptors of FRET. The schematic theory of FRET is shown in **Figure 1-3**.

1-4 Nanoparticles stability - DLVO theory

DLVO theory was developed by Derjaguin, Landau, Verwey, and Overbeek in the 1940s and has been used to explain the stability of colloids in suspension. The theory describes that the force between charged surfaces interacts through a liquid medium. The stability of colloidal system is determined by the balance between two opposing forces: electrostatic repulsion and van der Waals attraction [Craig *et al.*, 1998; Schneider *et al.*, 2011]. The particle interaction forces are described in **Figure 1-4**.

The main cause of aggregation is the van der Waals attractive force between the particles, which is long-range forces [Shaw, 1980; Segets *et al.*, 2011]. Van der Waals attraction is

actually the result of attractive forces acting between individual particles in colloid system. The effect is accumulative. One particle has a van der Waals attraction to other particles in the same system. This phenomenon repeats for each particle in the colloid system, which then causes total attractive forces. The variation in van der Waals force with distance between the particles is demonstrated by an attractive energy curve [Zeta-Meter, Inc. 1993; Pashley and Karaman, 2005; Hwang *et al*., 2010].

The DLVO theory proposes that an energy barrier resulted from the repulsive force prevents particles aggregation. The particles would suspend in the solution, and the system would be stable. However, when the particles collide with sufficient energy to overcome that barrier, the attractive force would pull them approaching and adhering to each other. Therefore, the particles would be irreversibly aggregation. An electrostatic repulsion curve is used to indicate the energy that must be overcome if the particles are forced together. The maximum energy is related to the surface potential and the zeta potential. Therefore, the repulsive forces play an important role in maintaining the stability of the colloidal system. There are two essential mechanisms that affect dispersion stability.

Steric repulsion: The stability of colloidal dispersions is enhanced by adding suitable materials (protective agents) to adsorb or otherwise attach to the particle surfaces and prevent the particles coming into close contact [Shaw, 1980; Persoons and Verbiest, 2006; Schneider *et al*., 2011]. If the materials adsorbed to the particles are enough, the coating is sufficient to keep particles separated by steric repulsions between the polymer layers, and the van der Waals forces are too weak to cause the particles to aggregate. The mechanism of steric stabilization is simple and requires just the addition of the suitable materials. However, the materials might be expensive, and in some cases the materials are undesirable for subsequently aggregation of the particles if that is required.

Electrostatic or charge stabilization: The effect of the particles interaction results in the distribution of charged species in the colloid system. Energy is required for overcoming this repulsion. An electrostatic repulsion curve is used to indicate the energy that must be overcome if the particles are forced together. The maximum energy is related to the surface potential and the zeta potential. This mechanism can stabilize or aggregate the particles in the system by altering the concentration of ions in the solution. This process is simple and potentially inexpensive [Zeta-Meter, Inc. 1993; Pashley and Karaman, 2005; Segets *et al.*, 2011].

1-5 Applications of AuNPs

1-5-1 Applications of AuNPs in biosensors

AuNPs have great potential applications in the field of biosensors due to many interesting electrical and optical properties. AuNPs could exhibit surface plasmon resonance and plasmon absorption in red-shift due to interparticle plasmon interactions [Wang *et al.*, 2009]. This optical property of AuNPs establishes a highly selective and sensitive optical assay for molecular recognition events [Jena and Raj, 2008; Chandra *et al.*, 2010]. AuNPs-based colorimetric assays for detection are mainly dependent on the analyte inducing interparticle distance change of AuNPs that result in color change of AuNPs. Since the first AuNPs-based DNA sensor was developed by Mirkin and coworkers [Mirkin *et al.*, 1996], the AuNPs-based platform has been increasingly applied for the detection of various targets, including nucleic acids [Cao *et al.*, 2005; Li *et al.*, 2005; Boisselier and Astruc, 2009], proteins [Tsai *et al.*, 2005; Chen *et al.*, 2008; Uehara *et al.*, 2010], enzyme activity [Xu *et al.*, 2007; Jiang *et al.*, 2009], and metal ions [Liu and Lu, 2007; Slocik *et al.*, 2008; Lin *et al.*, 2011].

In addition, the exceptional quenching ability of AuNPs makes them excellent materials for FRET-based biosensors [Sapsford *et al.*, 2006; De *et al.*, 2008; de Dios and Díaz-García,

2010]. The fluorescence of many fluorophores is quenched when they are in close proximity to AuNPs surface [Dulkeith *et al*., 2002; Lee *et al*., 2010]. For detecting analytes, AuNPs are conjugated with ligands that specifically bind to the analyte modified with fluorophores. When the analyte and ligand have interaction, the fluorophores are closely linked to the AuNPs, and their fluorescence is quenched. Another detection scheme works slightly different. In this case, the spacer links fluorophores to AuNPs. In the presence of the analyte, the spacer molecule changes its conformation and these results in quenching or releases the fluorescence of the fluorophore. The FRET-based biosensors has been used for detecting nucleic acids [Maxwell *et al*., 2002; Ray *et al*., 2006] and proteins [Oh *et al*., 2006; Huang *et al*.,2007; Kang *et al*., 2011].

Finally, AuNPs are also used for transfering electrons in redox reactions because of their conductivity and catalytic properties [De *et al*., 2008; Ozdemir *et al*., 2010]. In the electrochemical biosensor, enzyme specifically oxidizes (or reduces) the analyte, and the flow of electrons released (or required) in this redox reaction is measured as electrical current. Additionally, enzyme is conjugated with the AuNPs [Xiao *et al*., 2003] and immobilized on the surface of an electrode that is connected to an amplifier for current detection. Alternatively, AuNPs could be first immobilized on the electrode and then modified with enzymes [Xiao *et al*., 1999; Norouzi *et al*., 2010]. These AuNPs-based modifications on the electrode could improve the surface area, which increase the quantity of immobilized enzyme, and the enzyme conjugated with the AuNPs could also facilitate the electron transport, these modifications enhance the electrical currents [Sperling *et al*., 2008; Bonanni and del Valle, 2010].

1-5-2 Applications of AuNPs in drug delivery system

AuNPs have been used for a long time as drug delivery system (DDS). Biology molecules are adsorbed on the surface of AuNPs and introduced into the cells. The

methods for particles introduction into cells are either forced as in the case of gene guns or achieved naturally by cell endocytosis. These molecules will eventually detach themselves from the surface of the AuNPs inside the cells [Sperling *et al*., 2008].

The method of gene guns is using AuNPs as massive nanobullets for ballistic projectile introduction of DNA into cells. DNA is adsorbed onto the surface of AuNPs and then shot into the cells. This method has been used successfully for gene delivery [Tischer *et al*., 2002; Lee *et al*., 2008].

Another method for AuNPs application of drug delivery is achieved naturally by cell endocytosis. As good biocompatible materials, AuNPs could be modified with bio-molecules and would not destroy their biological activity. Furthermore, AuNPs are uptake by cells naturally, either specifically (via receptor-ligand interaction) or nonspecifically [Chithrani *et al*., 2006; Johnston *et al*., 2010]. For specifically uptake, the ligands specific recognized to receptors on the cell membrane are conjugated to the surface of AuNPs. In this way, ligand-modified AuNPs are predominantly incorporated by cells that possess receptors for these ligands, and it is more effective than nonspecific uptake [Sperling *et al*., 2008]. It is possible to make particles specifically to cancer cells by conjugating them with biomarkers on the surface of cancer cells [Jain *et al*., 2007; Kim *et al*., 2010]. After ingestion, the AuNPs are stored in vesicular compartments inside the cells [Chithrani and Chan, 2007]. In order to release the particles from the vesicular structures to the cytosol, their surfaces are coated with membrane-disruptive peptides or relying on the acidic condition in tumors, inflamed tissues (pH = 6.8), and cellular compartments including endosomes (pH = 5.5 - 6.0) and lysosomes (pH = 4.5 - 5.0) [de la Fuente and Berry, 2005; Yang *et al*., 2005]. AuNPs uptake-mediated delivery of molecules into cells is used mainly for two applications. First, DNA used for gene therapy is introduced into cells, which subsequently causes the expression or silence of the corresponding proteins [Salem *et al*., 2003; Sullivan *et al*., 2003].

Second, targeting anti-cancer drugs are specifically delivered to the cancer tissues [Rojo *et al*., 2004; Jain *et al*., 2007; Chithrani, 2010].

1-5-3 Applications of AuNPs in bioimaging

AuNPs have been primarily used for bioimaging, based on the interaction between AuNPs and light. AuNPs are very attractive contrast agent as they could be visualized with a number of different techniques [Sousa *et al*., 2010].

Immunostaining is one of the traditional methods that used AuNPs in biology. First, AuNPs are conjugated with the antibodies for molecular recognition. The antibody-modified AuNPs will bind to the antigen or target region containing the antigen. The antibody-modified AuNPs are added to the fixed and permeabilized cells. Targets on the cell-membrane or in the cells could be labeling by AuNPs in this way. The AuNPs then provide excellent contrast for transmission electron microscopy imaging with high lateral resolution, and larger structures are also imaged by optical microscopy [Faulk and Taylor, 1971; De Mey *et al*., 1982; Cobley *et al*., 2011].

AuNPs are not only used for visualizing structures in the single cell but also applied for providing contrast *in vivo* to whole organs in the animal, and this technique is potentially applied in human. Initially, AuNPs are conjugated with antibodies or ligands which bind specifically to the organ of interest in the animal. When modified AuNPs are injected into the blood vessel of the animal, these particles label at the target organs via receptor-ligand interaction [Boisselier and Astrue, 2009]. AuNPs bound to the organ provides contrast for imaging and resolving the structure of the organ. For example, X-rays, which penetrates skin and organs deep inside the body, could image or address functional AuNPs for therapy or diagnosis [Hainfeld *et al*., 2004; Glazer and Gurley, 2010]. Furthermore, AuNPs have the predominance of causing less cytotoxic damage than quantum dots, and that makes AuNPs possess more potential to be applied in medical applications.

1-6 Matrix metalloproteinases

Matrix metalloproteinases (MMPs) are the family of extracellular zinc-dependent endopeptidases [Birkedal-Hansen *et al*., 1993; Bourboulia and Stetler-Stevenson, 2010] that are able to degrade all components of the extracellular matrix (ECM), including fibrillar and non-fibrillar collagens, gelatin, fibronectin, laminin, and basement membrane glycoproteins [Fedarko *et al*., 2004; Lombard *et al*., 2005; Jacobsen *et al*., 2010]. MMPs not only play important roles in ECM remodeling in physiologic situations, such as embryonic development, cell migration, tissue regeneration, wound repair, apoptosis, angiogenesis and inflammatory, but also in pathological conditions, including rheumatioid arthritis, osteoarthritis, atherosclerotic plaque rupture, tissue ulceration and involved in the processes of tumors metastasis and growth [Miyazaki *et al*., 1990; Roeb and Matern, 2001; Roy *et al*.,2009]. The levels of MMPs could be determined in patient serum or urine. When the MMPs concentrations elevate over a particular threshold, it could sometimes indicate the progression or prognosis. In addition, due to the activity of MMPs are related to the tumor critically, scientists have developed or designed various inhibitors to block MMPs activity for treating diseases [Devel *et al*., 2010] (**Table 1-3**).

MMPs are generally divided into six groups, collagenases (MMP-1, -8, and -13), stromelysins (MMP-3, -10, and -11), matrilysins (MMP-7 and MMP-26), gelatinases (MMP-2 and MMP-9), membrane-type matrix metalloproteinases (MT-MMPs) (MMP-14, -15, -16, -17, -24, and -25) and others [Jones *et al*., 2003; Jacobsen *et al*., 2010]. Although MMPs are sub-classified based on their ability to degrade various proteins of the ECM, they also play other important roles such as the activation of cell surface receptors and chemokine [Stefanidakis and Koivunen, 2006]. In addition, MMP-2 has proteolytic activity to specific targets within the cell to cause acute, reversible contractile dysfunction in cardiac disease [Cauwe and Opdenakker, 2010].

The regulation of MMPs occurs at many levels, including transcription (the major one), post- transcriptional modulation of mRNA stability, secretion, localization, zymogen (proenzyme) activation, and inhibition of activity by natural inhibitors of MMPs, tissue inhibitor of metalloproteinases (TIMPs). The TIMP gene family consists of 4 members: TIMP-1, -2, -3, and -4. TIMPs inhibit the activity of MMPs by binding to activated MMPs in a 1:1 molar stoichiometry [Brew *et al*, 2000]. TIMPs could also inhibit the growth, invasion and metastasis of malignant tumors [Pasternak and Aspenberg, 2009; Brew and Nagase, 2010].

1-6-1 Gelatinase A

In 1978, Sellers *et al*. were first to separate a gelatinase activity from collagenase and stromelysin in the culture medium of rabbit bone [Sellers *et al*., 1978]. Similar enzyme acting on basement membrane type IV collagen was reported by Liotta *et al*. [Liotta *et al*., 1979] in the following years. Gelatinase was purified from human skin, mouse tumor cells, rabbit bone, and human gingival. Gelatinase A was a triple repeat of fibronectin type I domains inserted in the catalytic domain. This domain participates in binding to the gelatin substrates of the enzyme [Libson *et al*., 1995; Kandasamy *et al*., 2010]. MMP-2 is ubiquitously expressed in the cells which comprise the heart and is found in normal cardiomyocytes, as well as in endothelium, vascular smooth muscle cells, and fibroblasts [Coker *et al*., 1999; Kandasamy *et al*., 2010]. In particular, MMP-2 is overexpressed in many cancers, including breast cancers, and is an indicator of cancer invasiveness, metastasis, angiogenesis, and treatment efficacy [Kessenbrock *et al*., 2010]. Therefore, many novel analyzing methods for MMP-2 activity detection are developed in recent years [Kupai et al., 2010; Ryu *et al*., 2010; Hyafil *et al*., 2011].

1-6-2 Activation of MMPs

The MMPs are produced as zymogens. The basic structure of MMPs is divided into three structural well-preserved domain motifs, including a catalytic domain, a N-terminal domain, and a C-terminal domain. Zinc-dependent catalytic domain (about 170 amino acids) of MMPs contains a zinc binding motif HEXXHXXGXXH as the zinc binding active site, and has an additional structural zinc ion and 2-3 calcium ions. These ions are required for the stability and the expression of enzymic activity [Nagase and Woessner, 1999; Jacobsen *et al*., 2010]. The N-terminal domain (propeptide domain; about 80 amino acids) contains a unique PRCG (V/N) PD sequence in which the cysteine residue interacts with the catalytic zinc atom in the active site, prohibiting the activity of the MMPs. Thus, the interaction has to be disrupted to "open" the cysteine switch in the process of MMPs activation [Van Wart and Birkedal-Hansen, 1990; Sela-Passwell *et al*., 2010], which is a critical step that leads ECM breakdown [Carmeli *et al*., 2004; Shiomi *et al*., 2010]. The C-terminal hemopexin domain (about 210 amino acids) of MMPs has a four-bladed propeller structures and contributes to substrate specificity [Wallon and Overall, 1997]. In membrane-type MMPs, the hemopexin domain contains a transmembrane domain for anchoring the protein in the membrane. Additionally, the hemopexin domain in MMP-2 also has a function in the activation of the enzyme [Morgunova *et al*., 1999; Tallant *et al*., 2010].

All MMPs are synthesized in the latent form and require extracellular activation. MMPs can be activated *in vitro* by various mechanisms [Kupai *et al*., 2010]. The activation of latent MMPs is believed to occur by the dissociation of the sulfhydryl group on the cysteine from the active zinc site and the replacement with a water molecule that plays a role in catalysis [Murphy *et al*., 1980; Galazka *et al*., 1996; Zhang and Kern, 2009]. Disruption of the Cys-zinc bond could be achieved by heavy metal ions, oxidants, organomercurials, sulfhydryl alkylating agents, or disulfide compounds [Macartney and Tschesche, 1983; Weiss

et al., 1985; Mallya and Van Wart., 1989; Tallant *et al*.,2010]. Latent MMPs are also activated by conformational changes of the polypeptide chain induced by detergents or chaotropic agents [Birkedal-Hansen and Taylor, 1982; Springman *et al*., 1990], and also by limited cleavage of the propeptide by proteolytic enzymes such as trypsin or chymotrypsin [Stricklin *et al*., 1983; Okada *et al*., 1990; Sela-Passwell *et al*., 2010].

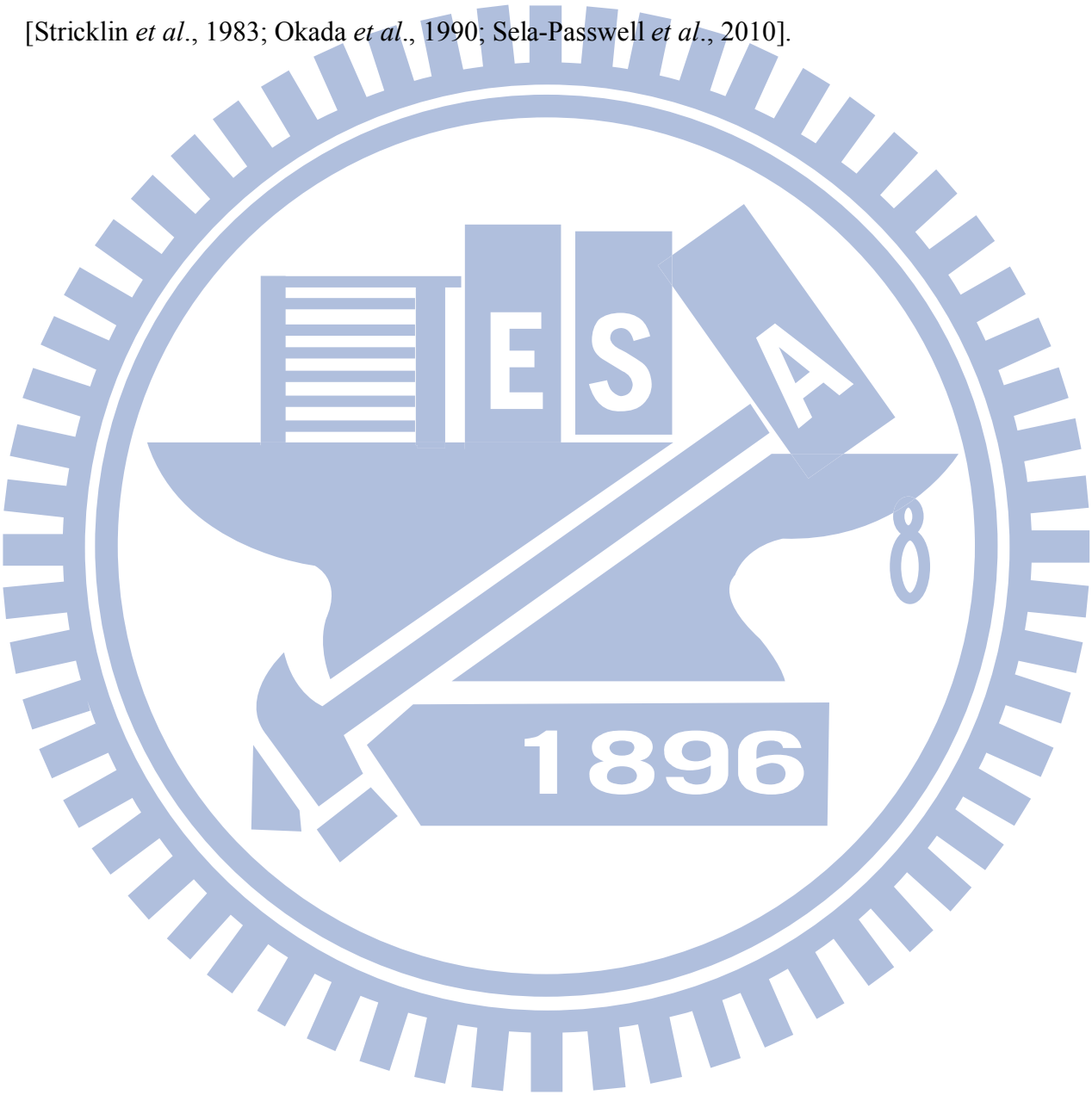

Table 1-1. The applications of AuNPs

Applications	Detecting method	Assistant technology	Reference
Biosensor			
Detection of DNA	Colorimetric detection	Self-assembly	Mirkin *et al*., 1996 Suzuki *et al*., 2009
Detection of metal ion	Colorimetric detection	Aptamers Ligands	Liu and Lu, 2007 Knecht and Sethi, 2009
Detection of enzyme activity and screening of inhibitors	Colorimetric detection	Self-assembly	Jiang *et al*., 2009 Chuang *et al*., 2010
Protein-protein interaction	Colorimetric detection	Self-assembly	Tsai *et al*., 2005
Detection of Protein/peptide concentrations	Colorimetric detection	Polymer modification	Uehara *et al*., 2010
Detection of DNA	Fluorescence resonance energy transfer	Self-assembly	Maxwell *et al*., 2002
Protein-protein interaction	Fluorescence resonance energy transfer	Quenching protein fluorophore	Oh *et al*., 2005
Detection of enzyme activity and screening of inhibitors	Fluorescence resonance energy transfer	Self-assembly	Lee *et al*., 2008
In vivo tumor targeting	Surface enhance Raman	Raman shift	Qian *et al*., 2008
Detection of pH value in cell	Surface enhance Raman	Raman shift	Boisselier and Astruc, 2009
Detection of glucose	Elechemical	AuNPs modified with oxidase	Xiao *et al*., 2003 Ozdemir *et al*., 2010

Continued

Detection of hydrogen peroxide	Elechemical	AuNPs immobilized on the electrode surface	Norouzi *et al*., 2010
Drug delivery system			
Drug delivery	Endocytosis	Self-assembly	Rojo *et al*., 2004
Drug delivery	Intravenously injection	Self-assembly	Ghosh *et al*., 2008
Gene delivery	Endocytosis	Self-assembly	Ghosh *et al*., 2008
Gene delivery	Gene gun	Self-assembly	Lee *et al*., 2008
Bioimaging			
Cells migrating	Endocytosis	Self-assembly	Kennedy *et al*., 2011
Visualization of microtubules in plants	Immuno-gold staining	Self-assembly	Faulk and Taylor, 1971
Organ detection by computer microtomography	Luminescence	Self-assembly	Sousa *et al*., 2010

Table 1-2. The synthesis methods of AuNPs

Core size (diameter)	Synthetic methods	Capping agents	Reference
1-2 nm	Reducing AuCl (PPh_3) with diborane or sodium borohydride	Phosphine	Schmid, 1992; Ghosh *et al*., 2008
1.5-5 nm	Biphasic reducing of $HAuCl_4$ by sodium borohydride in the presence of thiol capping agents	Alkanethiol	Brust *et al*., 1994; Rodriguez *et al*., 2003
10-150 nm	Reducing $HAuCl_4$ with sodium citrated in water	Citrate	Templeton *et al*., 2000; Ghosh *et al*., 2008
20-80 nm	Reducing $HAuCl_4$ with water and ethanol by ultrasound	Water and ethanol	Daniel and Astruc, 2004
2-200 nm	Reducing $HAuCl_4$ by bacterial reductant	Different from various kinds of microbe	Narayanan and Sakthivel, 2010

Table 1-3. Pharmacological inhibitors of MMPs in experimental studies

Drug	Action	Effects	References
BB-94	Broad spectrum MMPs inhibitor	◆ Blocks both the growth and metastatic spread of malignant tumors ◆ Inhibits lung coloization and spontaneous lymphatic metastases	Asahi *et al.*, 2000 Horstmann *et al.*, 2003 Lee *et al.*, 2006 Zhao *et al.*, 2006
BB-1101	Broad spectrum MMPs and TNF-α inhibitor	◆ Reduces BBB opening ◆ Reduces brain edema ◆ Reduces the ECM degradation ◆ Inhibits the releasing of TNF-α	Sumii and Lo, 2002 Liu *et al.*, 2009
GM6001	MMPs (collagenase) inhibitor	◆ Reduces ischemic lesion size ◆ Reduces cell proliferation ◆ Decreases delayed neurovascular remodeling ◆ Decreases protrusive activity through a downregulation of Rac activity	Suzuki *et al.*, 2007 Sood *et al.*, 2008
FN-439	Broad spectrum MMPs inhibitor	◆ Decreases delayed neurovascular remodeling	Lee *et al.*, 2006 Zhao *et al.*, 2006
SB-3CT	MMPs (gelatinase) inhibitor	◆ Rescues neurons from apoptosis	Kang *et al.*, 2008
Antibody clone 6-6B	MMP-9 monoclonal antibody	◆ Reduces ischemic lesion size	Romanic *et al.*, 1998
Indomethacin	COX inhibitor	◆ Reduces BBB injury ◆ Reduces brain edema ◆ Inhibits monocyte MMP-9 induction	Kurzepa *et al.*, 2006
Tandrolapril	ACE inhibitor	◆ Reduces MMP-9 in plasma level and left ventricular remodeling ◆ Improves neurological outcome	Candelario-Jalil *et al.*, 2007
Minocycline	Tetracycline	◆ Reduces the production of MMP-9 ◆ Attenuates T cell migration ◆ Inhibits MMP enzymatic activity	Amaro *et al.*, 2009 Tu *et al.*, 2009
ONO-4817	Broad spectrum MMPs inhibitor	◆ Reduces tissue injury and inflammation ◆ Has therapeutic potential in treating fibrosis	Ro *et al.*, 2007

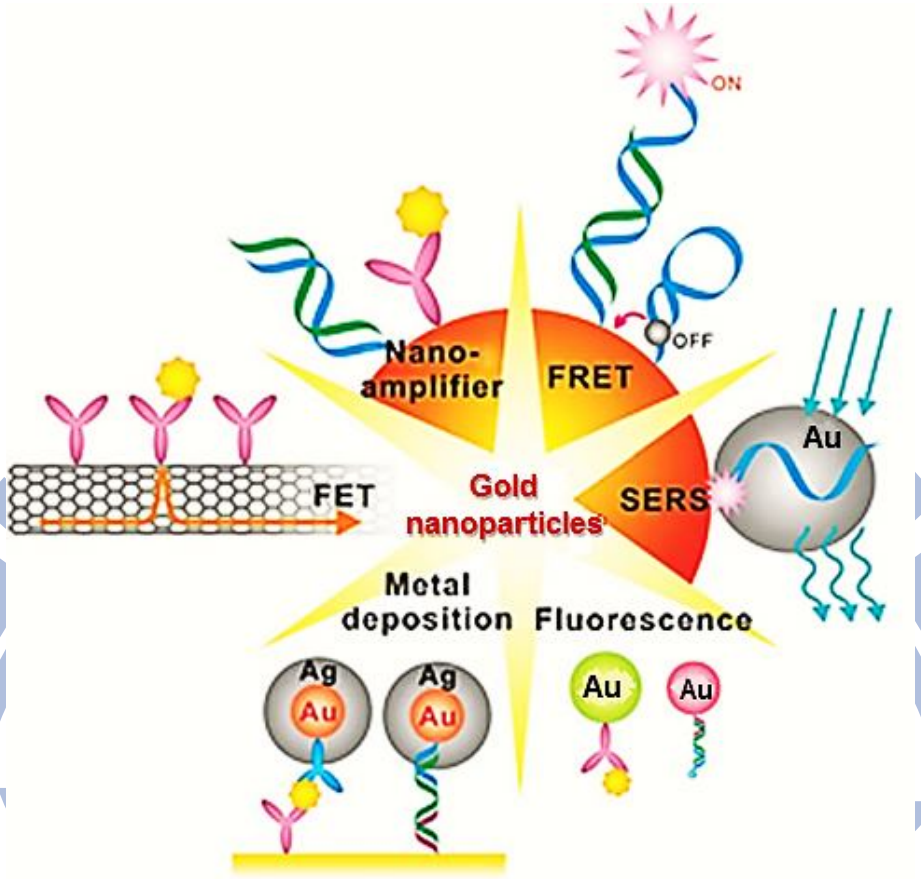

Figure 1-1. Schematic AuNPs properties and its applications. AuNPs provide almost unlimited combinations of various compositions, sizes, dimensions and shapes of materials, which can be tailored to couple different biomolecules in order to develop nanoprobes with desired properties. First, the AuNPs has excellent biocompatibility as well as readily available conjugation chemistry at gold surfaces. Moreover, AuNPs also possess highly attractive plasmonic coupling, fluorescent quenching as well as high conductivity. In addition, some recent advances have demonstrated that multiple biomolecules can be assembled onto one AuNP because of its high surface-to-volume ratio [Song *et al.*, 2010].

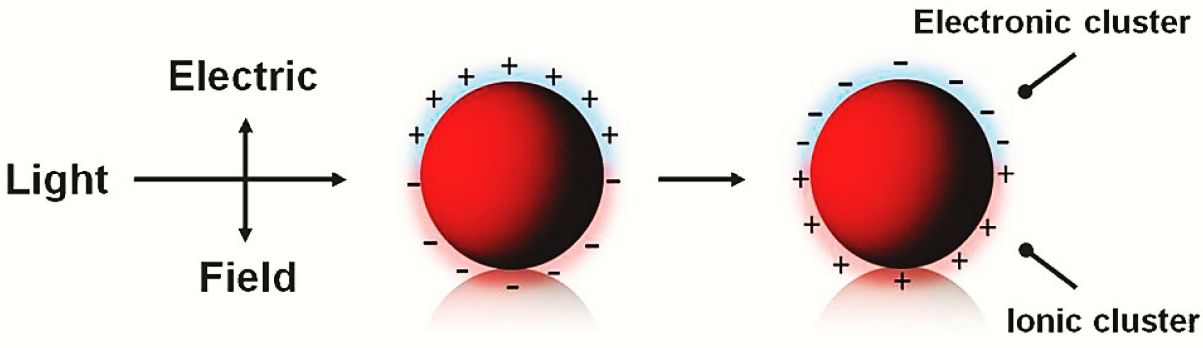

Figure 1-2. Schematic presentation of the surface plasmon resonance. A schematic representation illustrating the optical response of a metal colloid to an electric field (an incident light wave) leading to a dipolar surface plasmon. The negative charges (the conduction electrons) move under the influence of the external field. The phenomenon induces surface electron oscillation of metal colloid is so-called surface plasmon resonance (SPR) [Swierczewska *et al*., 2011].

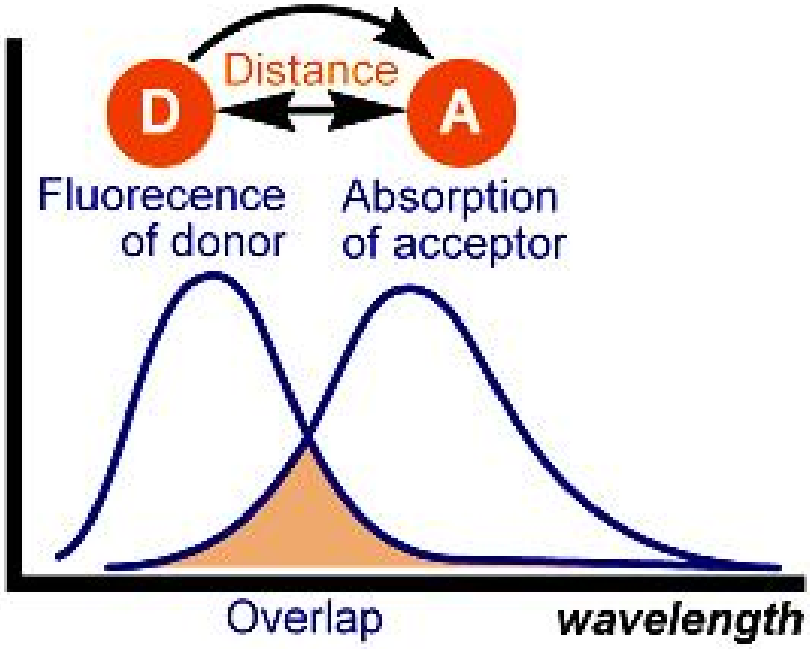

Figure 1-3. The schematic presentation of the Förster resonance energy transfer (FRET). A donor chromophore, initially in its electronic excited state, may transfer energy to an acceptor chromophore (in proximity, typically less than 10 nm) through non-radiative dipole-dipole coupling. FRET is analogous to near field communication, in that the radius of interaction is much smaller than the wavelength of light emitted. In the near field region, the excited chromophore emits a virtual photon that is instantly absorbed by a receiving chromophore. These virtual photons are undetectable, since their existence violates the (conservation of energy and momentum, and hence FRET is known as a radiationless mechanism [Lakowicz, 1999].

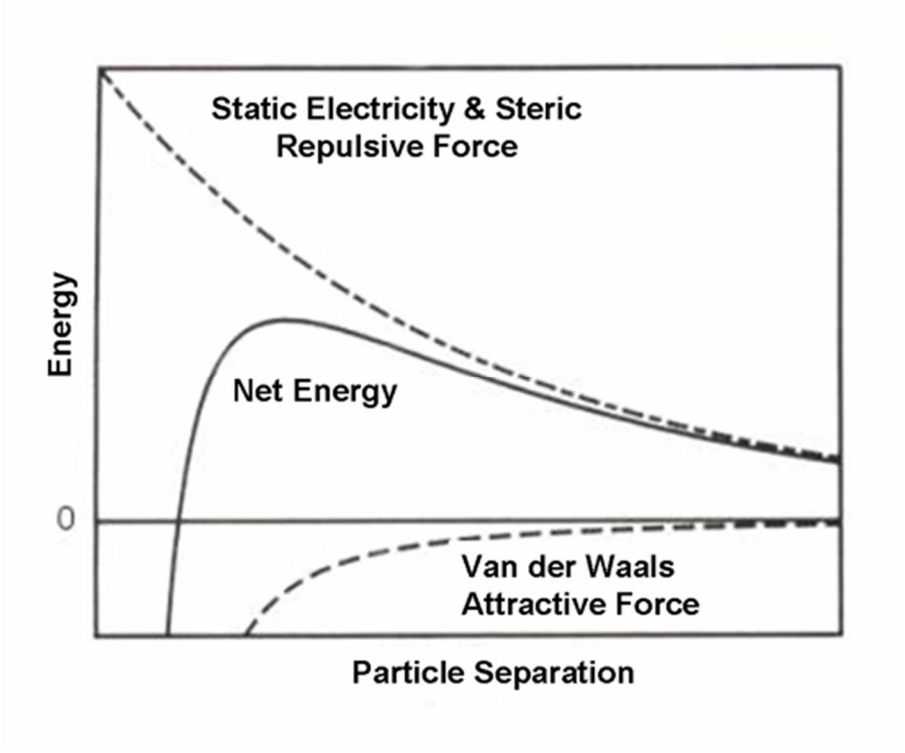

Figure 1-4. The DLVO theory. DLVO theory was developed by Derjaguin, Landau, Verwey and Overbeek in the 1940s, and has been used to explain the stability of colloids in suspension. The theory describes the force between charged surfaces interacting through a liquid medium. The stability of colloidal system is determined by the balance between two opposing forces, electrostatic repulsion and van der Waals attraction [Craig *et al*., 1998].

II. Research Strategy

Traditional methods for analyzing the activity of MMPs include the zymography and fluorescein-labeled synthetic peptides conjugated with chemical quencher [Leber and Balkwill, 1997; Netzel-Arnett *et al*., 1991]. The zymography is time consuming and complicated for MMPs activity and inhibition studies [Hu and Beeton, 2010]. Moreover, fluorescein-labeled synthetic peptide with chemical quencher is high cost of diagnosis, expensive instruments needed, and hard to design or improve the quenching ability of quencher [Mayilo *et al*., 2009]. Therefore, the SPR property of AuNPs is used to establish the AuNPs-based optical and fluorescence biosensing platforms for measuring peptidase activity and screening the inhibitors of peptidase.

Most of AuNPs-based diagnoses for the detection of enzyme activity mainly depend on the enzyme properties to induce the aggregation of AuNPs [Wang *et al*., 2006; Jiang *et al*., 2009]. However, using AuNPs to establish a platform for detecting enzyme activity may encounter the following problems. First, ions concentration effects enzyme activity and AuNPs aggregation [Giljohann *et al*., 2010]. When enzymes carry out their function, the change of the niche (such as pH, temperature, metal ion, or salt concentration) would affect the activity of enzymes. Therefore, the diagnostic system should provide an adequate environment for enzyme working. In terms of AuNPs, AuNPs would easily aggregate while surface charge is neutralized by counter ions. In previous AuNPs-based sensing systems, AuNPs aggregation relies on the electrostatic interaction. For instance, while the surface charges of receptor-modified AuNPs become neutral upon the addition of target analyte, the attractive force among AuNPs would increase and lead AuNPs aggregation [Sato *et al*., 2003; Zhao *et al*., 2007; Wang *et al*., 2009]. Above all, when the AuNPs-based optical sensing system is applied to assay enzyme activity, not only the analyte would make monodispersed AuNPs to aggregate, but also the cations which are supplied by the enzyme buffer may induce

AuNPs to aggregate. It would result in false-positive results and interfere with the analysis of enzyme activity.

Moreover, according to the DLVO theory, the stability of colloidal system is determined by the balance between two opposing forces, electrostatic repulsion and van der Waals attraction [Craig *et al*., 1998; Schneider *et al*., 2011]. When the bio-recognition element is modified on AuNPs as the substrate, the bio-element molecule provides the steric repulsion and prevents the AuNPs coming into close contact [Persoons and Verbiest, 2006; Schneider *et al*., 2011]. In the detection of protein-protein interaction like proteinase digestion, the steric hindrance between the proteins would lead AuNPs to dispersion, and the slow enzyme kinetics would prolong the detection time. In addition, AuNPs have high affinity for biomolecules [Lu *et al*., 2007; Nguyen *et al*., 2010], which could conjugate with amino acids that have thiol, amino, carboxylic, or hydroxyl groups in their side chains [Nguyen *et al*., 2011]. Therefore, the protein which is digested by proteinase would adsorb on AuNPs again and then interferes with the aggregation of AuNPs.

To overcome these arduous problems, in this study, the colloidal AuNPs are modified with peptide as peptidase substrate, which could avoid the highly spatial barrier just like protein but provide enough repulsion effect to protect AuNPs from aggregation. **Figure 2-1** illustrates the schema of this AuNPs-based optical platform. When AuNPs are modified with peptide by thiol group on cysteine, the peptide adsorbed on AuNPs surface not only as peptidase substrate but also increasing the steric repulsion of AuNPs, preventing the particle surfaces coming into close contact. After peptidase digested the AuNPs/peptide, the AuNPs would lose their shelter and the repulsion effect from original peptide. This digestion leads AuNPs become aggregation to others. Additionally, the peptidase digests the peptide in middle, indicating that there is half of peptide remains on AuNPs surface which then becomes the blocker to avoid free peptide sticks to AuNPs surface again leading stronger repulsion

effect among AuNPs.

In this system, the maximum wavelength (λ_{max}) could be measured by UV/Vis spectroscopy. Additionally, the method could serve as an alternative platform for efficient screening of the peptidase inhibitors. When the peptidase is inhibited by candidate drugs, the drugs block activity of peptidase, the AuNPs/peptide are intact and stable in the solution without the color change. Therefore, the novel AuNPs-based optical biosensing platform could not only detect the activity of peptidase rapidly, but also screen a great deal of effective inhibitor for peptidase.

Despite the AuNPs-based optical biosensing platform is low cost and convenient, the detection range and detection limit of it is still too high to analyze some kinds of peptidase activity. To figure out this problem, based on the FRET property of AuNPs [Iosin *et al*., 2009], the peptide modified on AuNPs is exchanged for peptide-FITC to improve the sensitivity of the AuNPs-based biosensing system in detecting peptidase activity. The peptide-FITC could be detected though fluorescence spectrophotometer in slight quantity after peptidase digestion and release from AuNPs surface. Different from the traditional fluorescein-labeled synthetic peptides with chemical quencher, AuNPs could quench various dyes with perfect quenching efficiency [Lee *et al*., 2008] due to its long-term and broad quenching ability [Mayilo *et al*., 2009]. Therefore, this AuNPs-based flurescence system increases the applications, decreases the cost of chemical quencher and reduces difficulties of experimental design. **Figure 2-2** illustrates the schema of this AuNPs-based fluorescence platform.

Except using AuNPs in biosensing field, AuNPs could also apply in drug delivering because of its good bio-complementary and multi-functional property, which could resolve the barrier of traditional drug delivery system (non-targeting, high dose treatment and non-tracing) [Ghosh *et al*., 2008; Kim *et al*., 2011]. Based on this concept, in this study,

AuNPs are multi-functionalized by target (hGH), tag (MGITC) and drug (doxorubicin), and these AuNPs-complexes (AuNPs/MGITC, AuNPs/hGH, AuNPs/hGH-MGITC, and AuNPs/hGH-doxorubicin) are treating HepG2 cells for demonstrating their cytotoxicity and functions (targeting and tagging). **Figure 2-3** illustrates the schema of this AuNPs-based drug delivery system. In addition, **Figure 2-4** shows the experimental flow chart of these researches.

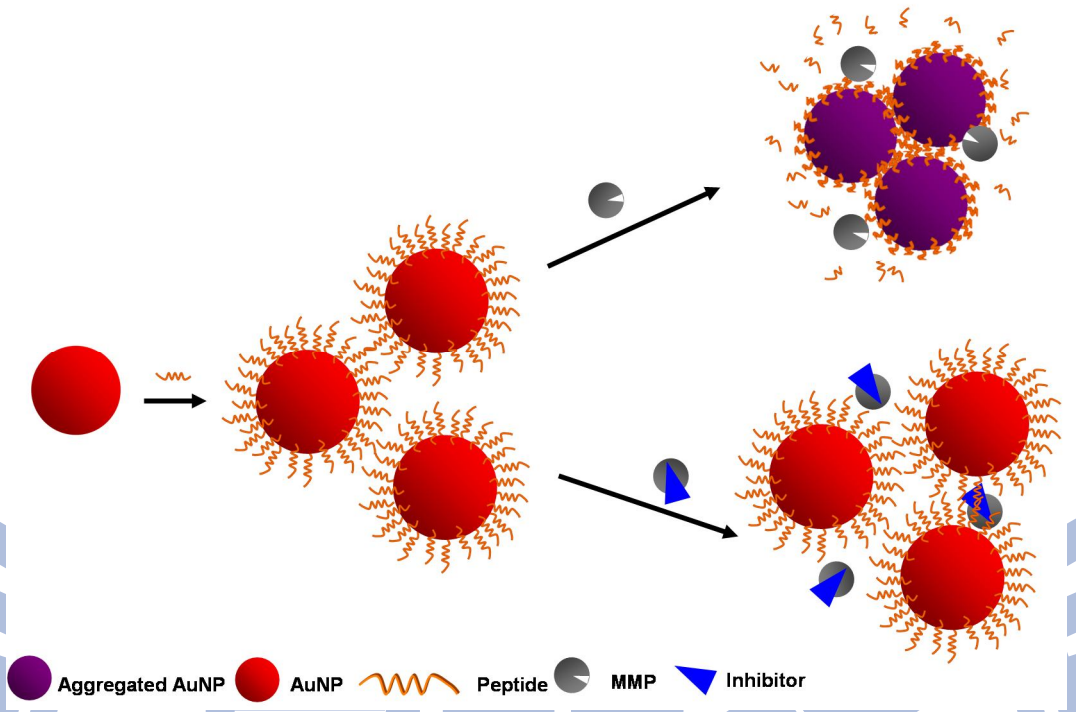

Figure 2-1. A schematic illustration of the AuNPs-based optical biosensing platform to assay peptidase activity. The AuNPs were functionalized with peptide as peptidase substrate for the colorimetric detection. When peptide was digested by peptidase, the AuNPs/peptidase lost shelter to cause aggregation. Aggregation of AuNPs would result in a change of color from pink red to violet blue. In addition, when the peptidase activity was blocked by inhibitor, no further color changes in the AuNPs/peptide. Therefore, this system could be used to efficiently assay peptidase activity and screen the inhibitors of peptidase.

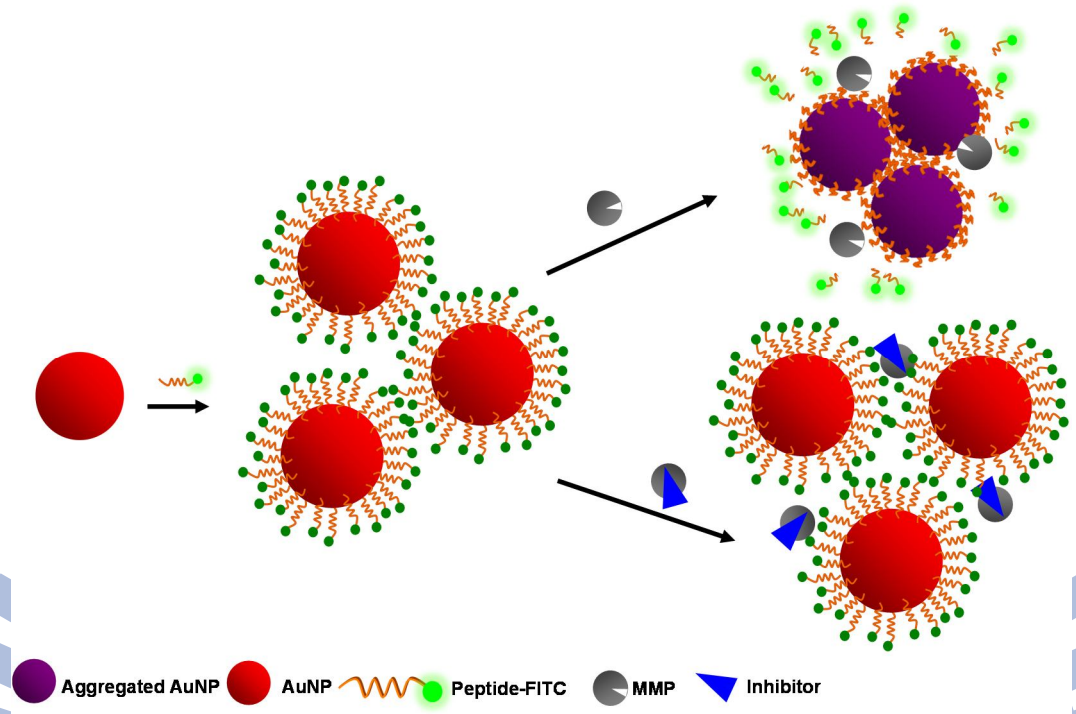

Figure 2-2. A schematic illustration of the AuNPs-based fluorescence platform to assay peptidase activity. The AuNPs were functionalized with peptide-FITC as peptidase substrate for the fluorescence detection. When peptide-FITC was digested by peptidase, the releasing peptide-FITC could be detected its fluorescence intensity. Releasing of peptide-FITC would result in a change of fluorescence intensity at 515 nm. In addition, when the peptidase activity was blocked by inhibitor, no further fluorescence intensity changes in the AuNPs/peptide-FITC. Therefore, this system could be used to efficiently assay peptidase activity and screen the inhibitors of peptidase.

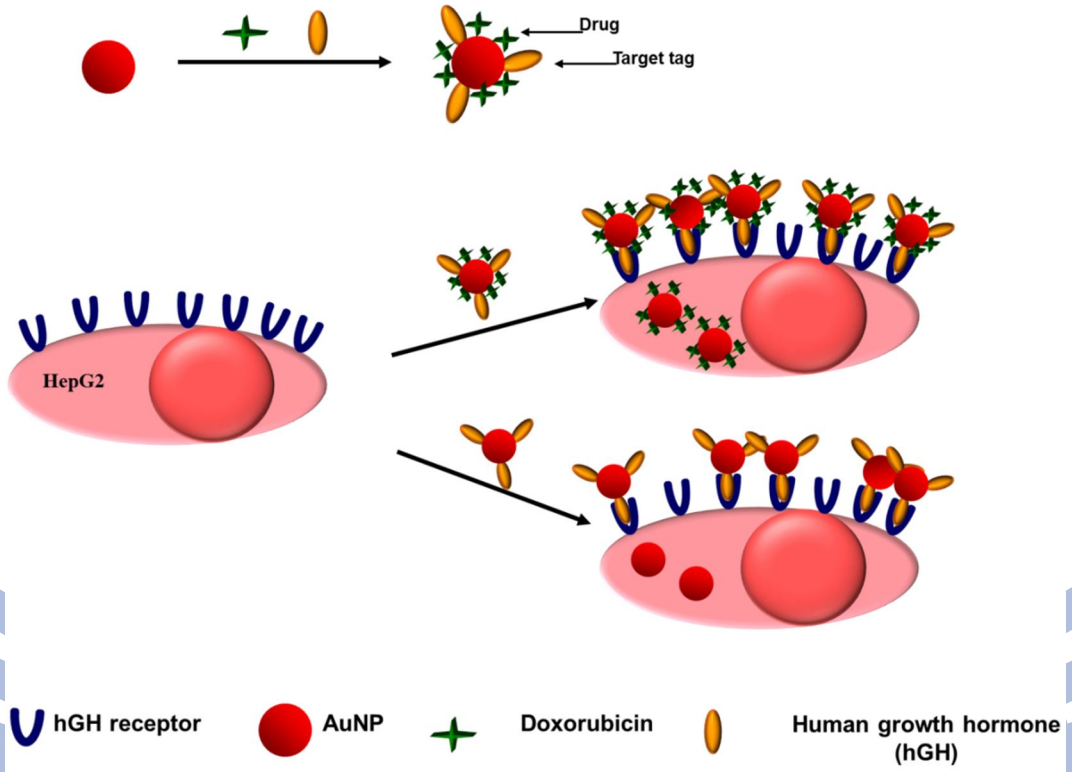

Figure 2-3. A schematic illustration of the AuNPs-based drug delivery platform. The AuNPs could be functionalized with target and drug on the same surface for using as high specifically drug delivery system. In this study, hGH was choose as target, which could bind with hGH receptors on HepG2 cells membrane specifically, and the AuNPs/hGH would be uptaken by HepG2 cells easily with no cell toxicity than bare AuNPs or non-targeted modified AuNPs treatment. Additionally, AuNPs were also modified with doxorubicin, one kind of anticancer drug, which interacts with DNA through intercalation and inhibits the progression of topoisomerase II. Thus, AuNPs/hGH-doxorubicin could inhibit HepG2 cells growth more efficiently than free doxorubicin treatment through specific targeting.

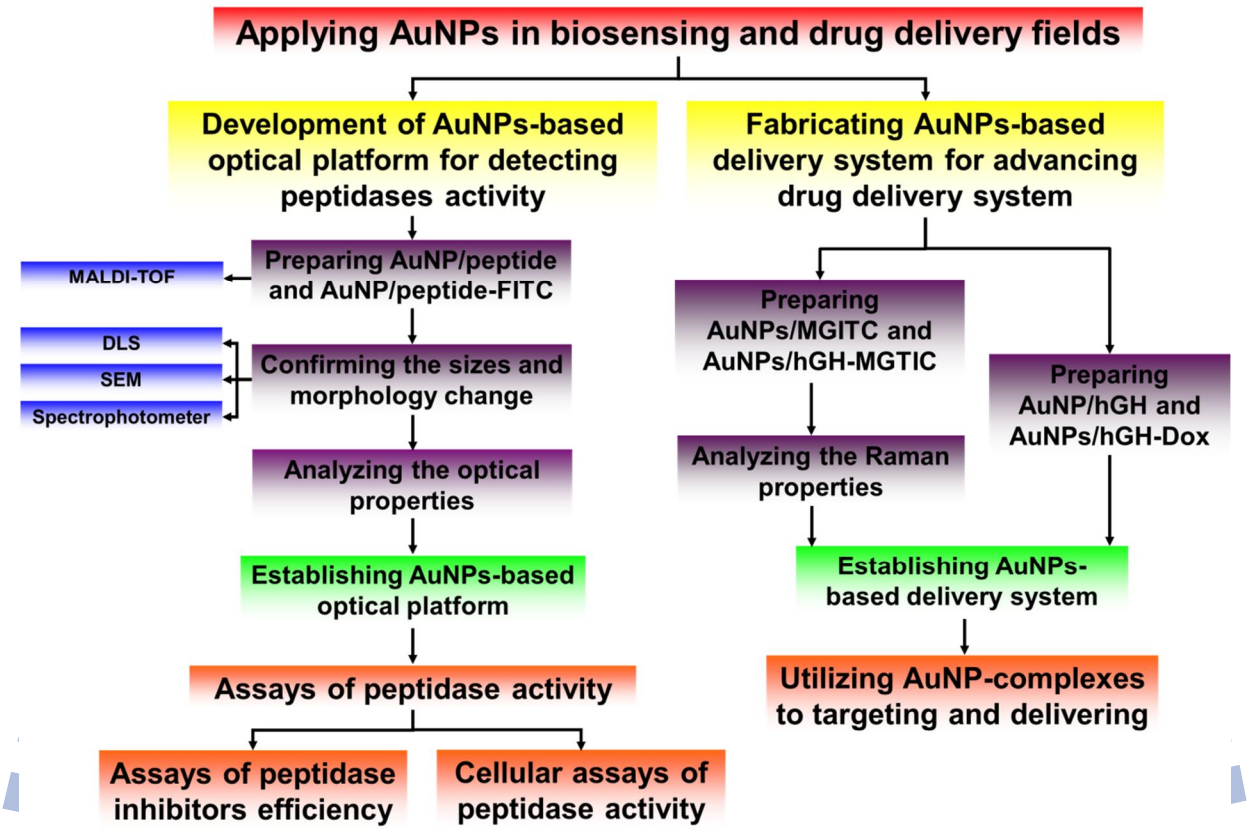

Figure 2-4. The experimental flowchart of the research strategies. In this research, AuNPs were functionalized with different biomolecules and chemical compounds, and the AuNPs-complexes could be applied in biosensing and drug delivery fields. In the first system, AuNPs were modified with peptide and peptide-FITC to establish AuNPs-based optical biosensing platforms for assay of peptidase activity and assay the inhibitors of peptidase. The peptide digested by MMP-2 was revealed by matrix-assisted laser desorption/ionization time-of-flight mass spectrometry (MALDI-TOF). The characteristic change of AuNPs was investigated by dynamic light scattering (DLS), scanning electron micrographs (SEM), and UV-Vis absorption spectrum. Finally, the AuNPs-based optical biosensing platforms were applied in screening the inhibitors of peptidase, detection of peptidase activity, and analyzing cellular peptidase activity. In the other platform, AuNPs were modified with hGH as target and doxorubicin as drug or MGITC as Raman tag to demonstrate an AuNPs-based drug delivery system for targeting and drug delivering. The Raman characteristic change of AuNPs/MGITC was analyzed by surface enhance Raman shift (SERS), and the efficiency of AuNPs/hGH-doroxubicin was detected by MTT assay.

III. Materials and Methods

3-1 Apparatus

Absorption spectra of AuNPs and its complex were observed by UV-Vis spectrophotometer (SpectraMAx 190; Molecular Devices Corporation, Sunnydale, CA, USA). Absorbance values of MTT assay were recorded at 595 nm using a spectrophotometer (Molecular Devices Corporation, Sunnydale, CA, USA). The morphology of AuNP-complexes were performed with SEM (JEOL, Tokyo, Japan), and the size changing of AuNP-complexes were measured by DLS (Brookhaven Instruments Corporation, Holtsville, NY, USA). The mass-to-charge ratio of peptide was detected by Bruker autoflex III MALDI-TOF MS (Billerica, MA, USA). The Raman shift characteristics of AuNP-complexes were performed with Raman spectroscopy (LabRAM HR800, HORIBA Jobin Yvon, Tokyo, Japan). The fluorescence signals of AuNPs/peptide-FITC were analyzed by fluorescence spectrometer (F-2700; Hitachi, Tokyo, Japan).

3-2 Materials

All chemicals were of analytical grade and were used without further purification. Sodium citrate ($C_6H_5Na_3O_7 \cdot 2H_2O$), HPLC-grade acetonitrile (ACN), and trifluoroacetic acid (TFA) were obtained from Merck (Darmstadt, Germany). Tris HCl, minimum essential medium (MEM), Dulbecco's modified Eagle's medium (DMEM), Dulbecco's phosphate buffer saline (DPBS), fetal bovine serum (FBS), 4',6-diamidino-2-phenylindole (DAPI; $C_{16}H_{15}N_5$), and malachite green isothiocyanate (MGITC; $C_{24}H_{24}ClN_3O_4S$) were purchased from Invitrogen (San Diego, LA, USA). Sodium chloride (MGITC) was purchased from USB (Cleveland, OH, USA). ONO-4817 ($C_{22}H_{28}N_2O_6$) was purchased from Tocris (Ellisville, MO, USA). GM6001 (Ilomastat; Galardin; $C_{20}H_{28}N_4O_4$) was purchased from USBiological (Swampscott, MA, USA). Calcium chloride ($CaCl_2$), trypsin, triton X-100, dimethyl

sulfoxide (DMSO), hydrogen tetrachloroaurate(III) ($HAuCl_4 \cdot 3H_2O$), MMP-2 human (expressed in mouse NSO cells), MMP-9 human, MMP-7 human, MMP-1 human, phosphate-buffered saline (PBS), Brij™ 35 solution 30% (w/v), poly-l-lysine, and doxorubicin hydrochloride were obtained from Sigma-Aldrich (St. Louis, MO, USA). Human growth hormone protein (hGH; ab51232) was purchased from Abcam (Cambridge, UK). Disodium dihydrogen ethylenediaminetetraacetate dehydrate (EDTA) was purchased from Amresco (Buenos Aires, Argentina). Sinapinic acid and α–cyano-4-hydroxycinnamic acid (CHCA) used as MALDI matrix, which was saturated in 50% H_2O: 50% ACN (v/v) solution, were obtained from Bruker (Billerica, MA, USA). Nanopure water was obtained by passing twice-distilled water through a Milli-Q system (18 MΩ· cm; Millipore, Bedford, MA, USA).

3-3 Peptides

The substrate of MMP-2 used in the AuNPs-based optical detecting system has the following sequence: 10-mer peptide, Cys-Gly-Pro-Leu-Gly-Leu-Ala-Gly-Hyp-Cys. The peptide was synthesized by Biomertech (Pleasanton, CA, USA). The peptide could be recognized and digested by MMP-2 specifically, and the peptide was separated to Cys-Gly-Pro-Leu-Gly and Leu-Ala-Gly-Hyp-Cys after digestion [Seltzer *et al*., 1990]. The peptide was dissolved in 50% H_2O: 50% ACN (v/v) solution and was preserved in -80ºC.

The substrate of MMP-2 used in the AuNPs-based fluorescence platform has the following sequence: 9-mer peptide, Gly-Pro-Leu-Gly-Leu-Ala-Gly-Hyp-Cys conjugated with fluorescein isothiocyanate (FITC) at N-terminal. The peptide-FITC was synthesized by Pruigo (Taipei, Taiwan). The peptide could be recognized and digested by MMP-2 specifically, and the peptide was separated to FITC-Gly-Pro-Leu-Gly and Leu-Ala-Gly-Hyp-Cys after digestion [Seltzer *et al*., 1990]. The peptide was dissolved in H_2O and was preserved in -20 ºC.

3-4 Preparation of the AuNPs/peptide

3-4-1 Synthesis of 20 nm AuNPs

The 20 nm AuNPs were prepared by citrate reduction of $HAuCl_4 \cdot 3H_2O$ according to the literature procedure [Saraiva and de Oliveira, 2002; Nath and Chilkoti, 2004]. A 25 mL aqueous solution consisting of 2.5 mM $HAuCl_4 \cdot 3H_2O$ was brought to a vigorous boil with stirring in a conical flask, and then 38.8 mM sodium citrate (2.5 mL) was added to the solution rapidly. This solution was boiled with vigorous stirring for another 15 min, resulted in the color change from the originally yellow solution to deep red. The solution was cooled to room temperature with continuous stirring for 15 min. The colloidal AuNPs with an average diameter of 20 nm were produced, and was stored at 4ºC.

Diameter of the prepared 20 nm AuNPs was measured by SEM and DLS. Moreover, the absorption spectra change of AuNPs was measured by UV-Vis spectrophotometer, and the peptide modified on the AuNPs was also detected by MALDI-TOF.

3-4-2 Modification of AuNPs/peptide

The technique of AuNPs conjugated with protein and peptide was based on previously published methods [Lee *et al*., 2008], the peptide was modified on AuNPs surface due to its thiol group of cysteine on the terminal. The process of modified AuNPs/peptide was monitored by observing the spectral change after adding peptide to colloidal AuNPs. The peptide was coated on the AuNPs surface according to the below procedures:

The 100 μL of aqueous peptide solution (1 mg/mL in 50% ACN) was added to 900 μL of the aqueous 20 nm AuNPs solution. After gently mixing, the mixture was incubated and shaken at 4°C for 24 hr. The mixture was then centrifuged for 6 min at 10,000 rpm 4°C to remove the excess peptide, and the supernatant was carefully removed. After two centrifuge/wash cycles, the colloids was resuspended in 1,000 μL of TCNB buffer (50 mM

Tris, with 10 mM calcium chloride, 150 mM sodium chloride and 0.05% Brij 35, pH 7.5), and the AuNPs/peptide was stored at 4°C for 12 hr before used in the further experiment.

3-5 Confirmation of size and morphology change of AuNPs/peptide

3-5-1 Dynamic light scattering

DLS, also known as photon correlation spectroscopy or quasi-elastic light scattering, is a technique which can be used to determine the size distribution of small particles in solution. The method utilizes laser as light source which is monochromatic and coherent, and observes a time-dependent fluctuation in the scattering light intensity to determine the translational diffusion coefficient of small particles.

The AuNPs samples were diluted with TCNB buffer (filtered through 0.22 μm syringe filters) and filled into the light scattering cuvette. Light scattering experiments were performed using the BI-200SM Goniometer (Brookhaven Instruments Corporation, Holtsville, NY, USA) at a temperature of 20°C. The laser wavelength was 532 nm, and measurements were conducted at an angle of 90°. The DLS data were analyzed by Brookhaven Instruments-Dynamic Light Scattering software.

3-5-2 Scanning electron micrographs

High resolution SEM images of modified-AuNPs were obtained with a field-emission SEM instrument JSM-6700F (JEOL, Tokyo, Japan) and operated at 15 kV. The samples were prepared by dropping 10 μL of AuNPs solution onto a golden chip and incubated samples at 37°C for 30 min. Finally, the chips were rinsed thoroughly with distilled water and air-dried for scanning.

3-5-3 Matrix-assisted laser desorption/ionization time-of-flight mass spectrometry

All MALDI-TOF were acquired on a Bruker autoflex III MALDI-TOF mass spectrometer with a pulsed 337 nm nitrogen laser. The sample was dotted on a MTP 384 target plate polished steel TFA. The instrument (positive ion detection) was performed in reflection mode and collision-induced dissociation (CID) was accomplished with Argon as the collision gas. The extraction voltage was 37 kV, and gated matrix suppression was applied to prevent detector saturation by matrix ions with *m/z* lower than 200. Peptide samples (1 μL), original peptide, peptide digested by MMP-2, AuNPs and AuNPs/peptide, were mixed with matrix solution (saturated solution of CHCA in 50 % ACN/H_2O) at 1:1 ration and was able to dry. All data were reprocessed utilizing the flexanalysis (3.1) and biotools (3.1) software.

3-5-4 UV-Vis spectrophotometer

UV-Vis absorption spectroscopy of AuNPs was recorded on a spectrophotometer (Molecular Devices Corporation, Sunnydale, CA, USA). Aliquots of the solution were taken out and the samples were cooled in room temperature to quench the reaction.

3-6 Assay of peptidase activity

3-6-1 Activation of MMP-2

Preliminary experiments were undertaken to determine the concentrations MMP-2 required for maximal activation of each sample. The lyophilized powder MMP-2 was resuspended in 0.1 mL of TCNB buffer (composed of 50 mM Tris, 10 mM $CaCl_2$, 150 mM $NaCl_2$ and 0.05% Triton-X100, pH 7.5), and activated by *p*-Aminophenylmercuric acetate (APMA).

APMA is an organomercurial agent used for the activation of latent MMPs *in vitro*.

The procedure for activation is discribed as follows:

The stock solution of APMA was prepared by dissolve 3.5 mg APMA in 1 mL 0.1 M NaOH, this stock solution should be 10 mM. Then neutralize the high base by diluting 4 folds in Tris-Triton-Calcium buffer (50 mM Tris-HCl, 1 mM $CaCl_2$ and 0.05% Triton X-100, pH 7.5). For activated MMP-2, the APMA solution was mix with MMP-2 sample to give a final concentration of 0.25 mM. Then activation times will vary depending upon the samples. MMP-2 generally requires short activation time. This final activated MMP-2 solution can be used directly without dialyzing away the APMA [Sellers *et al.*, 1977].

3-6-2 Peptidase activity assayed by AuNPs-based optical biosensing platform

For the assay of peptidase activity, the measurement were performed in TCNB buffer as a control experiment and observed result. TCNB buffer would not influence the absorbance of AuNPs and not promote the AuNPs/peptide to aggregate. The concentration of peptide modified-AuNPs was adjusted to 5 nM for the further assay of peptidase activity. In the peptidase activity assay, an amount of 1 μL MMP-2 samples solution with different concentrations (the concentration of MMP-2 was from 100 to 2,000 ng/mL) was added into 100 μL of modified-AuNPs, and then the mixture was incubated at 37°C. The incubation time of AuNPs/peptide treated with MMP-2 was adjusted to 60 min. After peptidase digested, 100 μL of mixture solutions were transferred into 96-well plate. All of samples were analyzed with UV-Vis absorption spectrophotometer and recorded their wavelength. After MMP-2 digested the substrate of AuNPs/peptide, the absorption band around 530 nm decreased, and a new broad absorption above 625 nm emerged. The absorbance spectrum around 530 nm reduced was because of the free AuNPs/peptide decreasing. The new broad absorption above 625 nm emerged was due to the AuNPs/peptide began aggregation and resulted in a red-shift of absorption spectrum. The ratio of $A_{625\ nm}/A_{530\ nm}$ was used to quantify the MMP-2 activity. All of the tests were performed in triplates.

3-7 Assay of MMP inhibitors

In order to apply AuNPs-based optical system for drug screening, two broad-spectrum MMP inhibitors (MMPIs) and one broad-spectrum peptidase inhibitor were used in this study. EDTA is widely used for peptidase inhibitor because of their chelated function, which could bind with metal ions. MMPIs are synthetic molecules and behave as MMPs competitive inhibitors [Augé *et al*., 2004]. GM6001 (galardin) is a potent hydroxamate-type MMPI with a broad inhibitory profile [Sood *et al*., 2008]. ONO-4817 is a novel synthetic hydroxamic acid-based nonpeptide compound designed to be administered orally. ONO-4817 binds reversibly to the zinc-binding region of MMPs and has a selective inhibitory spectrum [Ro *et al*., 2007]. Both of them have been used to inhibit the MMP-2 activity through binding to its active site and developed the treatment of MMP-related diseases [Galardy *et al*., 1994; Yamada *et al*., 2000; Bai *et al*., 2005].

3-7-1 Assay of the efficiency of MMP inhibitors by AuNPs-based optical biosensing platform

For drug screening assay of MMP-2, the procedure was similar with peptidase activity assay. In this inhibitors screening assay, 1 μL of MMP-2 (1,000 ng/mL) with different kinds of MMPIs was added into 200 μL of AuNPs/peptide (5 nM), and the mixtures were incubated at 37°C for 60 min. Finally, the mixture solution was transferred into 96-well plate, then the color change and UV-Vis absorption spectra were collected by SpectraMax 190 UV-Vis spectrophotometer. $A_{625\ nm}/A_{530\ nm}$ of AuNPs/peptide was used to show the inhibitors blocking the activity of MMP-2.

3-8 Specificity of AuNPs-based optical biosensing platform used in the detection of MMPs activity

To confirm the specificity of AuNPs-base optical system in detecting MMPs activity, different types of MMPs were used as samples in the experiment. In this specificity testing, 1 μL of MMP-1, -2, and -7 was added into 200 μL AuNPs/peptide (5 nM) respectively, and the mixtures were incubated at 37°C for 60 min. Finally, the mixture solution was transferred into 96-well plate, then the color change, and UV-Vis absorption spectra were collected by SpectraMax 190 UV-Vis spectrophotometer. $A_{625\ nm}/A_{530\ nm}$ of AuNPs/peptide was used to show the specificity of AuNPs-based platform for MMP-2.

3-9 Preparation of the AuNPs/peptide-FITC

For analyzing peptidase activity, the peptide conjugated FITC was designed as peptidase substrate and modified on AuNPs. AuNPs would quench the fluorescence of FITC, and FITC could release its fluorescence intensity after peptidase digesting the peptide [Wang *et al*., 2010; Kang *et al*., 2011]. The process of modifying AuNPs/peptide-FITC was similar with AuNPs/peptide, due to the peptide-FITC would modified on AuNPs surface through the thiol group, which was the same as the peptide. Synthesizing AuNPs/peptide-FITC is described as follow:

Ten μL of aqueous peptide-FITC solution (1 mg/mL in H_2O) was added to 990 μL of the aqueous 20 nm AuNPs solution. After gently mixing, the mixture was incubated and shaken at 4°C for 24 hr. The mixture was then centrifuged for 8 min at 8,000 rpm in 4°C to remove the excess peptide, and the supernatant was carefully removed. After two centrifuge/wash cycles, the colloids was resuspended in 1,000 μL of TCNB buffer, and the AuNPs/peptide-FITC was stored at 4°C for 12 hr before used in the further experiment.

3-10 Peptidase activity assayed by AuNPs-based fluorescence biosensing platform

For the assay of peptidase activity, the measurement were performed in TCNB buffer as a control experiment and observed result. TCNB buffer would not influence the quenching ability of AuNPs, and TCNB buffer would not promote the AuNPs/peptide-FITC to aggregate. The concentration of peptide-FITC modified-AuNPs was adjusted to 5 nM for the further assay of peptidase activity. In the peptidase activity assay, an amount of 1 μL MMP-2 samples solution with different concentrations (the concentration of MMP-2 was from 0.01 to 5 ng/mL) was added into 100 μL of modified-AuNPs, and then the mixture was incubated at 37°C. The incubation time of AuNPs/peptide-FITC treated with MMP-2 was adjusted to 30 min. The mixture would be measured the fluorescence intensity after peptidase digestion. All of samples were analyzed with F-2700 fluorescence spectrophotometer and recorded their intensity (the excitation of FITC was 485 nm and the emission was 515 nm).

3-11 Assay of the efficiency of MMP inhibitors by AuNPs-based fluorescence biosensing platform

For drug screening assay of MMP-2, the procedure was similar with the peptidase activity assay. In this inhibitors screening assay, 1 μL of MMP-2 (1 ng/mL) with different kinds of MMPIs was added into 100 μL AuNPs/peptide-FITC (5 nM), and the mixtures were incubated at 37°C for 30 min. Finally, the mixture solution was analyzed with F-2700 fluorescence spectrophotometer and recorded their intensity (the excitation of FITC was 485 nm and the emission was 515 nm).

3-12 Specificity of AuNPs-based fluorescence biosensing platform used in the detection of MMPs activity

To confirm the specificity of AuNPs-base optical system in detecting MMPs activity, different types of MMPs were used as samples in the experiment. In this specificity testing, 1 μL of MMP-1, -2, -7, and -9 was added into 100 μL AuNPs/peptide-FITC (5 nM)

respectively, and the mixtures were incubated at 37°C for 30 min. Finally, the mixture solution was analyzed with F-2700 fluorescence spectrophotometer and recorded their intensity (the excitation of FITC was 485 nm and the emission was 515 nm).

3-13 Analysis of peptidase activity in cells

3-13-1 Cell culture

In this experiment, three kinds of cells were used as analytes, which were rat heart myoblasts (H9c2, #60096), primary human cardiac fibroblasts (HCF, #6300), and primary human cardiac myocytes (HCM, #6200). H9c2 cells were purchased from Food Industry Research and Development Institute (Hsin-Chu, Taiwan). The cells were seeded in 100-mm Petri dishes (2×10^6 cells/dish) or 24-well plate (5×10^4 cells/well), cultured in 90 % DMEM and 10 % FBS mixed medium with 100 U/mL penicillin and 100 U/mL streptomycin, and incubated in 5% CO_2, 37°C. The culture medium was changed every 2 days.

HCF and HCM were purchased from ScienCell Research laboratories (San Diego, CA, USA). The cells were seeded in 100-mm Petri dishes (2×10^6 cells/dish) or 24-well plate (5×10^4 cells/well) coated with 0.01% poly-l-lysine and cultured in commercial media (#2301 and #6201; ScienCell Research laboratories), which was maintained according to the manufacturer's instructions. The cells were incubated in 5% CO_2, 37°C, and the culture medium was changed every 2 days.

3-13-2 Analysis of cellular peptidase activity by AuNPs-based fluorescence system

For analyzing the cellular MMP-2 activity, the cell protein would be extracted by the following process:

The cells seeding in 100-mm dish were washed by PBS for three times. After 150 μL lysis buffer added in the dish, the cells were scraped down, transferred in the eppendorf, and

put in ice for 20 min. After centrifugation at 12,000 rpm for 5 min in 4 °C, the supernatant was retained and stored in -20°C for further use.

For detecting the cellular MMP-2 activity, the protein concentrations of HCF, HCM and H9c2 cells were measured first, and all cells protein concentration would be adjusted the same as each other by TCNB buffer before analyzing. In the AuNPs-based fluorescence peptidase activity assay, an amount of 1 μL samples (protein extracts of HCF, HCM, and H9c2 cells) were added into 100 μL of modified-AuNPs, and then the mixture was incubated at 37°C. The incubation time of AuNPs/peptide-FITC treated with MMP-2 was adjusted to 30 min. The mixture would be measured the fluorescence intensity (excitation was 485 nm and emission was 515 nm) after peptidase digestion.

3-13-3 Analysis of cellular peptidase activity by zymography

For analyzing cellular MMP-2 activity (HCF, HCM, and H9c2 cells), the cell protein was extracted as described above in *3-13-2*. The adjusted cellular protein solution was mixed with zymography buffer (composed of 0.5 M Tris-HCl, pH 6.8, glycerol, 10% (w/v) SDS, and 0.1% bromophenol blue) and stood at room temperature for 10 min. Then the samples were loaded on 8% SDS-polyacrylamide gel containing 0.1 mg/mL gelatin, and the gel was run with Tris-Glycine SDS running buffer at 80 V for 3.5 hr.

After doing electrophoresis, the gel was washed twice in renaturing buffer (2.5% Trixton X-100) with gentle agitation at room temperature for 30 min, in order to exchange SDS to Triton X-100. Finishing peptidase renature, the gel was transferred in developing buffer (50 mM Tris-HCl, 200 mM NaCl and 5 mM $CaCl_2$, pH 7.4) at room temperature for 30 min, then replaced with fresh developing buffer and incubated at 37°C for 24 hr.

The gel was then stained with coomassie staining solution (0.125% Coomassie Brilliant Blue R250, 50% (v/v) methanol, 10% (v/v) acetic acid) for 30 min, then was destained with

destain buffer (25% (v/v) methanol, 7.5% (v/v) acetic acid in ddH_2O). Gelatinolytic activities were identified as clear bands against a dark blue background where the peptidase had digested the substrate [Patricia *et al*., 2005; Hu and Beeton, 2010].

3-13-4 In vivo bioimage of cellular peptidase activity

Except analyzing cellular peptidase activity by peptidase assays, the activity of cellular peptidase could also be proved by optical image. The HCF, HCM and H9c2 cells were seeding on circular glasses in 24-well dish and would be incubated in serum free medium for 24 hr before experiment. After cells (HCF, HCM, and H9c2 cells) treated with AuNPs/peptide-FITC for 3 hr as the experimental group, the medium was changed as serum free medium again and incubated for 12 hr. Because cells were treated with AuNPs/peptide-FITC, the peptide was digested by cellular MMP-2, and the FITC would not be quenched by AuNPs that could be detected by confocal. The cells of control group were just incubated as experimental group except adding AuNPs/peptide-FITC. After cells incubation, the cells were washed by PBS for three times and fixed by 4% paraformaldehyde for 20 min in dark. The paraformaldehyde was then removed, and the cells were washed by PBS for three times again and dyed by DAPI for 5 min in dark. After cells dying, the cells were washed by PBS for three times, and the glasses, which had cells on them, would be mounted on microscope slide.

The cell images were acquired in the Olympus FV1000 spectral confocal microscope (Olympus, Latin America) with a 60 x 1.35 NA oil immersion objective. Excitations and filters were mentioned as follows:

DAPI, excitation was 405 nm, emission was 470 - 510 nm; FITC, excitation was 488 nm, emission was 500 - 530 nm; AuNPs, excitation was 543 nm, emission was 650 - 750 nm. Images were acquired in a frame mode.

3-14 Preparation of AuNPs/MGITC and AuNPs/hGH-MGITC

The technique of AuNPs conjugated with Raman reporter (MGITC) was based on previously published methods [Qian *et al*., 2008]. The MGITC could be modified on AuNPs because of its sulphur atom of isothiocyanate group [Biswas *et al*., 2010]. The processes of modified AuNPs/MGITC and AuNPs/hGH-MGITC were monitored by observing the spectral change and Raman shift after adding MGITC and hGH to colloidal AuNPs. The MGITC and hGH were coated on the AuNPs surface according to the below procedures:

The 150 μL of MGITC solution (4 μM in DMSO) was added to 850 μL of the aqueous AuNPs solution. After gently mixing, the mixture was incubated and shaken at 25°C for 10 min, and then 10 μL hexanthiol (1 mM) was added in the mixture incubated at 25°C for 60 min shaken. The hexanthiol was modified on AuNPs surface as a shelter. The mixture was then centrifuged for 8 min at 8,000 rpm to remove the excess MGITC and hexanthiol, and the supernatant was carefully removed. After two centrifuge/wash cycles, the AuNPs/MGITC colloids were resuspended in 100 μL of 0.1% PBST.

To modify AuNPs/hGH-MGITC, 10 μL hGH (100 μg/mL) was added in 840 μL AuNPs with gently mixing. After incubating and shaking in 4°C for 24 hr, the AuNPs/hGH was modified with MGITC as previous description. The AuNPs/hGH-MGITC colloids were then resuspended in 100 μL of 0.1 % PBST, and stored in 4°C.

3-15 Confirmation of Raman shift of AuNPs-complexes

3-15-1 Raman shift signal of AuNPs-complexes

All signals of Raman shift were measured by Raman spectrometer, LabRAM HR800, with 20 mW 633 nm Helium-Neon laser due to the absorption spectrum of MGITC was 632.8 nm (the gratin was 600, integrating time was 10 s, the range of detected wavelength was 1,100 - 1,800 cm^{-1}). All samples (AuNPs, MGITC, and AuNPs/MGITC) were seeded on

silicon wafer (for low background signal), dried in air and fixed on the plate for detection.

3-15-2 Cell culture of HepG2 cells

Human hepatoblastoma cells (HepG2, #60025) were purchased from Food Industry Research and Development Institute (Hsin-Chu, Taiwan). The cells were seeded in 100-mm Petri dishes (2×10^6 cells/dish), 6-well plate (5×10^5 cells/well) or 24-well plate (5×10^4 cells/well), cultured in 90 % MEM and 10 % FBS mixed medium with 100 U/mL penicillin and 100 U/mL streptomycin, and incubated in 5% CO_2, 37°C. The culture medium was changed every 2 days.

3-15-3 Raman shift signal of AuNPs-complexes in HepG2 cells

The HepG2 cells were transferred to 6-well plate, seeded on silicon wafer, and cultured in serum-free medium for 24 hr before experiment treatments. The cells were treated with 50 μL AuNPs/MGITC (5 nM) or AuNPs/hGH-MGITC (5 nM) for 24 hr, washed with PBS for three times, fixed with 4 % paraformaldehyde for 20 min, and washed with PBS for three times again before detection. The instrument condition was as the same as part *3-15-1* description.

3-16 Preparation of AuNPs/hGH-doxorubicin

The modification process of AuNPs/hGH is described as follow: 10 μL hGH (100 μg/mL) was added in 950 μL AuNPs with gently mixing. After incubating and shaking in 4°C for 24 hr, the AuNPs/hGH colloids were then centrifuged for 8 min at 8,000 rpm to remove the excess hGH, and the supernatant was carefully removed. After two centrifuge/wash cycles, the AuNPs/hGH colloids was resuspended in 100 μL of 0.1 % PBST.

To modify AuNPs/hGH-doxorubicin, 40 μL doxorubicin (1.8 mM) was added in 960 μL AuNPs/hGH mixture and mixed gently. After 2 hr incubating and shaking in 37°C, the

AuNPs/hGH-doxorubicin colloids were centrifuged for 8 min at 8,000 rpm to remove the excess hGH and doxorubicin, and the supernatants were carefully removed. After two centrifuge/wash cycles, the AuNPs/hGH-doxorubicin colloids were resuspended in 100 μL of 0.1% PBST.

The concentration of doxorubicin on AuNPs could be measured by using dithiothreitol (DTT) to replace the doxorubicin from AuNPs surface [Lee *et al*., 2008] and then detecting the concentration of doxorubicin through spectrometer (the absorption spectrum of doxorubicin was 480 nm). 100 μL of AuNPs/hGH-doxorubicin was mixed with 10 μL 0.1 M DTT, and then the mixture was centrifuged for 8 min at 8,000 rpm to get the supernatant which had exchanged doxorubicin. After centrifuging, the supernatant and the different standard concentrations of doxorubicin were transferred to 96-well dish and measured the absorbance at 480 nm.

3-17 In vitro cytotoxicity of AuNPs/hGH-doxorubicin, AuNPs/hGH, and doxorubicin

The cytotoxicity of HepG2 cells treated with AuNPs/hGH, AuNPs/hGH-doxorubicin, and free doxorubicin was detected by a 3-(4,5-dimethylthiazole-2-yl)-2,5-diphenylte -trazolium bromide (MTT) assay. The assay was based on the ability of mitochondrial dehydrogenases in live cells to reduce MTT compound, a yellow soluble tetrazolium salt, to blue formazan crystal. The cells were transferred to 24-well plate and incubated with serum free medium for 24 hr before treatment. HepG2 cells were treated with different concentrations of AuNPs/hGH ranging from 0 to 37.5 nM (AuNPs), and different doses of AuNPs/hGH-doxorubicin and free doxorubicin ranging from 0 to 100 μM (doxorubicin). After 24 hr incubating, the cells were placed into 90 % serum free medium with 10 % MTT reagent (5 mg/mL) and incubated for 4 hr in 37°C. The medium was removed from plate, and 200 μL DMSO was added in these wells respectively. After mixing, the blue formazan

crystal would be dissolved in DMSO, and the absorption wavelength was measured by spectrophotometer at 595 nm.

IV. Results

4-1 Synthesis of AuNPs and AuNPs/peptide

In the study, the 20 nm AuNPs were used to establishing an optical biosensing platform to assay peptidase activity. The 20 nm AuNP were produced by sodium citrate reduction method. The absorption spectra of 20 nm AuNPs and modified-AuNPs (AuNPs/peptide) were measured by Ultrospec 3300 pro UV-Vis spectrophotometer (Amersham Biosciences). The extinction coefficients of the AuNPs are normally very high [Jena and Raj, 2008]. In the previous reports, the optical spectrum was used to estimate the particles size of AuNPs, and the maximum absorbance (λ_{max}) of 20 nm AuNPs was located at 525nm [Brozek and Zharov, 2008].

The UV-Vis absorption spectra of 20 nm AuNPs and AuNPs/peptide were measured to confirm the modification of AuNPs/peptide (data not shown). The red-colored AuNPs (20 nm in diameter) had surface plasmon resonance band at 525 nm. When the 20 nm AuNPs were modified with peptide, the λ_{max} of AuNPs/peptide shifted from 525 to 530 nm because of the AuNPs size changing.

4-2 The mass-to-charge ratio (m/z) change of peptide and AuNPs/peptide

The *m/z* of original peptide (Cys-Gly-Pro-Leu-Gly-Leu-Ala-Gly-Hyp-Cys) was 1,954, shown in **Figure 4-1A**. The peptide was separated in two parts after digested by MMP-2 (Cys-Gly-Pro-Leu-Gly and Leu-Ala-Gly-Hyp-Cys), and the *m/z* were 972 and 994, which were detected by MALDI-TOF (**Figure 4-1B**). The peptide was made as MMP-2 substrate, so MMP-2 could recognize the sequence (Gly-Pro-Leu-Gly-Leu-Ala-Gly-Hyp) and cut the peptide in middle. Additionally, the cysteine was designed at N- and C-terminal of peptide for modifying on AuNPs surface through thiol groups [Song *et al*., 2010].

To confirm the modification of AuNPs/peptide, bare AuNPs and AuNPs/peptide were adhered on the matrix, and the components on AuNPs surface would be ionized by the laser and be analyzed by MALDI-TOF (**Figure 4-1C** and **4-1D**). AuNPs would not be detected by positive mode MALDI-TOF because AuNPs had negative charge on the surface (the AuNPs was synthesis through sodium citrate reducing Au^{3+}), and the detection range of the machine was also set from 500 to 4,000 *m/z*, which was too small for 20 nm AuNPs. The result shows that, there was a significant *m/z* signal of peptide (Cys-Gly-Pro-Leu-Gly-Leu-Ala-Gly-Hyp-Cys), 1,954, from ionizing AuNPs/peptide (**Figure 4-1D**), and there was lack of specific *m/z* signal on bare AuNPs surface. It indicated that the peptide was modified on AuNPs indeed.

4-3 Identification of the size and morphology change of modified-AuNPs

The size change of modified-AuNPs was investigated by DLS (**Figure 4-2**), and the morphology change of modified-AuNPs was observed by SEM (**Figure 4-3**). In the process of the 20 nm AuNPs synthesized by sodium citrate reduction, citrate ions and free chloride ions were adsorbed on the surface to AuNPs, and provided negative charge to AuNPs surface [Saraiva and de Oliveira, 2002; Nguyen *et al*., 2010]. The average particle size of non-modified AuNPs was about 24.03 nm (**Figure 4-2A**), and the non-modified AuNPs was dispersive on the chip (**Figure 4-3A**) due to the negative charge of AuNPs would repel each other.

When the 20 nm AuNPs was modified with peptide, the diameter of AuNPs/peptide was estimated about 34.55 nm (**Figure 4-2B**), and the peptide increased the steric repulsion of AuNPs which could prevent the AuNPs from aggregation (**Figure 4-3B**).

After peptidase digested the AuNPs/peptide, AuNPs/peptide displayed a dramatic aggregation due to the peptides around AuNPs were shorter. The shorter peptide reduced

repulsive force among AuNPs that leaded AuNPs come together easily and become aggregation (**Figure 4-3C**).

4-4 Time-dependent absorption spectra of AuNPs-based optical biosensing platform

Time-dependent changed of absorbance spectrum of AuNPs-based optical biosensing platform is shown in **Figure 4-4**. After peptidase (MMP-2) digested the substrate of AuNPs/peptide, the absorption band around 530 nm decreased gradually. Concomitantly, a new broad absorption above 625 nm emerged, and its intensity increased by prolonging the reaction time. The absorbance spectrum around 530 nm reduced was because of the free AuNPs/peptide decreasing. The new broad absorption above 625 nm emerged was due to the AuNPs/peptide began aggregation and resulted in a red-shift of absorption spectrum. Therefore, the value of absorption spectra ratio ($A_{625\ nm}/A_{530\ nm}$) was stand for the ratio of aggregated AuNPs and free AuNPs, which could be used to quantity peptidase activity.

4-5 Assay of MMP-2 activity by AuNPs-based optical biosensing platform

In this study, the AuNPs/peptide was used to assay the MMP-2 activity by optical method. The 5 nM of AuNPs/peptide solutions were incubated with different concentrations of MMP-2 (from100 to 2,000 ng/mL) at 37°C for 60 min. As the concentrations of MMP-2 rising, the aggregation degree of AuNPs/peptide increased, and resulted in a remarkable color change from wine-red to purple. In addition, large absorption spectra variation would be observed (**Figure 4-5A**). To estimate the activity of MMP-2, the ratios of absorbance at 625 and 530 nm ($A_{625\ nm}/A_{530\ nm}$) at 60 min after adding MMP-2 were plotted as the function of MMP-2 concentrations (**Figure 4-5B**). The absorbance was chosen to represent the corrilation amount of aggregating and suspending AuNPs.

When plotting $A_{625\ nm}/A_{530\ nm}$ against the MMP-2 concentrations, it is found that the correlation coefficients (R^2) was 0.9703 for the determination of MMP-2 in the concentration ranges from 100 to 1,500 ng/mL, and the detection limit of this method could reach to as low as 100 ng/mL for MMP-2.

4-6 Assay of the efficiency of MMPs inhibitors by AuNPs-based optical biosensing platform

This convenient AuNPs-based optical biosensing platform was further applied for MMP-2 inhibitors screening. EDTA, a broaden peptidase inhibitor, was chosen as candidate to test the AuNPs-based optical biosensing system applied on peptidase inhibitor assay. GM6001 and ONO-4817, two well-known inhibitors for MMP-2, were selected as examples to demonstrate the application in MMP-2 inhibitor screening. The AuNPs/peptide solutions containing MMP-2 (1,000 ng/mL) and different MMP-2 inhibitors were measured after the solutions incubated at 37°C for 1 hr.

In the presence of an efficient inhibitor in the AuNPs/peptide solution, no detectable color change occurred, and the solutions were indefinitely stable without showing signs of aggregation. These results could be observed from absorbance spectra (shown in **Figure 4-6A**), since EDTA, GM6001 and ONO-4817 could inhibit the activity of MMP-2, the aggregation of AuNPs/peptide would become slow, and resulted in less absorption variation (and less color change). **Figure 4-6B** displays the $A_{625\ nm}/A_{530\ nm}$ obtained during the MMPs inhibitors to block the MMP-2 activity. According to the data, MMP-2 could digest substrate on AuNPs and induce AuNPs aggregation well, while the inhibitors blocked MMP-2 activity and leaded no obvious aggregation among AuNPs. Therefore, the AuNPs-based optical biosensing platform not only is possible to perform a colorimetric assay for peptidase activity, but also has potential for further applications in anti-MMPs drugs screening.

4-7 Specificity of AuNPs-based optical biosensing platform used in the detection of MMPs activity

Excluding quantifying peptidase activity and peptidase inhibitors screening, the specificity of AuNPs-based platform for MMPs detection also should be confirmed. The peptide modified on AuNPs was designed as MMP-2 substrate. Thus, different kinds of MMPs could be chosen as examples to test the specificity of the AuNPs-based system. MMP-1 is one kind of collagenases, which could digest six types of collagen [Kessenbrock *et al*., 2010]. MMP-7 is belonged to one of matrilysins, which digests elastin, fibronectin and laminin [Bourboulia and Stetler-Stevenson, 2010]. Both MMP-1 and MMP-7 were selected as the candidates to demonstrate the specificity of AuNPs-based biosensing system.

In the presence of MMP-1 or MMP-7 in the AuNPs/peptide solution, no detectable color change occured, and the solutions were indefinitely stable without showing signs of aggregation. These results could be observed from absorbance spectra (shown in **Figure 4-7A**). Since MMP-1 and MMP-7 could not digest the peptide, the aggregation of AuNPs/peptide would become slow, and resulted in less absorption variation (and less color change). **Figure 4-7B** shows the $A_{625\ nm}/A_{530\ nm}$ obtained during the MMP-1 and MMP-7 could not digest the peptide on AuNPs. According to the data, MMP-2 could digest substrate on AuNPs and induce AuNPs aggregation well, while MMP-1 and MMP-7 have no activities on the peptide and lead no obvious aggregation among AuNPs. Therefore, the AuNPs-based optical biosensing platform has high specificity for MMP-2 activity detection.

4-8 Assay of MMP-2 activity by AuNPs-based fluorescence biosensing platform

In this part of research, the AuNPs-base optical system was changed to AuNPs-based fluorescence system for analyzing lower peptidase activity. The AuNPs/peptide was exchanged to peptide-FITC used as substrate modified on AuNPs, and the peptide-FITC would be quenched by AuNPs before peptidase digestion. After peptidase digested

peptide-FITC, released FITC could be detected intensity by F-2700 fluorescence spectrophotometer.

The 5 nM of AuNPs/peptide-FITC solutions were incubated with different concentrations of MMP-2 (from 0.01 to 5 ng/mL) at 37°C for 30 min. As the concentrations of MMP-2 rising, the number of releasing peptide-FITC increased, which could be measured by fluorescence intensity (excitation was 485nm, and emission was 515nm) (**Figure 4-8A**). To estimate the activity of MMP-2, the delta intensity of 515 nm at 30 min after adding MMP-2 were plotted as a function of MMP-2 concentrations (**Figure 4-8B**).

When plotting delta fluorescence intensity at 515 nm against the MMP-2 concentrations, it was found that the correlation coefficients (R^2) was 0.9759 for the determination of MMP-2 in the concentration ranges from 0.01 to 2 ng/mL, and the detection limit of this method could reach to as low as 0.01 ng/mL for MMP-2.

4-9 Assay of the efficiency of MMPs inhibitors by AuNPs-based fluorescence biosensing platform

This AuNPs-based fluorescence biosensing platform was further applied for MMP-2 inhibitor screening. EDTA, GM6001 and ONO-4817, one broad peptidase inhibitor and two well-known inhibitors for MMP-2, were selected as examples to demonstrate the application in MMP-2 inhibitor screening. The AuNPs/peptide-FITC solutions containing MMP-2 (1 ng/mL) and different MMP-2 inhibitors were measured after the solutions incubated at 37°C for 30 min.

In the presence of an efficient inhibitor in the AuNPs/peptide-FITC solution, no obvious fluorescence intensity change occurred, and the solutions were indefinitely stable without showing aggregation. These results could be observed from fluorescence intensity, since EDTA, GM6001 and ONO-4817 could inhibit the activity of MMP-2 and lead the releasing of peptide-FITC would become slow, and resulted in less fluorescence intensity variation.

Figure 4-9 displays the delta fluorescence intensity at 515 nm. The delta intensity obtained during the MMPs inhibitors to block the MMP-2 activity. According to the data, MMP-2 could digest substrate on AuNPs and induce peptide-FITC releasing, while the inhibitors blocked MMP-2 activity and leaded less peptide-FITC separating from AuNPs surface. Therefore, the AuNPs-based fluorescence biosensing platform not only possible to perform an assay for peptidase activity, but also has potential for further applications in anti-MMPs drugs screening.

4-10 Specificity of AuNPs-based fluorescence biosensing platform used in the detection of MMPs activity

Excluding quantifying peptidase activity and peptidase inhibitors screening, the specificity of AuNPs-based platform for MMPs detection also should be confirmed. The peptide-FITC modified on AuNPs was designed as MMP-2 substrate. Thus, different kinds of MMPs could be chosen as examples to test the specificity of the AuNPs-based system. MMP-1, -7 and -9 (gelatinase B), were selected as the candidates to demonstrate the specificity of AuNPs-based fluorescence biosensing system.

In the presence of MMP-1 or MMP-7 in the AuNPs/peptide-FITC solution, no detectable fluorescence intensity change occurred, and the solutions were indefinitely stable without showing signs of aggregation. These results could be observed from fluorescence intensity, since MMP-1 and MMP-7 could not digest the peptide, the releasing of peptide-FITC would become slow, and resulted in less intensity variation. **Figure 4-10** displays the delta fluorescence intensity at 515 nm, which obtained during the MMP-1 and MMP-7 could not digest the peptide-FITC on AuNPs. As the result shown, MMP-2 and MMP-9 could digest substrate on AuNPs and induce peptide-FITC releasing well, while MMP-1 and MMP-7 had no activities on the peptide-FITC and leaded no obvious peptide-FITC releasing from AuNPs surface. Therefore, the AuNPs-based fluorescence biosensing platform has high specificity

for MMP-2 and MMP-9 activity detection.

4-11 Assay of cellular peptidase activity by AuNPs-base fluorescence system and zymography

Excepting pure compounds analysis, AuNPs-based fluorescence system could also apply on assay cellular peptidase activity. For demonstrating this platform, high (HCF and HCM) and low (H9c2 cells) MMP-2 expression cells were chosen as analytes, and their cellular MMP-2 activity would be measured by AuNPs-based fluorescence system and zymography as the same time. As the result shown (**Figure 4-11A and 4-11B**), the delta fluorescence intensity of HCF and HCM extracts were much higher than H9c2 cells in the same protein concentration, and the MMP-2 (72 kDa) band on zymography gel of HCF and HCM were also much stronger than H9c2 cells. Therefore, both assays displayed the same trend, the expression of MMP-2 in HCF and HCM were high while H9c2 cells were low. This result means that AuNPs-based fluorescence system had the ability to analyze not only pure MMP-2 and its inhibitors but also bio-samples. Additionally, AuNPs/peptide-FITC could be used as an in-cell peptidase activity detector. Three kinds of cell (HCF, HCM, and H9c2 cells) were treated with AuNPs/peptide-FITC, and then the MMP-2 in the cells would digest peptide-FITC leading FITC releasing, which could be observed by confocal. As the pictures shown (**Figure 4-11C**), HCF, HCM and H9c2 cells endocyted similar number of AuNPs-complexes (shown in red), but the intensity of FITC (shown in green) in HCF and HCM was much stronger than in H9c2 cells in the same detecting condition. Thus, AuNPs/peptide-FITC has a promising potential to become a real-time detector of MMP-2 activity in cell or *in vivo*.

4-12 Synthesis of AuNPs/MGITC and the SERS profile of AuNPs/MGITC

MGITC is usually used as a Raman reporter due to it had several significant Raman shift signals after modified on metal particles surface reported in studies before [Lin *et al*., 2008;

Qian *et al*., 2008]. In this study, AuNPs were used as Raman enhancer according to its SPR characteristic, which could enhance the signal intensity of analytes [Abalde-Cela *et al*., 2010]. Therefore, the modification of AuNPs/MGITC would be confirmed by surface enhance Raman scattering (SERS).

The Raman shifts (cm^{-1}) of bare AuNPs, MGITC, and AuNPs/MGITC are shown in **Figure 4-12**. The result shows that, bare AuNPs had no specific Raman signal, and MGITC had few unique Raman signals with low intensity that was hard to identify. However, after MGITC modified on AuNPs surface through its sulphur atom of isothiocyanate group, the AuNPs/MGITC showed several significant Raman shifts (1,169, 1,365, 1,590, and 1,615 cm^{-1}), and the intensity of these signals were amplified ten times then MGITC only. This data indicated the MGITC was modified on AuNPs, and AuNPs enhanced the intensity of MGITC Raman signal indeed.

4-13 The SERS profile of AuNPs/MGITC and AuNPs/hGH-MGITC treated HepG2 cells

In the previous results, the process of the modification and the SERS characteristic of AuNPs/MGITC had been confirmed. To apply the modified AuNPs into cell, hGH protein was used as the target tag on AuNPs in this study. As the results shown, the intensity of SERS signals of HepG2 cells treated with AuNPs/hGH-MGITC for 24 hr was four times higher than the cells treated with AuNPs/ MGITC (**Figure 4-13**). In addition, the main Raman signal of MGITC on AuNPs (1,169, 1,365, 1,590 and 1,615 cm^{-1}) had no obvious shifting whether hGH modified on AuNPs. This meant the hGH would not influence the SERS property of MGITC.

4-14 The cytotoxicity of AuNPs/hGH in HepG2 cells

For applying AuNPs-based platform as drug delivery system in cell, the cytotoxicity of AuNPs-complex (AuNPs/hGH) was tested first. As the result shown, the viability ratio of

HepG2 cells treated with different concentrations AuNPs/hGH were almost around 100%. This meant AuNPs/hGH would not affect HepG2 cells growth or survive in 24 hr (**Figure 4-14**).

4-15 The viability of HepG2 cells treated with AuNPs/hGH-doxorubicin, and doxorubicin

In previous study, AuNPs/hGH was proved to be no cytotoxicity for HepG2 cells in short time interval. This indicated that AuNPs-based platform would not affect HepG2 cells viability. For demonstrating AuNPs-based drug delivery system, doxorubicin was chose as the candidate. Doxorubicin is one kind of anticancer drug and could interact with DNA through intercalation and inhibit the progression of topoisomerase II. Therefore, after HepG2 cells treated with AuNPs/hGH-doxorubicin or free doxorubicin, the cell viability of HepG2 cells would decrease. As the result shown (**Figure 4-15**), the viability of HepG2 cells treated with doxorubicin was higher than AuNPs/hGH-doxorubicin in the same doxorubicin concentrations (from 0.01 μM to 100 μM). In addition, AuNPs/hGH-doxorubicin decreased the viability of HepG2 cells 30% than doxorubicin treatment. This result shows that AuNPs/hGH-doxorubicin could inhibit HepG2 cells growth more efficient than doxorubicin only.

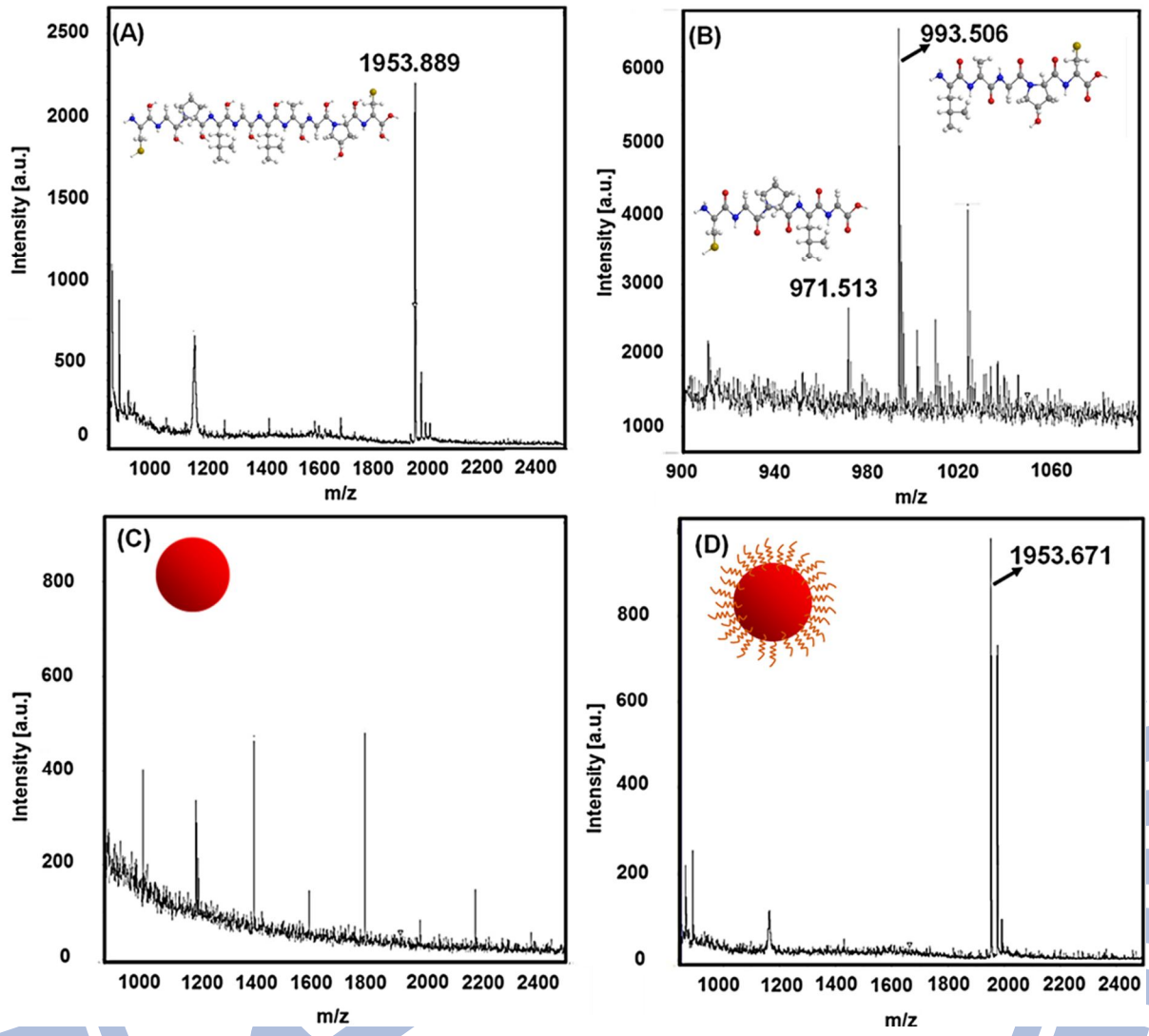

Figure 4-1. The MALDI-TOF profile of peptide and AuNPs/peptide. The mass-to-charge ratio of peptide and AuNPs/peptide was measured by MALDI-TOF in positive mode. (**A**) The mass-to-charge ratio (*m/z*) of original peptide (Cys-Gly-Pro-Leu-Gly-Leu-Ala-Gly-Hyp-Cys) was about 1,954. After MMP-2 digestion, the peptide would separate to two parts that were Cys-Gly-Pro-Leu-Gly and Leu-Ala-Gly-Hyp-Cys. (**B**) The *m/z* of Cys-Gly-Pro-Leu-Gly was about 972 and the *m/z* of Leu-Ala-Gly-Hyp-Cys was about 994. (**C**) and (**D**) was bare AuNPs and AuNPs/peptide, respectively.

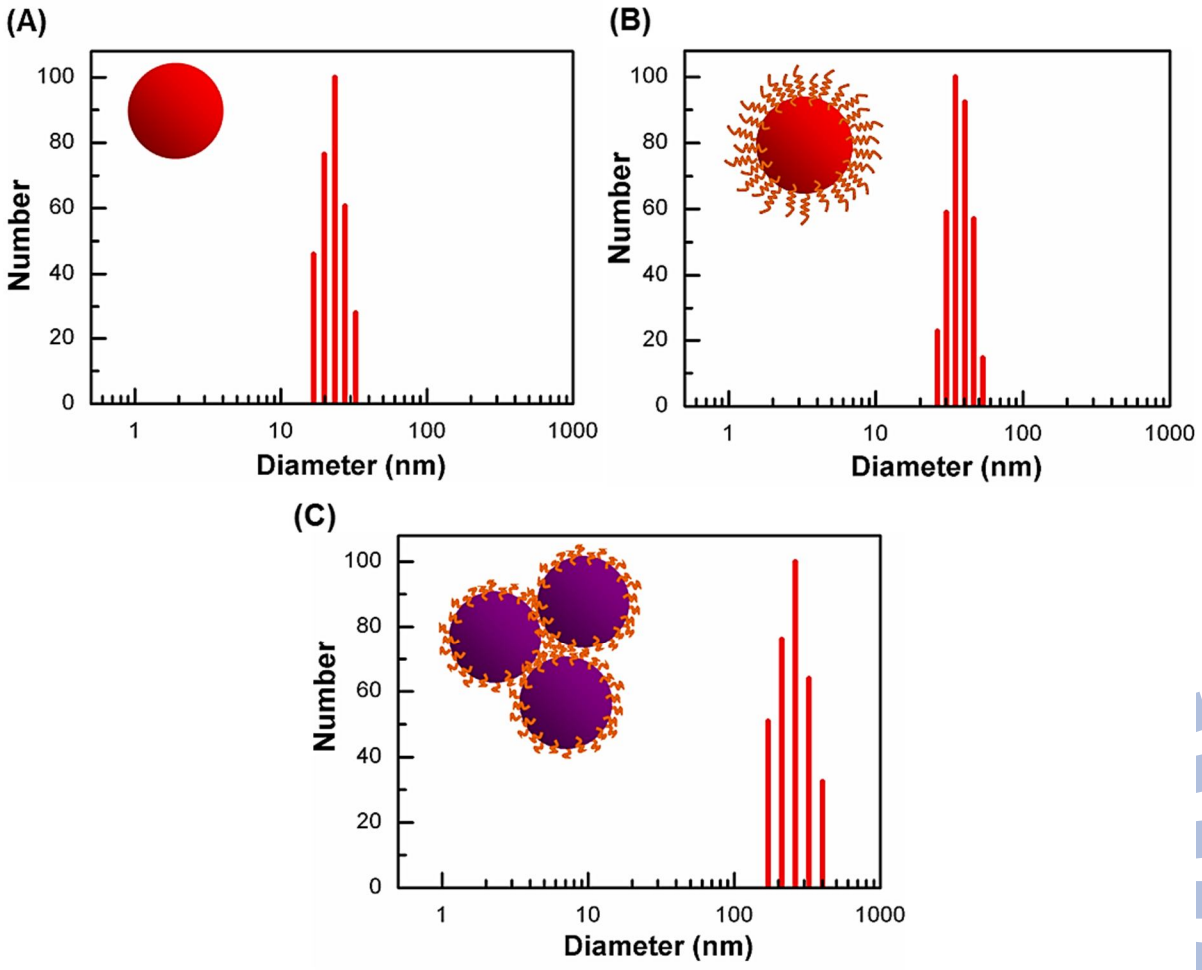

Figure 4-2. Investigation of the size change of modified-AuNPs by DLS. The average particle size of modified/ bare-AuNPs were investigated by DLS and analyzed at 20°C. The bare-AuNPs (**A**) was estimated about 24.03 nm, and the AuNPs/peptide (**B**) was estimated about 34.55nm. The AuNPs/peptide treated with MMP-2 (**C**) was measured about 260.53 nm. X-axis represents the diameter of particles on a diameter scale. Y-axis represents the relative number of collected particles.

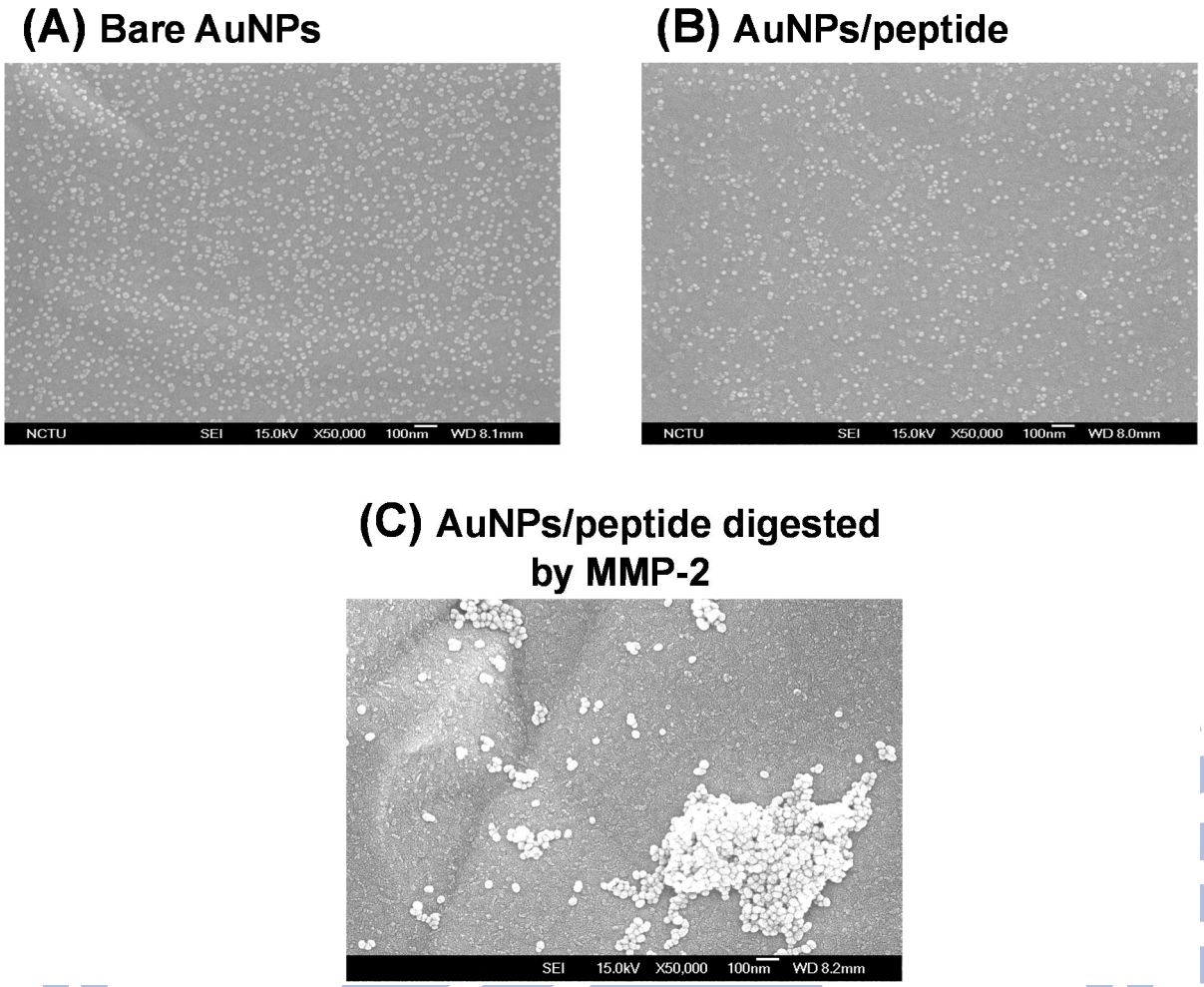

Figure 4-3. SEM micrographs of the modified-AuNPs mophology. Bare-AuNPs (**A**); The AuNPs/peptide before (**B**) and after digested with MMP-2 (**C**). The bare-AuNPs were dispersive on the golden chip because of their negative charge of AuNPs surface, which would repel from each other. The morphology of AuNPs/peptide was similar with bare-AuNPs, but the AuNPs/peptide showed slightly aggregation due to the peptide decreasing repulsive effect of AuNPs. After MMP-2 digestion, AuNPs/peptide was lose shutter and became seriously aggregation.

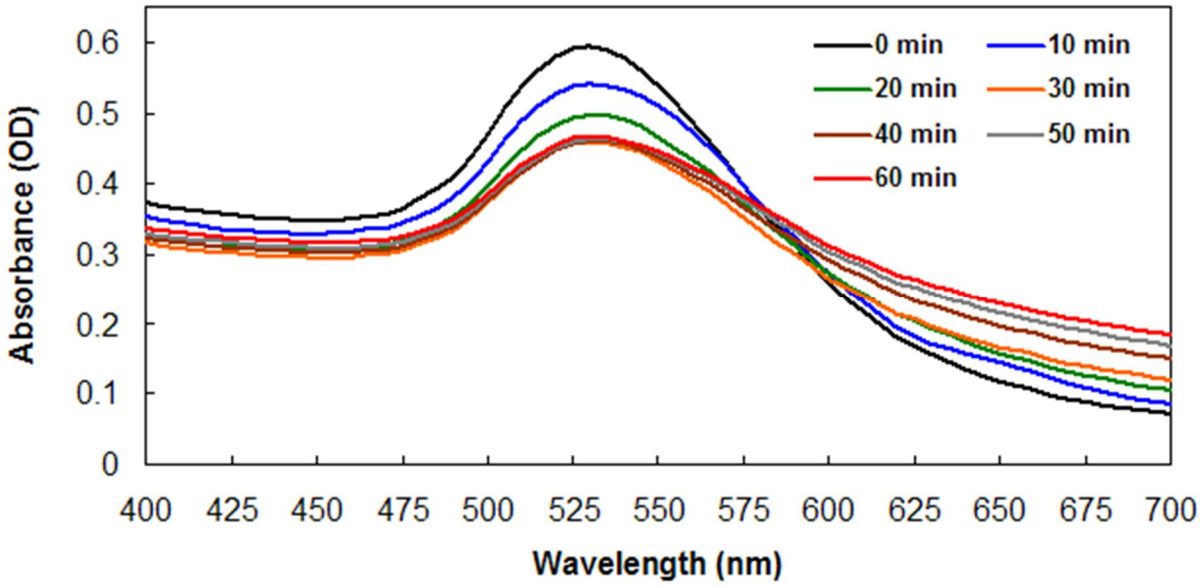

Figure 4-4. Time-dependent absorption spectra changes of AuNPs-based optical biosensing platform. Absorption spectra of AuNPs/peptide were taken for 60 min at 10 min interval after MMP-2 digested the substrate. The solution under investigation was composed of 100 μL AuNPs/peptide (5 nM) and MMP-2 (500 ng/mL). Both of the decreased absorbance spectra at 530 nm and the increased absorbance spectra at 625 nm were observed with increasing time. The broad absorption at 625 nm was raised due to the AuNPs/peptide became aggregation. Because of the reason, in this AuNPs-based optical biosensing platform, the absorption ratio ($A_{625\ nm}$/ $A_{530\ nm}$) of AuNPs/peptide was used to quantify the peptidase activity.

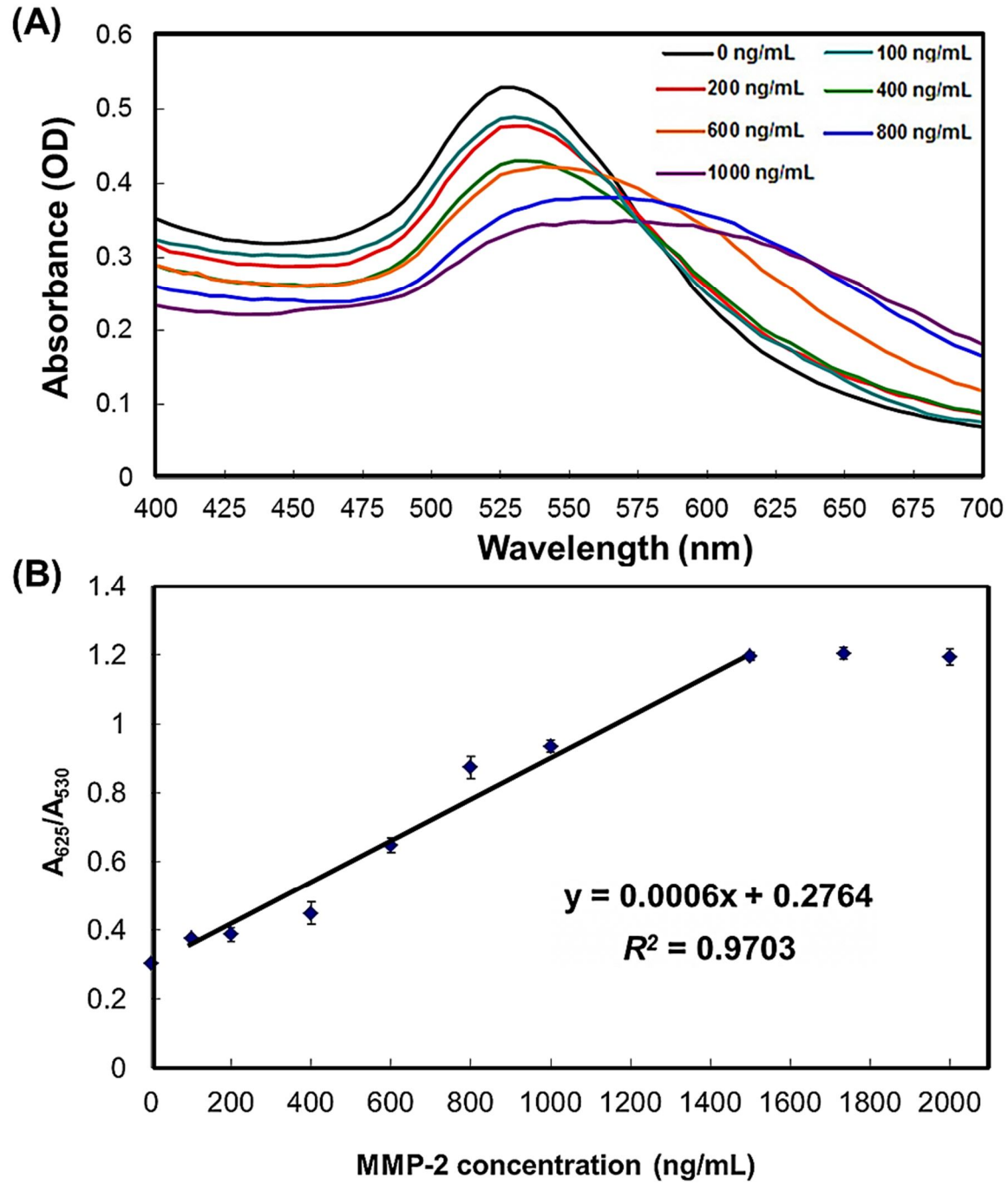

Figure 4-5. The absorption spectra changes of AuNPs/peptide treated with MMP-2. The solution was composed of AuNPs/peptide (100 μL) and different concentrations of MMP-2 (from 100 to 2,000 ng/mL). (**A**) The absorption spectra were measured after AuNPs/peptide treated with MMP-2. (**B**) Plot of absorption ratio ($A_{625\ nm}/A_{530\ nm}$) of AuNPs/peptide against MMP-2 concentration. The samples were incubated in 37 °C for 60 min before measurement. The leaner relationship of MMP-2 concentration is ranged from 100 to 1,500 ng/mL with regression equation, y = 0.0006x + 0.2764, R^2 = 0.9703. The detection limit is determined as 100 ng/mL. The S.D. (error bars) were calculated based on three independent detections (n = 3).

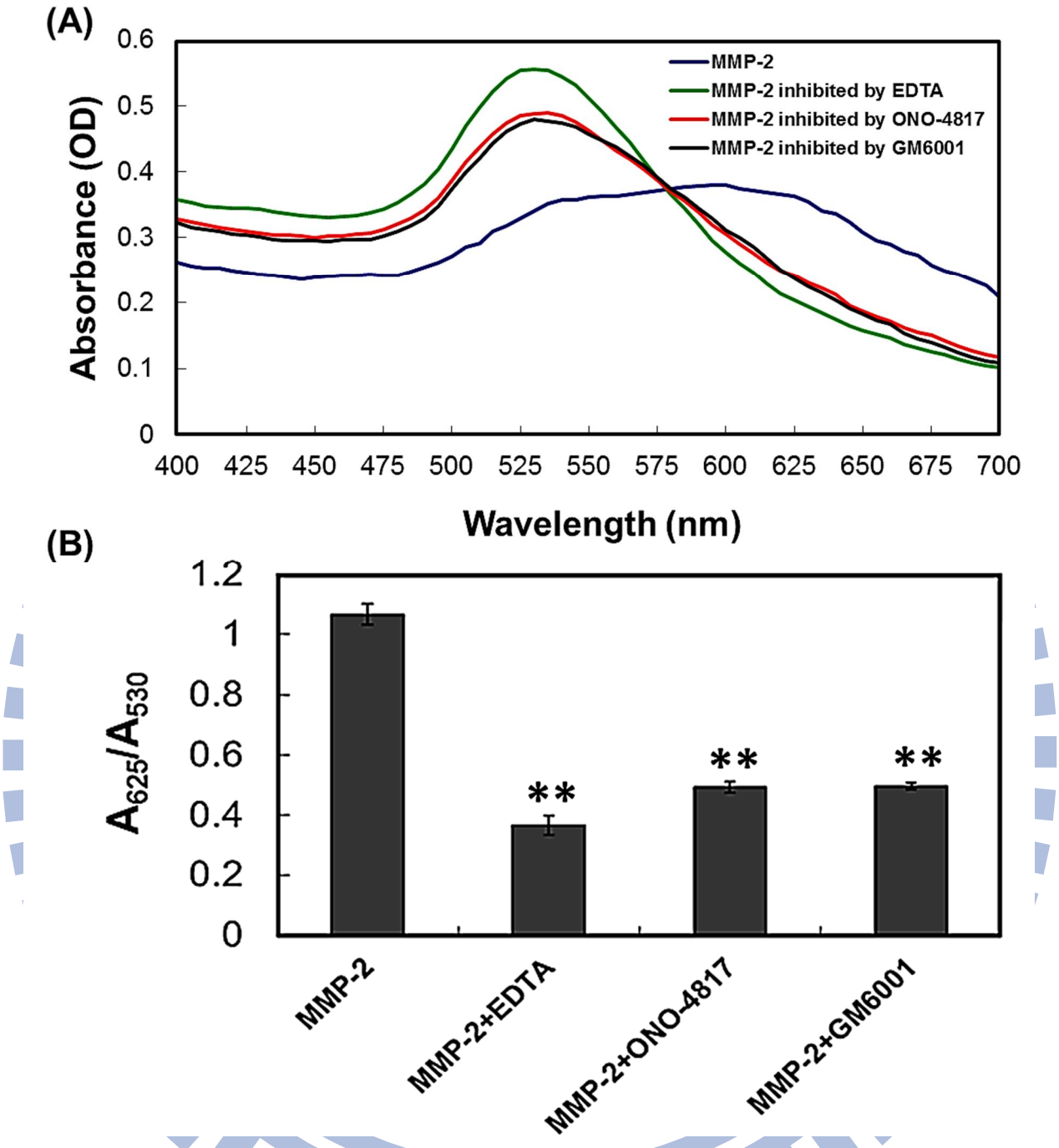

Figure 4-6. Using the AuNPs-based optical platform to assay different MMPs inhibitors. The solution was composed of AuNPs/peptide (100 μL), MMP-2 (1,000 ng/mL), and MMPs inhibitors (EDTA, ONO-4817, and GM6001). (**A**) The absorption spectra were analyzed after AuNPs/peptide treated with MMP-2 and its inhibitor in 37 ^{o}C, 60 min. (**B**) Plot of absorption ratio ($A_{625\ nm}/A_{530\ nm}$) of AuNPs/peptide against MMP-2 and its inhibitors. The values ($A_{625\ nm}/A_{530\ nm}$) of AuNPs/peptide treated with MMP-2 only and MMP-2 inhibited by EDTA, ONO-4817 and GM6001 were 1.07, 0.37, 0.49 and 0.50, respectively. The S.D. (error bars) were calculated based on three independent detections (n = 3). Asterisk (**) indicates $P < 0.01$.

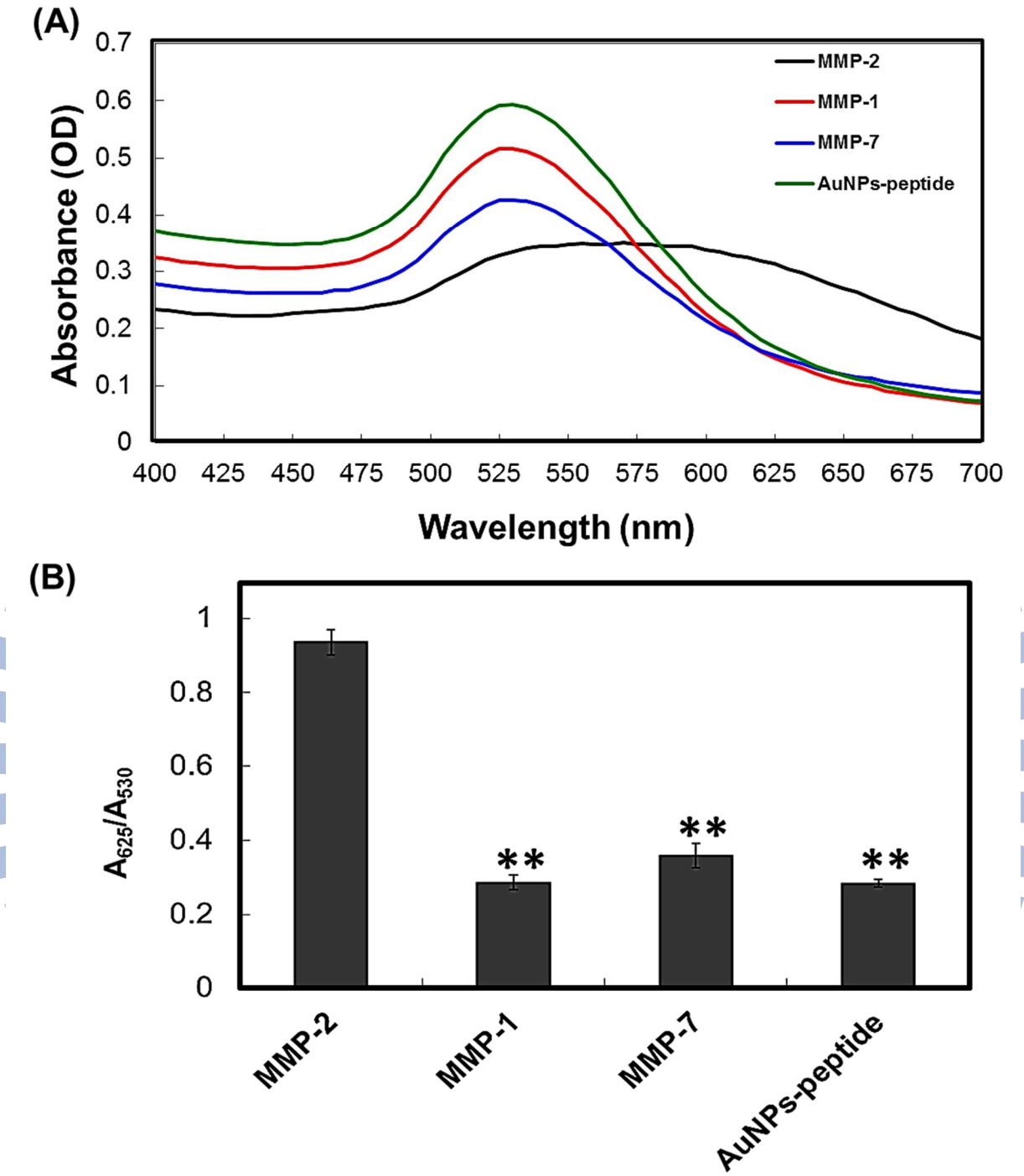

Figure 4-7. Specificity of AuNPs-based optical platform used in the detection of MMPs activity. The solution was composed of AuNPs/peptide (100 μL) and different MMPs (MMP-2, -1, and -7). (**A**) The absorption spectra were analyzed after AuNPs/peptide treated with different MMPs in 37 ^{o}C, 60 min. (**B**) Plot of absorption ratio ($A_{625\ nm}/A_{530\ nm}$) of AuNPs/peptide against MMP-2, -1, and -7. The values ($A_{625\ nm}/A_{530\ nm}$) of AuNPs/peptide treated with MMP-2, -1, -7 and AuNPs/peptide only were 0.94, 0.29, 0.36 and 0.28 respectively. The S.D. (error bars) were calculated based on three independent detections (n = 3). Asterisk (**) indicates $P < 0.01$.

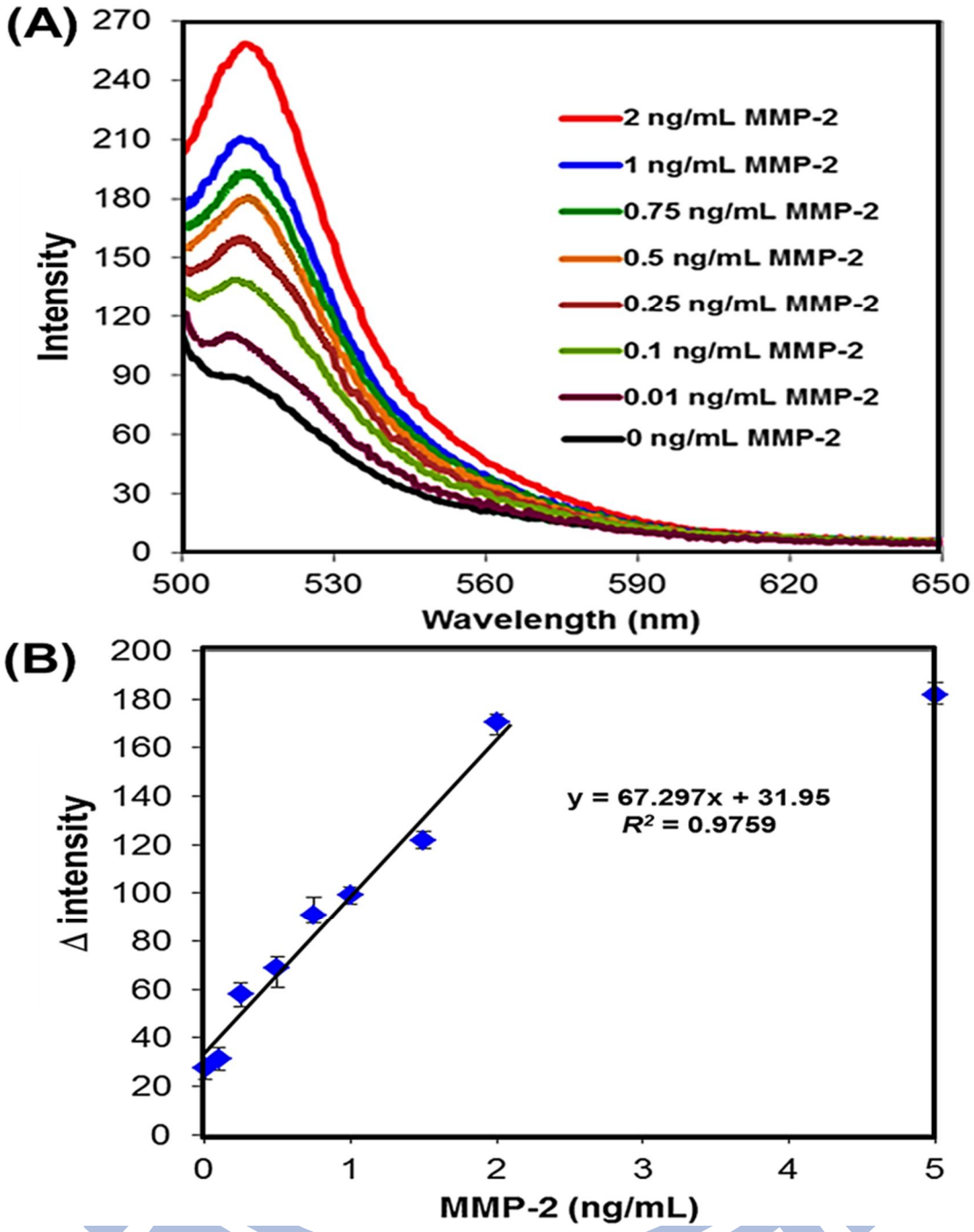

Figure 4-8. The fluorescence intensity change of AuNPs/peptide-FITC treated with MMP-2. The solution was composed of AuNPs/peptide-FITC (100 μL) and different concentrations of MMP-2 (from 0.01 to 5 ng/mL). (**A**) The fluorescence intensity was measured after AuNPs/peptide-FITC treated with MMP-2. (**B**) Plot of delta intensity (at 515 nm) of AuNPs/peptide-FITC against MMP-2 concentrations. The samples were incubated in 37 ^{o}C for 30 min before measurement. The leaner relationship of MMP-2 concentration is ranged from 0.01 to 2 ng/mL with regression equation, y = 67.297x + 31.95, R^2 = 0.9759. The detection limit is determined as 0.01 ng/mL. The S.D. (error bars) were calculated based on three independent detections (n = 3).

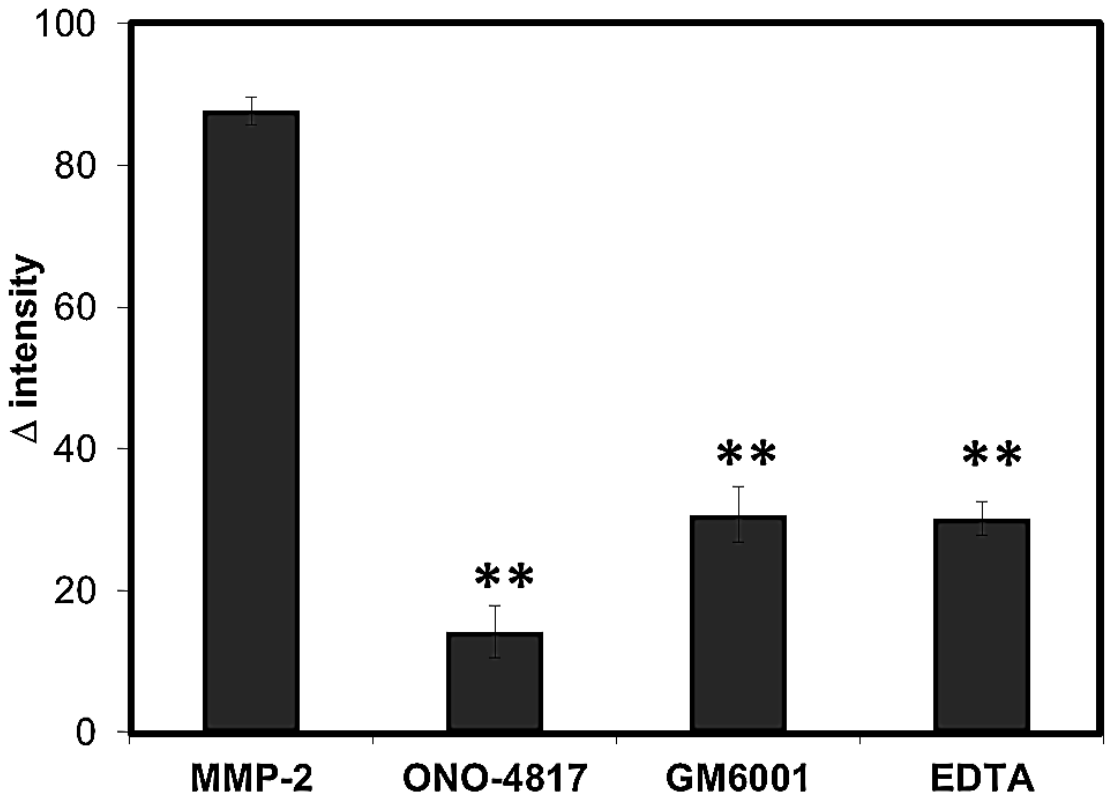

Figure 4-9. Using the AuNPs-based fluorescence platform to assay different MMPs inhibitors. The solution was composed of AuNPs/peptide-FITC (100 μL), MMP-2 (1 ng/mL), and MMPs inhibitors (ONO-4817, GM6001, and EDTA). The fluorescence intensity was analyzed after AuNPs/peptide-FITC treated with MMP-2 and its inhibitor in 37 ^{o}C, 30 min. Here shows the plot of delta intensity (at 515 nm) of AuNPs/peptide-FITC against MMP-2 and its inhibitors. The values of AuNPs/peptide-FITC treated with MMP-2 only and MMP-2 inhibited by ONO-4817, GM6001and EDTA were 87.68, 14.10, 30.70 and 30.18, respectively. The S.D. (error bars) were calculated based on three independent detections (n = 3). Asterisk (**) indicates $P < 0.01$.

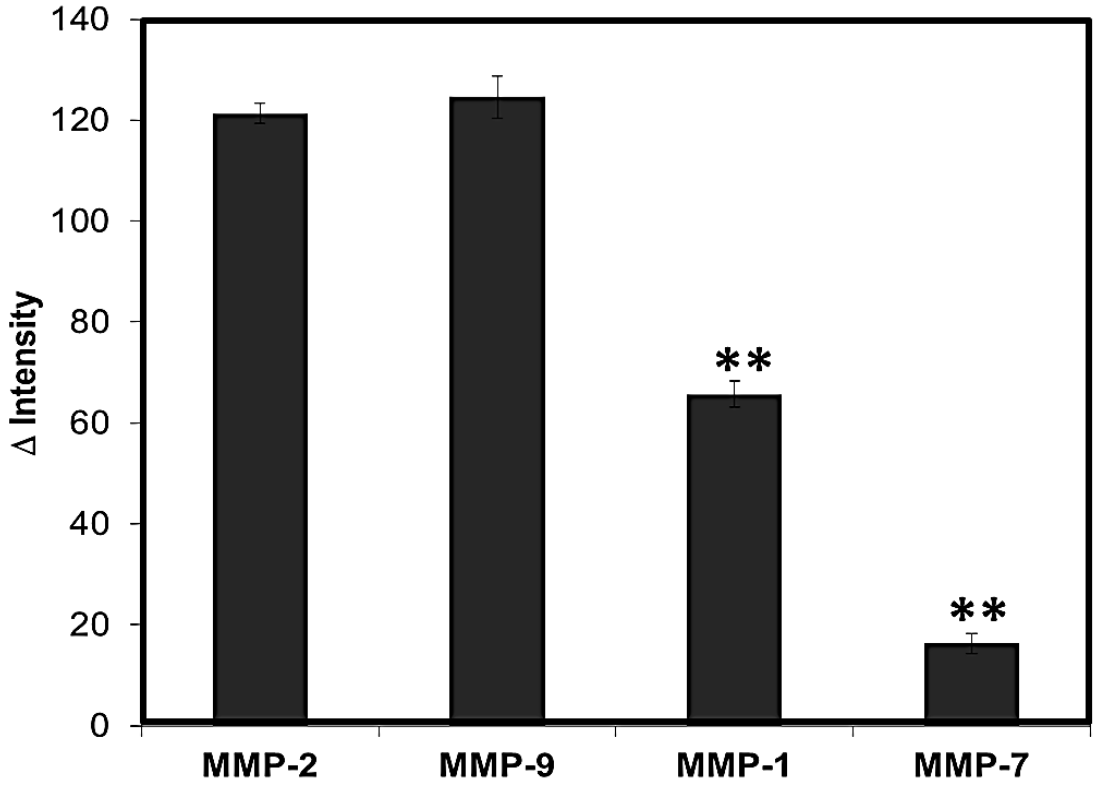

Figure 4-10. Specificity of AuNPs-based optical platform used in the detection of MMPs activity. The solution was composed of AuNPs/peptide-FITC (100 μL) and different MMPs (MMP-2, -9, -1, and -7). The fluorescence intensity was analyzed after AuNPs/peptide-FITC treated with different MMPs in 37 ^{o}C, 30 min. Here shows the plot of delta fluorescence intensity of AuNPs/peptide-FITC against MMP-2, -9, -1, and -7. The values of AuNPs/peptide-FITC treated with MMP-2, -9, -1 and -7 were 121.4, 124.6, 65.7 and 16.3, respectively. The S.D. (error bars) were calculated based on three independent detections (n = 3). Asterisk (**) indicates $P < 0.01$.

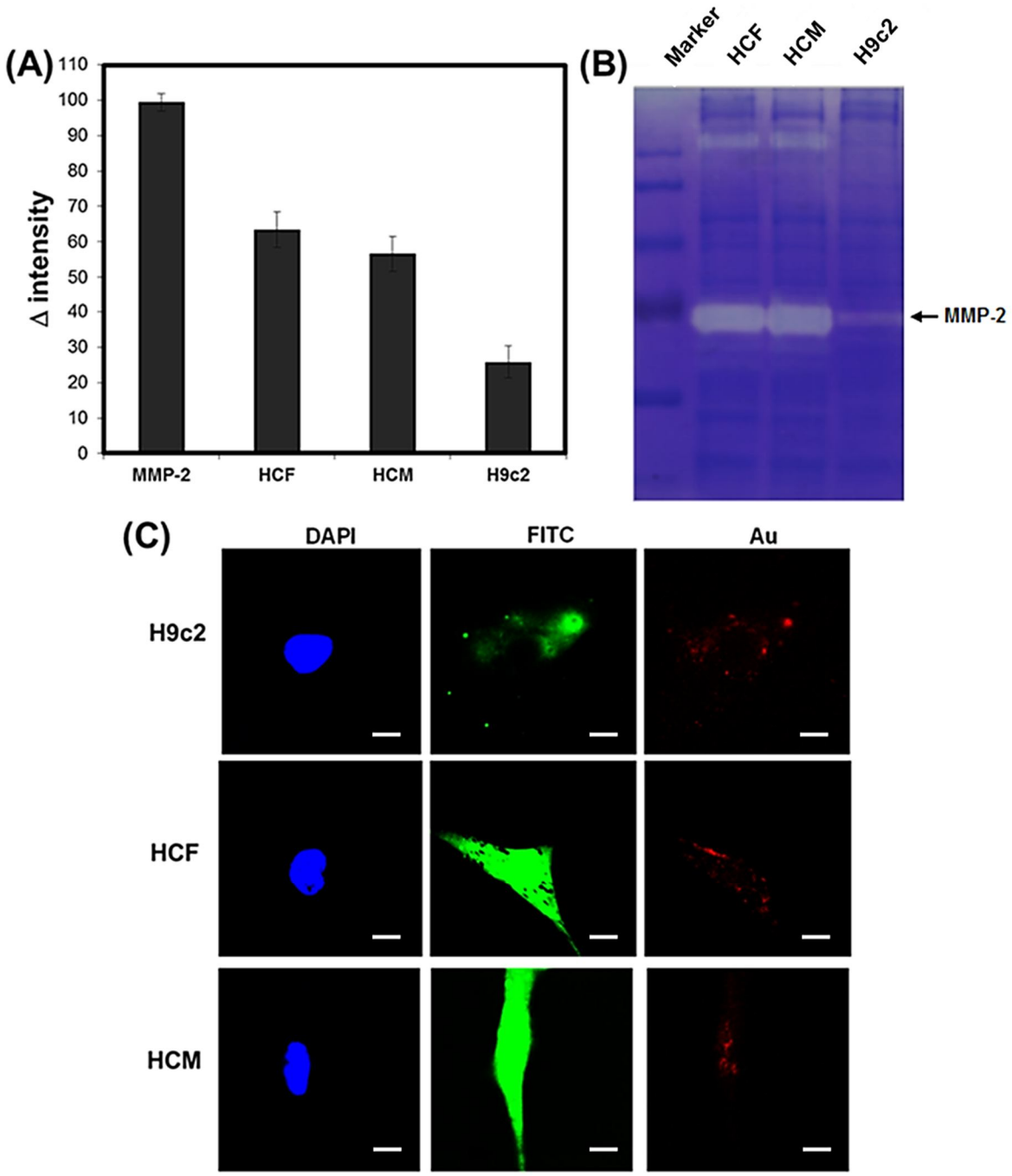

Figure 4-11. Using AuNPs-based fluorescence system and zymography to assay cellular MMP-2 activity. For demonstrating the platform, HCF, HCM and H9c2 cells were chose as analytes. The delta fluorescence intensity of HCF and HCM extracts were higher than H9c2 cells (**A**), and the MMP-2 band on zymography gel of HCF and HCM were also much broad than H9c2 cells (**B**). In addition, HCF, HCM and H9c2 cells endocyted similar number of AuNPs-complexes (displayed in red), but the intensity of FITC (shown as green) in HCF and HCM was much stronger than H9c2 cells in the same confocal detecting condition (**C**). The white bar represents 10 μm in (**C**). The S.D. (error bars) were calculated based on three independent detections (n = 3).

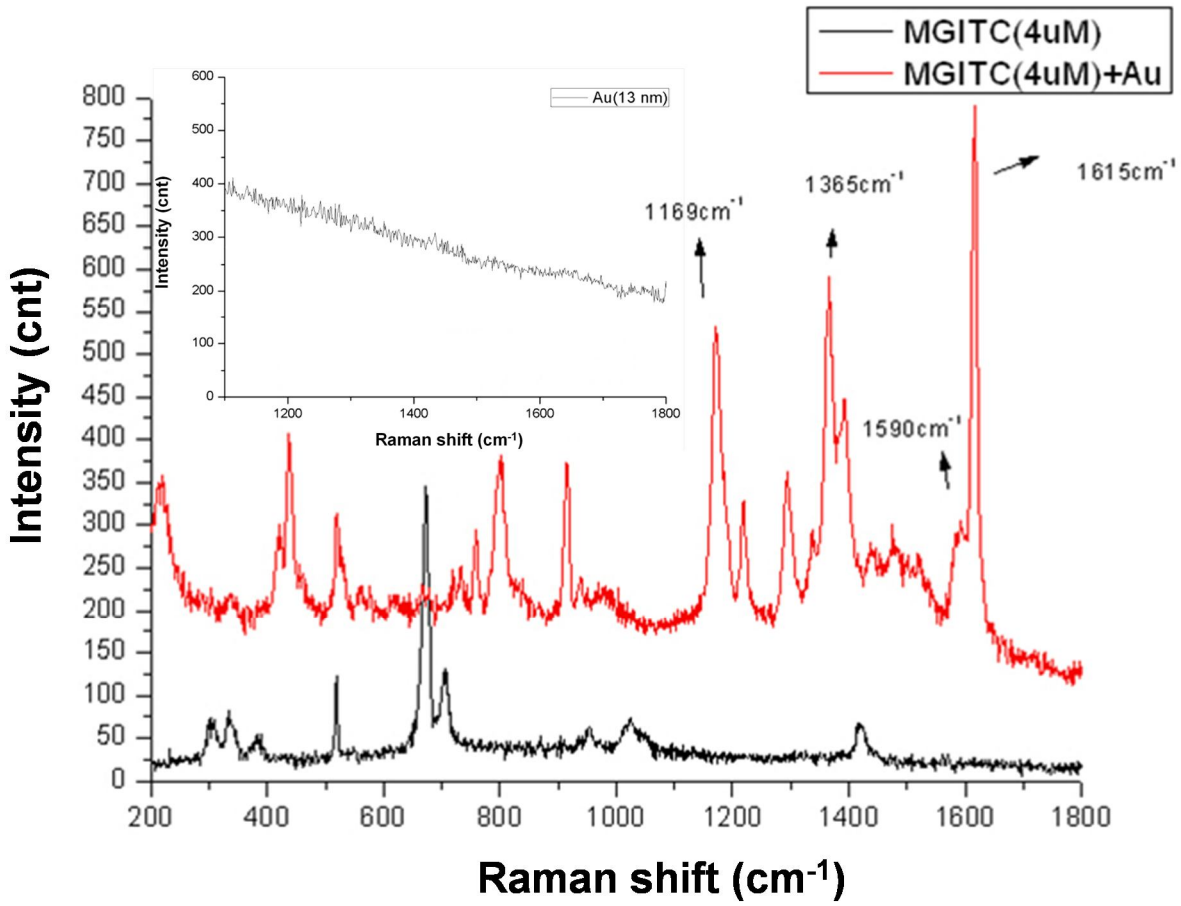

Figure 4-12. The surface enhance Raman shift of AuNPs, MGITC and AuNPs/MGITC. MGITC is a Raman reporter which has several meaningful peaks, and these peaks would be enhanced after modified on AuNPs during surface enhance effect. To measure AuNPs, MGITC and AuNPs/MGITC, the condition of the confocal is described as following: 633 nm laser, 600 optical gratin, and integrating 10 seconds. The results show that AuNPs has no significant Raman shift signal, and MGITC has weakly specific Raman shift. After modifying MGITC on AuNPS surface, there are four obvious MGITC Raman signals amplified 10 times by AuNPs (1,169, 1,365, 1,590 and 1,615 cm^{-1}). Thus, AuNPs/MGITC would use in further experiment.

.

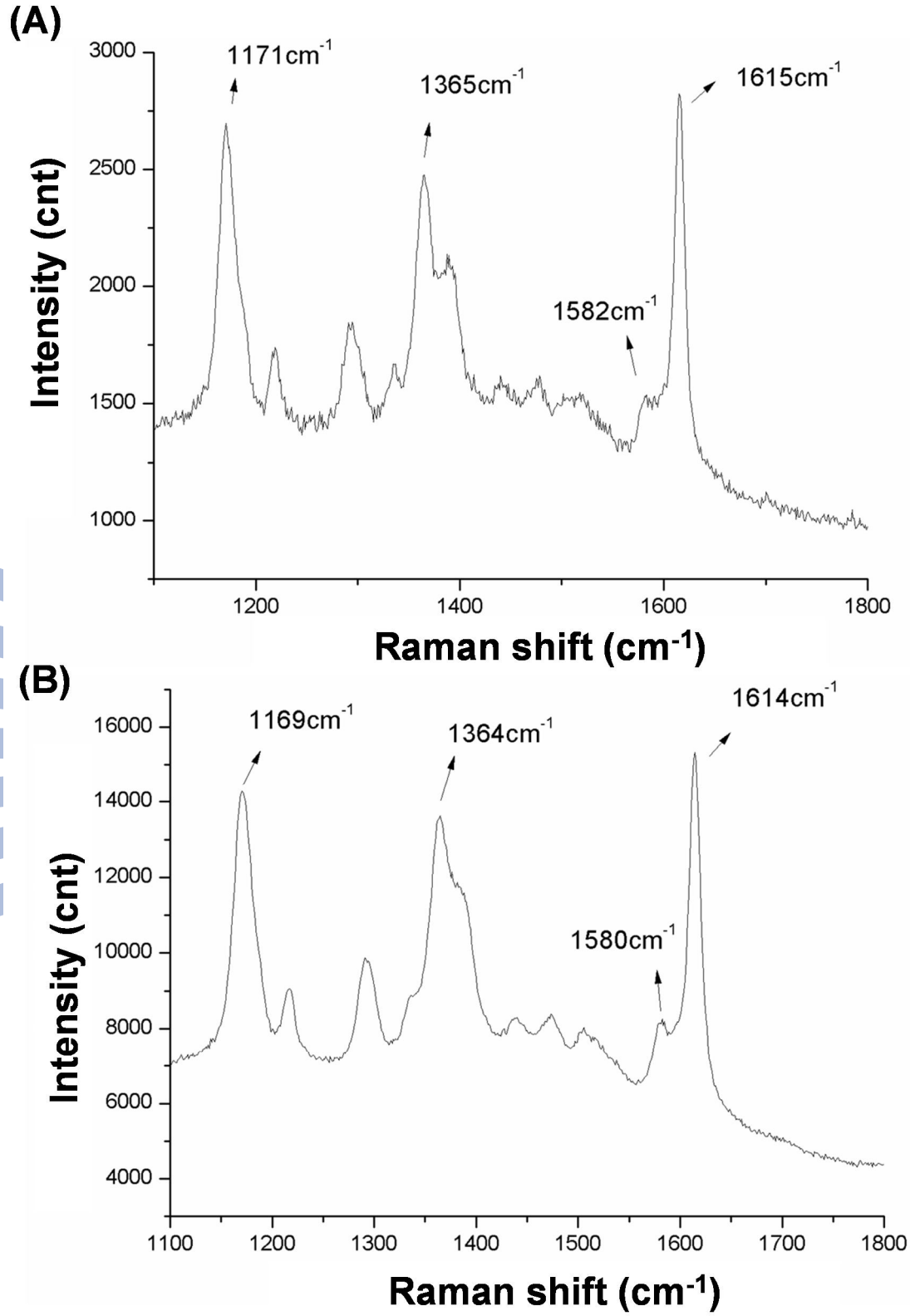

Figure 4-13. The surface enhance Raman shift of modified-AuNPs treated in HepG2 cells. The HepG2 cells were detected Raman shift intensity after treated with AuNPs/MGITC and AuNPs/MGITC-hGH for 24 hr. The Raman shift of MGITC in HepG2 cells was weaker when HepG2 cells only treated with AuNPs/MGITC (**A**) than both MGITC and hGH (**B**).

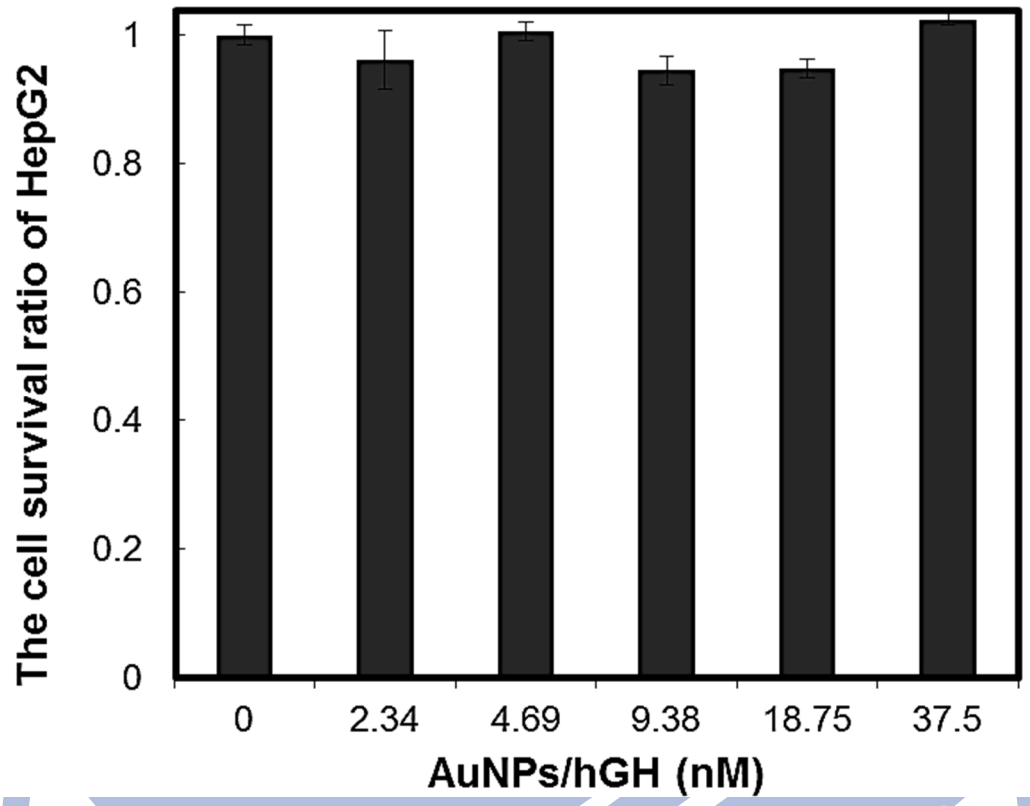

Figure 4-14. The cell viability of HepG2 cells after treated with AuNPs/hGH. The viability of HepG2 cells was detected by the MTT assay after treated with different concentrations of AuNPs/hGH for 24 hr. The HepG2 cells were detected the cell survival ratio after treated with AuNPs/hGH (from 0 to 37.5 nM). The cell survival ratio of HepG2 cells under different condition was similar, which meant there was no obvious effect of AuNPs/hGH to the growth of HepG2 cells. The S.D. (error bars) were calculated based on three independent detections (n = 3).

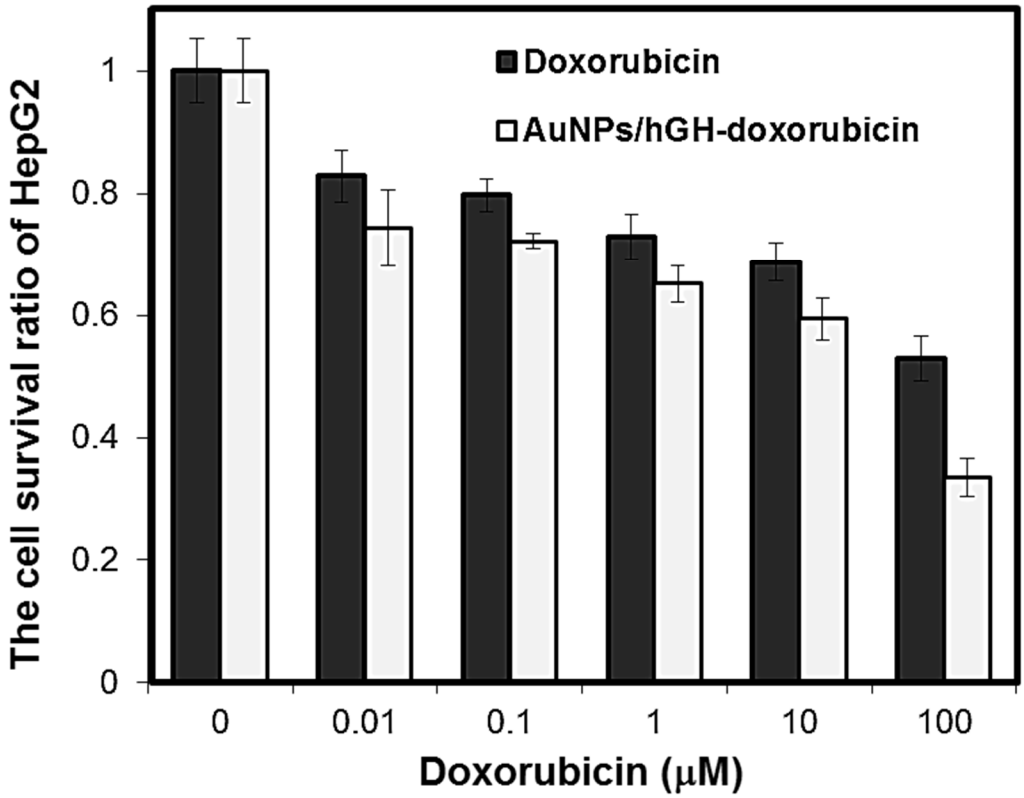

Figure 4-15. The cell viability of HepG2 cells after treated with doxorubicin and AuNPs/hGH-doxorubicin. The viability of HepG2 cells were detected by the MTT assay after treated with AuNPs/hGH-doxorubicin and free doxorubicin in various concentrations (from 0.01 to 100 μM) for 24 hr. According to the result, the cell survival ratio of HepG2 cells treated with AuNPs/hGH-doxorubicin was lower than doxorubicin treatment in concentration from 0.1 to 100 μM, which shows that AuNPs/hGH-doxorubicin has the better cytotoxicity than free doxorubicin. The S.D. (error bars) were calculated based on three independent detections (n = 3).

V. Discussion

5-1 Establishment of AuNPs-based optical biosensing system for peptidase activity detection

5-1-1 Synthesis of AuNPs and AuNPs/peptide

Because of the optical property of AuNPs (SPR), the synthesis and modification (size and shape) of AuNPs could be confirmed by spectrophotometer [Jena and Raj, 2008]. According to the result of absorption spectra of 20 nm AuNPs, after appropriate curve fitting and subtraction of the spectrum from the AuNPs absorption, the concentrations of AuNPs could be calculate from the absorbance by used the Beer–Lambert law:

$$\text{Absorbance} = \varepsilon bc$$

Here, ε is represented molar extinction coefficient, b is the path length of the sample, and c is molar concentration. The ε of 20 nm AuNPs at λ_{525} is 8.78×10^8/M cm [Liu *et al*., 2007]. By using the Beer–Lambert law, the concentration of modified-AuNPs were also calculated, and modified-AuNPs was adjusted to 5 nM for the further assay of peptidase activity.

Except using spectrophotometer, DLS and SEM were also used as tools to investigate the size and morphology of AuNPs, and the MALDI-TOF was used to provide the evidence that peptide were modified on AuNPs surface [Nimptsch *et al*., 2011]. As the data shown (**Figure 4-1** and **4-2**), after AuNPs modified with peptide, the mass profile showed the peak of peptide, and the diameter of the particles was increased, that indicated the increasing diameter of modified AuNPs was due to the peptide conjugated on AuNPs instead of the aggregation among AuNPs. In addition, the peptide was become a monolayer on AuNPs surface according to the data of DLS and SEM (**Figure 4-2** and **4-3**). Both results display the uniform morphology and almost unit average diameter. Nevertheless, the size of AuNPs samples measured by DLS would larger than that obtained from SEM study, that was mainly

because DLS measures the hydrodynamic radius, while SEM provided a more precise measurement of the hard AuNPs cores [Chen *et al*., 2009].

5-1-2 Assay of MMP-2 activity by AuNPs-based optical biosensing platform

For estimating the peptidase activity by AuNPs-based optical biosensing system, MMP-2 was choose as candidate, and the peptide modified on AuNPs was also designed as MMP-2 substrate. After MMP-2 adding in AuNPs/peptide solution, MMP-2 digested the peptide, AuNPs lost the shelter (peptide) [Seltzer *et al*., 1990], and the absorption value of 530 nm decreased, while 625 nm raised by the increasing reaction time. It was caused by the diminished suspending free AuNPs/peptide and raised aggregated AuNPs [Chuang *et al*., 2010]. Thus, through time-dependent spectra measuring (**Figure 4-4**), the value of 530 nm spectrum was stood for the quantity of AuNPs/peptide, the value of 625 nm spectrum was the degree of the aggregation among AuNPs, and the ratio of spectra ($A_{625\ nm}/A_{530\ nm}$) was represented as the ratio of aggregation versus free AuNPs/peptide. This absorption spectra ratio was then used to determine the activity of MMP-2.

The value of $A_{625\ nm}/A_{530\ nm}$ was increased due to not only the longer reaction time but also the raising concentration of MMP-2. As the absorption spectra shown (**Figure 4-5A**), when AuNPs/peptide treated with lower concentrations (100 to 400 ng/mL) of MMP-2, there was no obvious value increased at $A_{625\ nm}$ but apparent decreasing at $A_{530\ nm}$. This result represents that the some peptide around AuNPs was digested by MMP-2, but only decreasing less repulsion effect among AuNPs leaded no AuNPs aggregation [Adamczyk *et al*., 2011]. However, when AuNPs/peptide treated with 600 to 1,000 ng/mL MMP-2, not only $A_{530\ nm}$ decreased but also $A_{625\ nm}$ increased obviously. It indicated these concentrations of MMP-2 digested sufficient peptide, and AuNPs lost their shelter becoming aggregation [Segets *et al*., 2011]. Additionally, adding more than 1,000 ng/mL MMP-2 in AuNPs/peptide would lead fast and critical aggregation among AuNPs leading blue or black precipitation, and it let both

$A_{625\ nm}$ and $A_{530\ nm}$ decrease. Therefore, according to the inference above and the plot (**Figure 4-5B**), the detection range of AuNPs-based optical biosensing system were from 100 to 1,500 ng/mL of MMP-2, and the detection limit was 100 ng/mL MMP-2.

5-1-3 Assay of the efficiency of MMPs inhibitors and confirm the specificity by AuNPs-based optical biosensing platform

Excluding adding pure MMP-2 in AuNPs/peptide to demonstrate the ability of AuNPs-based optical biosensing system, the specificity and the inhibitor assaying should also be confirmed. For testing the AuNPs-based platform, EDTA, ONO-4817, and GM6001were chosen as candidates to block MMP-2 activity. After adding the inhibitors mixed with MMP-2 in AuNPs/peptide, the value of $A_{625\ nm}/A_{530\ nm}$ was no obvious different from AuNPs/peptide only (**Figure 4-6**). It meant that inhibitors blocked the activity of MMP-2 [Ro *et al*., 2007; Suzuki *et al*., 2007], and peptide maintained its original sequence leading no aggregation among AuNPs. This result also proves that the aggregation of AuNPs/peptide was due to MMP-2 digestion peptide and reducing the repulsion effect [Schneider *et al*., 2011], not because of changing buffer condition.

On the other hand, MMP-1, -2, and -7 were used to demonstrate the specificity of the AuNPs-based system. After MMP-1 and MMP-7 added in AuNPs/peptide, the value of $A_{625\ nm}/A_{530\ nm}$ was almost the same as AuNPs/peptide only (**Figure 4-7**). This indicated the peptide had high specificity of MMP-2 [Chuang *et al*., 2010], and the AuNPs/peptide would not aggregation without reacting with the target peptidase.

5-2 Establishment of AuNPs-based fluorescence biosensing system for peptidase activity detection

5-2-1 Assay of MMP-2 activity by AuNPs-based fluorescence biosensing platform

In spite of the AuNPs-based optical biosensing system is low cost and convenient, its detected range and limitation are still too high to analyze other kinds of MMPs activity (such as MMP-9) in normal human or patients [Ramos-Fernandez *et al.*, 2011]. It represents the AuNPs-based could be improved its measurement ability. Due to this concept, the peptide modified on AuNPs was exchanged with peptide-FITC, which would be quenched by AuNPs before peptidase digestion [Huang and Ren, 2011]. After peptidase digested peptide-FITC, released FITC was detected intensity by fluorescence spectrophotometer (**Figure 4-8**). Using AuNPs-based fluorescence method to analyze MMP-2 activity, the detected range and limitation were much lower than AuNPs-based optical method (comparing **Figure 4-8** with **Figure 4-5**) because of the higher sensitivity of fluorescence detection [Wang *et al*., 2010].

Additionally, AuNPs-based fluorescence system could also apply in inhibitors screening and has high specificity (**Figure 4-9** and **Figure 4-10**). The peptide-FITC would not release critically from AuNPs by adding inhibitors (dissolved in DMSO), but most of peptide-FITC was displacement after adding 100 μM DTT reagent (data not shown). This meant that the AuNPs/peptide-FITC was stable in ion or organic buffer without strong thiol groups solution [Lee *et al*., 2008]. However, AuNPs/peptide-FITC could be digested well by MMP-9, which is one kind of gelatinase and has most substrates same as MMP-2. After comparing the peptide sequence with MMP-9 cleavage site specificity on MEROPS (http://merops.sanger.ac.uk), the MMP-9 favorite cutting sequence was almost the same as the peptide designed for MMP-2 substrate, which explained the reason why MMP-9 could digest AuNPs/peptide-FITC (**Figure 4-10**).

5-2-2 Assay of cellular MMP-2 activity by AuNPs-base fluorescence system and zymography

AuNPs-based fluorescence system could not only analyze pure MMP-2 concentrations but also measure cellular MMP-2 activity. High MMP-2 expression cells (HCF and HCM) and low MMP-2 expression cells (H9c2 cells) were chosen as candidates for demonstrating in-cell biosensing platform. Through using zymography [Snoek-van Beurden and Von den Hoff, 2005] and AuNPs/peptide-FITC to detect MMP-2 activity of these cells (**Figure 4-11**), no matter the result of zymography, fluorescence method or confocal image had the similar trade. This indicated that AuNPs/peptide-FITC had the ability to analyze cellular MMP-2 activity and a possible potential to apply in *in vivo* MMP-2 activity tracing.

Moreover, comparing AuNPs-based optical and AuNPs-based fluorescence platforms with zymograpgy (**Table 5-1**), high surface-to-volume area of AuNPs provided more space that could not only enhance the immobilization density of peptide or peptide-FITC, but also raised the chance for MMP-2 to digest the substrate [Giljohann *et al*., 2009]. Additionally, because AuNPs-based fluorescence platform used peptide-FITC as substrate that could be detected in slight quantity, it had more sensitive analyzing ability than AuNPs-based optical system and zymography. The detection time for zymography of MMP-2 needs 24 hr at least [Kupai *et al*., 2010]; however, the AuNPs-based platforms can shorten detection time to 1 hr. On the other hand, when zymography was used to analyze the activity of MMP-2, the SDS would active MMP-2 and original activity of MMP-2 would change [Snoek-van Beurden and Von den Hoff, 2005], but the activity of MMP-2 would not be changed when AuNPs-based platforms were used [Song *et al.*, 2010]. Therefore, the AuNPs-based platforms not only are possible to perform the assay for MMPs activity, but also have potential for further applications in anti-MMPs drugs screening and apply for in-cell MMPs activity analysis.

5-3 Establishmet of AuNPs-based delivery system

5-3-1 The SERS profile of AuNPs-complexes

Because AuNPs has SPR property induced by laser excitationthat would increase the electric field around the AuNPs, and the Raman shift intensity is correlated with the strength of electric field, AuNPs could enhance the Raman signal of Raman reporter at most 10^{11} times [Jeanmaire and van Duyne, 1977]. According to the data (**Figure 4-12**), Raman signals of MGITC was amplified about 10^2 times by AuNPs, and the characteristic peaks of AuNPs/MGITC were 1,169, 1,365, 1,590 and 1,615 cm^{-1} These signals were assigned to phenyl-N stretching, ring breathing and stretching of the aromatic ring [Qian *et al.*, 2008; Biswas *et al*., 2010].

For applying Raman detection in cell, hGH was chosen as the target modified on AuNPs/MGITC to improve cell uptaking the particles. When hGH modified on AuNPs/MGITC (AuNPs/hGH-MGITC), the Raman profile and intensity of AuNPs/hGH-MGITC were as the same as AuNPs-MGITC (data not shown). This indicated that modifying hGH on AuNPs/MGITC would not influence its Raman property. After HepG2 cells incubated with AuNPs-complexes (**Figure 4-13**), HepG2 cells endocyted more AuNPs/hGH-MGITC than AuNPs/MGITC revealed on the Raman intensity. Because the high expression of hGH receptors on HepG2 cell membrane, HepG2 cells could easily up-take the colloids (AuNPs/hGH-MGITC) leading high intensity of AuNPs/hGH-MGITC [Wang and Thanou, 2010].

5-3-2 The cytotoxicity of AuNPs-complexes

For establishing AuNPs-based platform as drug delivery system in cell, the cytotoxicity of AuNPs/hGH needed to be tested. As the result shown (**Figure 4-14**), the viability ratio of HepG2 cells treated with different concentrations AuNPs/hGH were almost around 100%.

This result displays low cytotoxicity of AuNPs/hGH for HepG2 cells and means HepG2 could endure AuNPs in cell for at least 24 hr [Bhattacharya and Mukherjee, 2008]. Based on this result, the anticancer drug, doxorubicin, was modified on AuNPs/hGH, and using AuNPs/hGH-doxorubicin and free doxorubicin to treat HepG2 cells. As the result shown (**Figure 4-15**), the cell viability of HepG2 cells was lower when treated with AuNPs/hGH-doxorubicin than free doxorubicin treatment. This result has as the similar trade as **Figure 4-13** and proved that chemical compounds or biomolecules would not change their own characteristics after modified on AuNPs. Therefore, AuNPs have promising potential to apply in biomedical field.

Table 5-1. Comparisons of the AuNPs-based platform and zymography used to assay MMP-2 activity.

Method / Condition	Zymography*	AuNPs optical platform (AuNPs/peptide)	AuNPs fluorescence platform (AuNPs/peptide-FITC)
Detection time	>16 hr	60 min	30 min
Detection range	Limited to 10 pg	100 - 1,500 ng/mL	0.01 - 2 ng/mL
Signal detection	Densitometric analysis	UV-Vis spectrum	Fluorescence intensity
Decting process	Three-steps	One-step	One-step
Subtype identification	Yes	No	No

* Chuang *et al*., 2010; Kupai *et al*., 2010

VI. Conclusions

In this study, the AuNPs-based optical platform, the AuNPs/peptide was synthesized by combining 20 nm AuNPs and peptide. Moreover, the AuNPs/peptide was used to establish a simple and specific AuNPs-based optical biosensing platform for real-time and rapid assay of peptide activity and inhibitor screening. The key technology for this platform is using specific peptides as the bi-functions of peptidase substrate and AuNPs blocker. When AuNPs/peptide surface substrate digested by peptidase, AuNPs/peptide lost the steric stability and the interparticle distance shortened, followed by a rapid gathering phenomenon. The aggregation of AuNPs would change their optical property, i.e., plasmon resonance, and could be detected by UV-Vis spectroscopy to quantify accurately the concentration of peptidase. Using this low-cost platform of AuNPs, the detecting range of MMP-2 activity was from 100 to 1,500 ng/mL with linear correlation, and with a detection limit of 100 ng/mL. Furthermore, this AuNPs-based optical system could be also applied on inhibitor screening because the optical system possesses a high specificity.

On the other hand, the AuNPs-based fluorescence platform, the AuNPs/peptide-FITC was synthesized by combining 20 nm AuNPs and peptide-FITC. In addition, the AuNPs/peptide-FITC was used to establish a highly sensitive AuNPs-based fluorescence biosensing platform for real-time and rapid assay of peptidase activity, inhibitor screening, and cellular bio-image. The key technology for this platform is using peptide-FITC as the substrate of peptidase and using AuNPs as the quencher. When peptide-FITC modified on AuNPs, the fluorescence of FITC was quenched by AuNPs. However, after AuNPs/peptide-FITC digested by peptidase, AuNPs/peptide-FITC lost the steric stability and the interparticle distance shortened, followed by a rapid gathering phenomenon. Additionally, the peptide-FITC would release from AuNPs surface and the unquenched fluorescence intensity of FITC was detected by fluorescence spectrophotometer to quantify

the concentration of peptidase accurately. Using this fluorescence platform of AuNPs, the detecting range of MMP-2 activity was from 0.01 to 2 ng/mL with linear correlation, and with a detection limit of 0.01 ng/mL. Furthermore, this AuNPs-based fluorescence system could also apply on inhibitor screening with high specificity and utilize in cell level confocal image. Accordingly, the two simple AuNPs-based screening methods not only offer alternative platforms to assay of peptidase activity, also can be application in high-throughput screening of MMPs inhibitors and the activity assay of cellular peptidase.

Finally, in the AuNPs-based delivery system, the AuNPs-complexes were synthesized by combining AuNPs, hGH, MGITC, or doxorubicin. These AuNPs-complexes were used to demonstrate a targeting, tagging, and low cytotoxic AuNPs-based delivery platform for drug delivery and tracing. The key technology for this platform is using various biomolecule (hGH) or chemical compounds (MGITC and doxorubicin) to functionalize AuNPs. When hGH modified on AuNPs, the AuNPs/hGH could target the HepG2 cells and improve the cells endocyting the particles. In addition, after AuNPs conjugated with MGITC, AuNPs/MGITC was traced by Raman confocal through SERS method. Moreover, HepG2 cells had lower cell viability after incubated with AuNPs/hGH-doxorubicin than treated with free doxorubicin that revealed the drug delivering and targeting ability of AuNPs. Consequently, the AuNPs-based delivery system has promising potential to apply in *in vitro* or *in vivo* drug delivering.

VII. References

Abalde-Cela S, Aldeanueva-Potel P, Mateo-Mateo C, Rodríguez-Lorenzo L, Alvarez-Puebla RA, Liz-Marzán LM. 2010. Surface-enhanced Raman scattering biomedical applications of plasmonic colloidal particles. *Journal of the Royal Society Interface* 7:S435-S450.

Adamczyk Z, Nattich M, Wasilewska M, Zaucha M. 2011. Colloid particle and protein deposition: electrokinetic studies. *Advances in Colloid and Interface Science* doi:10.1016/j.cis.2011.04.002.

Allgeyer ES, Pongan A, Browne M, Mason MD. 2009. Optical signal comparison of single fluorescent molecules and Raman active gold nanostars. *Nano Letters* 9:3816-3819.

Amaro S, Obach V, Cervera A, Urra X, Gỏmez-Choco M, Planas AM, Chamorro A. 2009. Course of matrix metalloproteinase-9 isoforms after the administration of uric acid in patients with acute stroke: a proof-concept study. *Journal of Neurology* 256:651-656.

Anger P, Bharadwaj P, Novotny L. 2006. Enhancement and quenching of single-molecule fluorescence. *Physical Review Letter* 96:113002.

Asahi M, Asahi K, Jung JC, del Zoppo GJ, Fini ME, Lo EH. 2000. Role of matrix metalloproteinase 9 after focal cerebral ischemia: effects fo gene knockout and enzyme inhibition with BB-94. *Journal of Cerebral Blood Flow and Metabilism* 20:1681-1689.

Augé F, Hornebeck W, Laronze JY. 2004. A novel strategy for designing specific gelatinase A inhibitors: potential use to control tumor progression. *Critical Reviews in Oncology Hematology* 49:277-282.

Azzazy HME, Mansour MMH. 2009. *In vitro* diagnostic prospects of nanoparticles. *Clinica Chimica Acta* 403:1-8.

Bai S, Thummel R, Godwin AR, Nagase H, Itoh Y, Li L, Evans R, McDermott J, Seiki M, Sarras MP Jr. 2005. Matrix metalloproteinase expression and function during fin regeneration in zebrafish: Analysis of MT1-MMP, MMP2 and TIMP2. *Matrix Biology* 24:247-260.

Baptista P, Pereira E, Eaton P, Doria G, Miranda A, Gomes I, Quaresma P, Franco R. 2008. Gold nanoparticles for the development of clinical diagnosis methods. *Analytical and Bioanalytical Chemistry* 391:943-950.

Bhattacharya R, Mukherjee P. 2008. Biological properties of "naked" metal nanoparticles. *Advanced Drug Delivery Reviews* 60:1289-1306.

Birkedal-Hansen H, Moore WG, Bodden MK, Windsor LJ, Birkedal-Hansen B, DeCarlo A, Engler JA. 1993. Matrix metalloproteinases: a review. *Critical Reviews in Oral Biology and Medicine* 4:197-250.

Birkedal-Hansen H, Taylor RE. 1982. Detergent-activation of latent collagenase and resolution of its component molecules. *Biochemical and Biophysical Research Communications* 107:1173-1178.

Biswas A, Wang T, Biris AS. 2010. Single metal nanoparticle spectroscopy: optical characterization of individual nanosystems for biomedical applications. *Nanoscale*

2:1560-1572.

Boisselier E, Astruc D. 2009. Gold nanoparticles in nanomedicine: preparations, imaging, diagnostics therapies and toxicity. *Chemical Society Reviews* 38:1759-1782.

Bonanni A, del Valle M. 2010. Use of nanomaterials for impedimetric DNA sensors: a review. *Analytica Chimica Acta* 678:7-17.

Bourboulia D, Stetler-Stevenson WG. 2010. Matrix metalloproteinases (MMPs) and tissue inhibitors of metalloproteinases (TIMP): positive and negative regulators in tumor cell adhesion. *Seminars in Cancer Biology* 20:161-168.

Brew K, Dinakarpandian D, Nagase H. 2000. Tissue inhibitors of metalloproteinases: evolution, structure and function. *Biochimica et Biophysica Acta* 1477:267-283.

Brew K, Nagase H. 2010. The tissue inhibitors of metalloproteinases (TIMPs): an ancient family with structural and functional diversity. *Biochimica et Biophysica Acta* 1803:55-71.

Brozek EM, Zharov I. 2008. Surface modification and functionalization of colloidal nanoparitcles. http://archiv.ub.uni-marburg.de/diss/z2009/0061/pdf/dras.pdf

Brust M, Walker M, Bethell D, Schiffrin DJ, Whyman R. 1994. Synthesis of thiol-derivatised gold nanoparticles in a two-phase Liquid–Liquid system. *Journal of the Chemical Society, Chemical Communications* 801-802.

Cabdelario-Jalil E, Taheri S, Yang Y, Sood R, Grossetete M, Estrada EY, Fiebich BL, Rosenberg GA. 2007. Cyclooxygenase inhibition limits blood-brain barrier disruption following intracerebral injection of tumor necrosis factor-alpha in the rat. *Journal of Pharmacology and Experimental Therapeutics* 323:488-498.

Carmeli E, Moas M, Reznick AZ, Coleman R. 2004. Matrix metalloproteinases and skeletal muscle: a brief review. *Muscle and Nerve* 29:191-197.

Caruso RA, Ashokkumar M, Griese F. 2002. Sonochemical formation of gold sols. *Langmuir* 18:7831-7836.

Cao YC, Jin R, Thaxton CS, Mirkin CA. 2005. A two-color-change, nanoparticle-based method for DNA detection. *Talanta* 67:449-455.

Cauwe B, Opdenakker G. 2010. Intracellular substrate cleavage: a novel dimension in the biochemistry, biology and pathology of matrix metalloproteinases. *Critical Reviews in Biochemistry and Molecular Biology* 45:351-423.

Chandra P, Das D, Abdelwahab AA. 2010. Gold nanoparticles in molecular diagnostics and therapeutiecs. *Digest Journal of Nanomaterials and Biostructures* 5:363-367.

Chen LL, Lidstone EA, Finch KE, Heeres JT, Hergenrother PJ, Cunningham BT. 2009. A method for identifying small-molecule aggregators using photonic crystal biosensor microplates. *JALA: Journal of the Association for Laboratory Automation* 14:348-359.

Chen SH, Wu VC, Chuang YC, Lin CS. 2008. Using oligonucleotide-functionalized Au nanoparticles to rapidly detect foodborne pathogens on a piezoelectric biosensor. *Journal of Microbiological Methods* 73:7-17.

Chen SJ, Huang YF, Huang CC, Lee KH, Lin ZH, Chang HT. 2008. Colorimetric determination of urinary adenosine using aptamer-modified gold nanoparticles.

Biosensors and Bioelectronics 23:1749-1753.

Chen YM, Yu CJ, Cheng TL, Tseng WL. 2008. Colorimetric detection of lysozyme based on electrostatic interaction with human serum albumin-modified gold nanoparticles. *Langmuir* 24:3654-3660.

Chen YT, Hsu CL, Hou SY. 2008. Detection of single-nucleotide polymorphisms using gold nanoparticles and single-strand-specific nucleases. *Analytical Biochemistry* 375:299-305.

Cheng AK, Sen D, Yu HZ. 2009. Design and testing of aptamer-based electrochemical biosensors for proteins and small molecules. *Bioelectrochemistry* 77:1-12.

Chirea M, Cruz A, Pereira CM, Silva AF. 2009. Size-dependent electrochemical properties of gold nanorods. *Journal of Physical Chemistry C* 113:13077-13087.

Chithrani BD, Ghazani AA, Chan WC. 2006. Determining the size and shape dependence of gold nanoparticle uptake into mammalian cells. *Nano Letters* 6:662-668.

Chithrani BD, Chan WC. 2007. Elucidating the mechanism of cellular uptake and removal of protein-coated gold nanoparticles of different sizes and shapes. *Nano Letters* 7:1542-1550.

Chithrani DB. 2010. Nanoparticles for improved therapeutics and imaging in cancer therapy. *Recent Patents on Nanotechnology* 4:171-180.

Cho YK, Kim S, Kim YA, Lim HK, Lee K, Yoon D, Lim G, Pak YE, Ha TH, Kim K. 2004. Characterization of DNA immobilization and subsequent hybridization using in situ quartz crystal microbalance, fluorescence spectroscopy, and surface plasmon resonance. *Journal of Colloid and Interface Science.* 278:44-52.

Chuang YC, Li JC, Chen SH, Liu TY, Kuo CH, Huang WT. 2010. An optical biosensing platform for proteinase activity using gold nanoparticels. *Biomaterial* 31:6087-6095.

Clark LCJr, Lyons C. 1962. Electrode systems for continuous monitoring in cardiovascular surgery. *Annals of the New York Academy of Sciences* 102:29-45.

Cobley CM, Chen J, Cho EC, Wang LV, Xia Y. 2011. Gold nanostructures: a class of multifunctional materials for biomedical applications. *Chemical Society Reviews* 40:44-56.

Coker ML, Doscher MA, Thomas CV, Galis ZS, Spinale FG. 1999. Matrix metalloproteinase synthesis and expression in isolated LV myocyte preparations. *The American Journal of Physiology* 277:H777-H787.

Craig VSJ , Ninham BW, Pashley RM. 1998. Comment on "Deformation of fluid interfaces under double-layer forces stabilizes bubble dispersions". *Physical Review E* 57:7362-7363.

Daniel MC, Astruc D. 2004. Gold nanoparticles: assembly, supramolecular chemistry, quantum-size-related properties, and applications toward biology, catalysis and nanotechnology. *Chemical Review* 104:293-346.

de Dios AS, Díaz-García ME. 2010. Multifunctional nanoparticles: analytical prospects. *Analytica Chimica Acta* 666:1-22.

de la Fuente JM, Berry CC. 2005. Tat peptide as an efficient molecule to translocate gold nanoparticles into the cell nucleus. *Bioconjugate Chemistry* 16:1176-1180.

De M, Ghosh PS, Rotello VM. 2008. Applications of nanoparticles in biology. *Advanced Materials* 20:4225-4241.

De Mey J, Lambert AM, Bajer AS, Moeremans M, De Brabander M. 1982. Visualization of microtubules in interphase and mitotic plant cells of aemanthus endosperm with the immuno-gold staining method. *Proceedings of the National Academy of Sciences of the United States of Americ*a 79:1898-1902.

Devel L, Czarny B, Beau F, Georgiadis D, Stura E, Dive V. 2010. Third generation of matrix metalloprotease inhibitors: gain in selectivity by targeting the depth of the S_1' cavity. *Biochimie* 92:1501-1508.

Díaz-González M, González-García MB, Costa-García A. 2006. Detection of pneumolysin in human urine using an immunosensor on screen-printed carbon electrodes. *Sensors and Actuators B: Chemical* 113:1005-1011.

Dulkeith E, Morteani AC, Niedereichholz T, Klar TA, Feldmann J, Levi SA, van Veggel FC, Reinhoudt DN, Möller M, Gittins DI. 2002. Fluorescence quenching of dye molecules near gold nanoparticles: radiative and nonradiative effects. *Physical Review Letters* 89:203002.

Eck W, Nicholson AI, Zentgraf H, Semmler W, Bartling S. 2010. Specific contrast enhancement of peripheral lymph nodes in X-ray computed tomography of live mice. *Nano Letter* 10:2318-2322.

Faulk WP, Taylor GM. 1971. Communication to the editors: An immunocolloid method for the electron microscope. *Immunochemistry* 8:1081-1083.

Fedarko NS, Jain A, Karadag A, Fisher LW. 2004. Three small integrin binding ligand N-linked glycoproteins (SIBLINGs) bind and activate specific matrix metalloproteinases. *The FASEB Journal* 18:734-736.

Fournier-wirth C, Jaffrezic-Fenault N, Coste J. 2010. Detection of blood-transmissible agents: can screening be miniaturized. *Transfusion* 50:2032-2045.

Frens G. 1973. Controlled nucleation for the regulation of the particle size in monodisperse gold suspensions. *Nature Physics* 241:20-22.

Galardy RE, Grobelny D, Foellmer HG, Fernandez LA. 1994. Inhibition of angiogenesis by the matrix metalloprotease inhibitor N-[2R-2-(hydroxamidocarbonymethyl)-4-methylpentanoyl)]-L-tryptophan methylamide. *Cancer Research* 54:4715-4718.

Galazka G, Windsor LJ, Birkedal-Hansen H, Engler JA. 1996. APMA (4-aminophenylmercuric acetate) activation of stromelysin-1 involves protein interactions in addition to those with cysteine-75 in the propeptide. *Biochemistry* 35:11221-11227.

Gersten JI. 2005. Theory of fluorophore-metallic surface interactions. *Plenum Press: New York* 8.

Ghosh P, Han G, De M, Kim CK, Rotello VM. 2008. Gold nanoparticles in delivery applications. *Advanced Drug Delivery Reviews* 60:1307-1315.

Ghosh SK, Pal T. 2007. Interparticle coupling effect on the surface plasmon resonance of gold nanoparticles: From theory to applications. *Chemical Reviews* 107:4797-4862.

Giljohann DA, Seferos DS, Daniel WL, Massich MD, Patel PC, Mirkin CA. 2010. Gold nanoparticles for biology and medicine. *Angewandte Chemie International Edition* 49:3280-3294.

Glazer ES, Curley SA. 2010. Radiofrequency field-induced thermal cytotoxicity in cancer cells treated with fluorescent nanoparticles. *Cancer* 116:3285-3293.

Glomm WR. 2005. Functionalized gold nanoparticles for applications in bionanotechnology. *Journal of Dispersion Science and Technology* 26:389-414.

Goia DV, Matijevic E. 1998. Preparation of monodispersed metal particles. *New Journal of Chemistry* 22:1203-1215.

Goia DV, Matijevic E. 1999. Tailoring the particle size of monodispersed colloidal gold. *Colloids and Surfaces A, Physicochemical and Engineering Aspects* 146:139-152.

Grabar KC, Freeman RG, Hommer MB, Natan MJ. 1995. Preparation and Characterization of Au Colloid Monolayers. *Analytical Chemistry* 67:735-743.

Grabar KC, Brown KR, Keating CD, Stranick SJ, Tang SL, Natan MJ. 1997. Nanoscale characterization of gold colloid monolayers: a comparison of four techniques. *Analytical Chemistry* 69:471-477.

Gu Z, Cui J, Brown S, Fridman R, Mobashery S, Stongin AY, Lipton SA. 2005. A highly specific inhibitors of matrix metalloproteinsase-9 rescues lamini from proteolysis and neurons from apoptosis in transient focal cerebral ischemia. *Journal of Neuroscience* 25:6401-6408.

Guo S, Wang E. 2007. Synthesis and electrochemical applications of gold nanoparticles. *Analytica Chimica Acta* 598:181-192.

Hainfeld JF, Slatkin DN, Smilowitz HM. 2004. The use of gold nanoparticles to enhance radiotherapy in mice. *Physics in Medicine and Biology* 49:N309-N315.

Honeychurch KC, Gilbert L, Hart JP. 2010. Electrocatalytic behaviour of citric acid at a cobalt phthalocyanine-modified screen-printed carbon electrode and its application in pharmaceutical and food analysis. *Analytical and Bioanalytical Chemistry* 396: 3103-3111.

Horstmann S, Kalb P, Koziol J, Gardner H, Wagner S. 2003. Profiles of matrix metalloproteinases, their inhibitors, and laminin in stroke patients: influence of different therapies. *Stroke* 34:2165-2170.

Hu X, Beeton C. 2010. Detection of functional matrix metalloproteinsases by zymography. *Journal of Visurlized Experiments* doi: 10.3791/2455.

Huang CC, Huang YF, Cao Z, Tan W, Chang HT. 2005. Aptamer-modified gold nanoparticles for colorimetric determination of platelet-derived growth factors and their receptors. *Analytical Chemistry* 77:5735-5741.

Huang CC, Chiu SH, Huang YF, Chang HT. 2007. Aptamer-functionalized gold nanoparticles for turn-on light switch detection of platelet-derived growth factor. *Analytical Chemistry* 79:4798-4804.

Huang X, Ren J. 2011. Gold nanoparticles based chemiluminescent resonance energy transfer

for immunoassay of alpha fetoprotein cancer marker. *Analytica Chimica Acta* 686:115-120.

Hutter E, Fendler JH. 2002. Exploitation of localized surface plasmon resonance. *Advanced Materials* 16:1685-1706.

Hwang G, Lee CH, Ahn IS, Mhin GJ. 2010. Analysis of the adhesion of *Pseudomonas putida* NCIB 9816-4 to a silica gel as a model soil using extended DLVO theory. *Journal of Hazardous Materials* 179:983-988

Hyafil F, Vucic E, Cornily JC, Sharma R, Amirbekian V, Blackwell F, Lancelot E, Corot C, Fuster V, Galis ZS, Feldman LJ, Fayad ZA. 2011. Monitoring of arterial wall remodeling in atherosclerotic rabbits with a magnetic resonance imaging contrast agent binding to matrix metalloproteinases. *European Heart Journal* 32:1561-1571.

Iosin M, Baldeck P, Astilean S. 2009. Plasmon-enhanced fluorescence of dye molecules. *Nuclear Instruments and Methods in Physics Research Section B* 267:403-405.

Jacobsen JA, Jourden JLM, Miller MT, Cohen SM. 2010. To bind zinc or not to bind zinc: an examination of innovative approaches to improved metalloproteinase inhibition. *Biochimica et Biophysica Acta* 1803:72-94.

Jain PK, El-Sayed IH, El-Sayed MA. 2007. Au nanoparticles target cancer. *Nano Today* 2:18-29.

Jeanmaire DL, van Duyne RP. 1977. Surface Raman electrochemistry: part I. Heterocyclic, aromatic and aliphatic amines adsorbed on the anodized silver electrode. *Journal of Electroanalytical Chemistry and Interfacial Electrochemistry* 84:1-20.

Jena BK, Raj CR. 2008. Optical sensing of biomedically important polyionic drugs using nano-sized gold particles. *Biosensors and Bioelectronics* 23:1285-1290.

Jiang T, Liu R, Huang X, Feng H, Teo W, Xing B. 2009. Colorimetric screening of bacterial enzyme activity and inhibition based on the aggregation of gold nanoparticles. *Chemical Communications* 21:1972-1974.

Johnston HJ, Hutchison G, Christensen FM, Peters S, Hankin S, Stone V. 2010. A review of the in *vivo* and *in vitro* toxicity of silver and gold nanoparticles: particle attributes and biological mechanisms responsible for the observed toxicity. *Critical Review in Toxicology* 40:328-346.

Jones CB, Sane DC, Herrington DM. 2003. Matrix metalloproteinases: a review of their structure and role in acute coronary syndrome. *Cardiovascular Research* 59:812-823.

Kandasamy AD, Chow AK, Ali MAM, Schulz R. 2010. Matrix metalloproteinase-2 and myocardial oxidative stress injury: beyond the matrix. *Cardiovascular Research* 85:413-423.

Kang KA, Wang J, Jasinski JB, Achilefu S. 2011. Fluorescence manipulation by gold nanoparticles: from complete quenching to extensive enhancement. *Journal of Nanobiotechnology* doi: 10.1186/1477-3155-9-16.

Kennedy LC, Bear AS, Young JK, Lewinski NA, Kim J, Foster AE, Drezek RA. 2011. T cells enhance gold nanoparticle delivery to tumors *in vivo*. *Nanoscale Research Letters* 6:283-294.

Kessenbrock K, Plaks V, Werb Z. 2010. Matrix metalloproteinases: regulators of the tumor microenvironment. *Cell* 141:52-67.

Kim B, Han G, Toley B, Kim CK, Rotello VM, Forbes NS. 2010. Tuning payload delivery in tumour cylindroids using gold nanoparticles. *Nature Nanotechnology* 5:465-472.

Kim Y, Johnson RC, Hupp JT. 2001. Gold nanoparticle-based sensing of "spectroscopically silent" heavy metal ions. *Nano Letters* 1:165-167.

Knecht MR, Sethi M. 2009. Bio-inspired colorimetric detection of Hg^{2+} and Pb^{2+} heavy metal ions using Au nanoparticles. *Analyticl and Bioanalytical Chemistry* 394:33-46.

Kneipp J, Kneipp H, Kneipp K. 2008. SERS-a single-molecule and nanoscale tool for bioanalytics. *Chemical Society Reviews* 37:1052-1060.

Kumar CSSR, Aghasyan M, Modrow H, Doomes E, Henk C, Hormes J. 2004. Synthesis and characterization of S-Au interaction in gold nanoparticle bound polymeric beads. *Journal of Nanoparticle Research* 6:369-376.

Kumar S, Gandhi KS, Kumar R. 2007. Modeling of formation of gold nanoparticles by citrate method. *Industrial and Engineering Chemistry Research* 46:3128-3136.

Kupai K, Szucs G, Cseh S, Hajdu I, Csonka C, Csont T, Ferdinandy P. 2010. Matrix metalloproteinase activity assays: importance of zymography. *Journal of Pharmacological and Toxicological Methods* 61:205-209.

Kurzepa J, Szczepanska-Szerej A, Stryjecka-Zimmer M, Malecka-Massalska T, Stelmasiak Z. 2006. Simvastatin could prevent increase of the serum MMP-9/TIMP-1 ratio in acute ischaemic stroke. *Folia Biologica* 52:181-183.

Kwon SJ, Yang H, Jo K, Kwak J. 2008. An electrochemical immunosensor using *p*-aminophenol redox cycling by NADH on a self-assembled monolayer and ferrocene-modified Au electrodes. *The Analyst* 133:1599-1604.

Leber TM, Balkwill FR. 1997. Zymography: A single-step staining method for quantitation of proteolytic activity on substrate gels. *Analtical Biochemistry* 249:24-28.

Ladd J, Boozer C, Yu Q, Chen S, Homola J, Jiang S. 2004. DNA-directed protein immobilization on mixed self-assembled monolayers via a streptavidin bridge. *Langmuir* 20:8090-8095.

Lakowicz JR. 1999. Principle of fluorescence spectroscopy. *Plenum Publishing Corporation*

Lee K, Lee H, Bae KH, Park TG. 2010. Heparin immobilized gold nanoparticles for targeted detection and apoptotic death of metastatic cancer cells. *Biomaterials* 31:6530-6536.

Lee PW, Peng SF, Su CJ, Mi FL, Chen HL, Wei MC, Lin HJ, Sung HW. 2008. The use of biodegradable polymeric nanoparticles in combination with a low-pressure gene gun for transdermal DNA delivery. *Biomaterials* 29:742-751.

Lee S, Cha EJ, Park K, Lee SY, Hong JK, Sun IC, Kim SY, Choi K, Kwon IC, Kim K, Ahn CH. 2008. A Near-infrared-fluorescence-quenched gold nanoparticle imaging probe for *in vivo* drug screening and protease activity determination. *Angewandte Chemie Internaiotnal Edition* 47:2804-2807.

Lee SR, Kim HY, Rogowska J, Zhao BQ, Bhide P, Parent JM, Lo EH. 2006. Involvement of matrix metalloproteinase in neuroblast cell migration from the subventricular zone after stroke. *Journal of Neuroscience* 26:3491-3495.

Li CM, Sun CQ, Song S, Choong VE, Maracas G, Zhang XJ. 2005. Impedance labelless detection-based polypyrrole DNA biosensor. *Frontiers in Bioscience* 10:180-186.

Li J, Chu X, Liu Y, Jiang JH, He Z, Zhang Z, Shen G, Yu RQ. 2005. A colorimetric method for point mutation detection using high-fidelity DNA ligase. *Nucleic Acids Research* 33:e168.

Li JC. 2008. Establishing a gold nanoparticles-based optical biosensing platform for the assay of proteinase activity.

Libson AM, Gittis AG, Collier IE, Marmer BL, Goldberg GI, Lattman EE. 1995. Crystal structure of the haemopexin-like C-terminal domain of gelatinase A. *Nature Structural Biology* 2:938-942.

Lin XM, Wang X, Liu Z, Ren B. 2008. Enhanced Raman Scattering by polystyrene microspheres and application for detecting molecules adsorbed on Au single crystal surface. *Acta Physico-Chimica Sinica* 24:1941-1944.

Lin YW, Huang CC, Chang HT. 2011. Gold nanoparticle probes for the detection of mercury, lead and copper ions. *Analyst* 136:863-871.

Link S, El-Sayed MA. 1999. Size and temperature dependence of the plasmon absorption of colloidal gold nanoparticles. *The Journal of Physical Chemistry B* 103:4212-4217.

Liotta LA, Abe S, Robey PG, Martin GR. 1979. Preferential digestion of basement membrane collagen by an enzyme derived from a metastatic murine tumor. *Proceedings of the National Academy of Sciences of the United States of America* 76:2268-2272.

Liu J, Lu Y. 2007. Colorimetric Cu^{2+} detection with a ligation DNAzyme and nanoparticles. *Chemical Communications (Cambridge, England)* 14:4872-4874.

Liu W, Hendren J, Qin XJ, Shen J, Liu KJ. 2009. Normobaric hyperoxia attenuates early blood-brain barrier disruption by inhibiting MMP-9-mediated occluding degradation in focal cerebral ischemia. *Journal of Neurochemistry* 108:811-820.

Liu X, Atwater M, Wang J, Huo Q. 2007. Extinction coefficient of gold nanoparticles with different sizes and different capping ligands. *Colloids and Surfaces B: Biointerfaces* 58:3-7.

Lombard C, Saulnier J, Wallach J. 2005. Assays of matrix metalloproteinases (MMPs) activities: a review. *Biochimie* 87:265-272.

Lu W, Lin L, Jiang L. 2007. Nanogold hollow balls with dendritic surface for hybridization of DNA. *Biosensors and Bioelectronics* 22:1101-1105.

Macartney HW, Tschesche H. 1983. Latent and active human polymorphonuclear leukocyte collagenases. Isolation, purification and characterisation. *European Journal of Biochemistry / FEBS* 130:71-78.

Mallya SK, Van Wart HE. 1989. Mechanism of inhibition of human neutrophil collagenase by gold(I) chrysotherapeutic compounds. Interaction at a heavy metal binding site. *The Journal of Biological Chemistry* 264:1594-1601.

Maxwell DJ, Taylor JR, Nie S. 2002. Self-assembled nanoparticle probes for recognition and detection of biomolecules. *Journal of the American Chemical Society* 124:9606-9612.

Mayilo S, Kloster MA, Wunderlich M, Lutich A, Klar TA, Nichtl A, Kürzinger K, Stefani FD, Feldmann J. 2009. Long-range fluorescence quenching by gold nanoparticles in a sandwich immunoassay for cardiac troponin T. *Nano letters* 9:4558-4563.

Mirkin CA, Letsinger RL, Mucic RC, Storhoff JJ. 1996. A DNA-based method for rationally assembling nanoparticles into macroscopic materials. *Nature* 382:607-609.

Miyazaki K, Hattori Y, Umenishi F, Yasumitsu H, Umeda M. 1990. Purification and characterization of extracellular matrix-degrading metalloproteinase, Matrin, secreted from rectal carcinoma cell line. *Cancer Research* 50:7758-7764.

Morgunova E, Tuuttila A, Bergmann U, Isupov M, Lindqvist Y, Schneider G, Tryggvason K. 1999. Structure of human pro-matrix metalloproteinase-2: activation mechanism revealed. *Science* 284:1667-1670.

Murphy G, Bretz U, Baggiolini M, Reynolds JJ. 1980. The latent collagenase and gelatinase of human polymorphonuclear neutrophil leucocytes. *Biochemical Journal* 192:517-525.

Nagase H, Woessner JF Jr. 1999. Matrix metalloproteinases. *The Journal of Biological Chemistry* 274:21491-21494.

Nagel S, Genius J, Heiland S, Horstmann S, Gardner H, Wagner S. 2007. Diphenyleneiodonium and dimethylsufoxide for treatment of reperfusion injury in cerebral ischemia of the rat. *Brain Research* 1132:210-217.

Narayanan KB, Sakthivel N. 2010. Biological synthesis of metal nanoparticles by microbes. *Advances in Colloid and Interface Science* 156:1-13.

Nath N, Chilkoti A. 2004. Label free colorimetric biosensing using nanoparticles. *Journal of Fluorescence* 14:377-389.

Netzel-Arnett S, Mallya SK, Nagase H, Birkedal-Hansen H, Van Wart HE. 1991. Continuously recording fluorescent assays optimized for five human matrix metalloproteinases. *Analytical Biochemistry* 195:86-92.

Nguyen DT, Kim DJ, Myoung GS, Kim KS. 2010. Experimental measurements of gold nanoparticle nucleation and growth by citrate reduction of $HAuCl_4$. *Advanced Powder Technology* 21:111-118.

Nguyen DT, Kim DJ, Kim KS. 2011. Controlled synthesis and biomolecular probe application of gold nanoparticles. *Micron* 42:207-227.

Nimptsch A, Schibur S, Ihling D, Sinz A, Riemer T, Huster D, Schiller J. 2011. Quantitative analysis of denatured collagen by collagenase digestion and subsequent MALDI-TOF mass spectrometry. *Cell Tissue Research* doi: 10.1007/s00441-010-1113-2.

Norouzi P, Larijani B, Faridbod F, Ganjali MR. 2010. Hydrogen peroxide biosensor based on hemoglobin immobilization on gold nanoparticle in FFT continuous cyclic valtammetry flow injection system. *International Journal of Electrochemical Science* 5:1550-1562.

Oh E, Hong MY, Lee D, Nam SH, Yoon HC, Kim HS. 2005. Inhibition assay of biomolecules based on fluorescence resonance energy transfer (FRET) between quantum dots and gold nanoparticles. *Journal of the American Chemical Society* 127:3270-3271.

Oh E, Lee D, Kim YP- Cha SY, Oh DB, Kang HA, Kim J, Kim HS. 2006. Nanoparticle-based

energy transfer for rapid and simple detection of protein glycosylation. *Angewandte Chemie* 45:7959-7963.

Okada Y, Morodomi T, Enghild JJ, Suzuki K, Yasui A, Nakanishi I, Salvesen G, Nagase H. 1990. Matrix metalloproteinase 2 from human rheumatoid synovial fibroblasts. Purification and activation of the precursor and enzymic properties. *European Journal of Biochemistry / FEBS* 194:721-730.

Okammoto K, Takai S, Sasaki S, Miyazaki M. 2002. Trandolapril reduces infarction area after middle cerebral artery occlusion in rats. *Hypertension Research* 25:583-588.

Okitsu K, Yue A, Tanabe S, Matsumoto H, Yobiko Y. 2001. Formation of colloidal gold nanoparticles in an ultrasonic field: Control of rate of gold(III) reduction and size of formed gold particles. *Langmuir* 17:7717-7720.

Ozdemir C, Yeni F, Odaci D, Timur S. 2010. Electrochemical glucose biosensing by pyranose oxidase immobilized in gold nanoparticle-polyaniline/AgCl/gelatin nanocomposite matrix. *Food Chemistry* 119:380-385.

Park SJ, Taton TA, Mirkin CA. 2002. Array-based electrical detection of DNA with nanoparticle probes. *Science* 295:1503-1506.

Pashley RM, Karaman ME. 2005. Van der Waals forces and colloid stability. *Applied colloid and Surface Chemistry* 127-151.

Pasternak B, Aspenberg P. 2009. Metalloproteinases and their inhibitors: diagnostic and therapeutic opportunities in orthopedics. *Acta Orthopaedica* 80:693-703.

Patra CR, Bhattacharya R, Mukhopadhyay D, Mukherjee P. 2010. Fabrication of gold nanoparticles for targeted therapy in pancreatic cancer. *Advanced drug delivery reviews* 62: 346-361.

Persoons A, Verbiest T. 2006. An experimental study on the preparation of gold nanoparticles and their properties. *Katholieke universiteit Leuven.* https://repository.libis.kuleuven.be/dspace/bitstream/1979/254/2/thesis_finaal.pdf

Pellegrino T, Kudera S, Liedl T, Muñoz Javier A, Manna L, Parak WJ. 2005. On the development of colloidal nanoparticles towards multifunctional structures and their possible use for biological applications. *Small* 1:48-63.

Pissuwan D, Cortie CH, Valenzuela SM, Cortie MB. 2010. Funcitonalised gold nanoparticles for controlling pathogenic bacteria. *Trends in Biotechnology* 28:207-213.

Pividori MI, Lermo A, Bonanni A, Alegret S, del Valle M. 2008. Electrochemical immunosensor for the diagnosis of celiac disease. *Analytical Biochemistry* 388:229-234.

Privett BJ, Shin JH, Schoenfisch MH. 2008. Electrochemical sensors. *Analytical Chemistry* 80: 4499-4517

Qian X, Peng XH, Ansari DO, Yin-Goen Q, Chen GZ, Shin DM, Yang L, Young AN, Wang MD, Nie S. 2008. *In vivo* tumor targeting and spectroscopic detection with surface-enhanced Raman nanoparticle tags. *Nature Biotechnology* 26:83-90.

Ramos-Fernandez M, Bellolio MF, Stead LG. 2011. Matrix Metalloproteinase-9 as a marker for acute ischemic stroke: a systematic review. *Journal of Stroke and Cerebrovascular*

Diseases 20:47-54.

Rao CNR, Cheethama A. 2001. Science and technology of nanomaterials: current status and future prospects. *Journal of Materials Chemistry* 11:2887-2894.

Ray PC, Fortner A, Darbha GK. 2006. Gold nanoparticle based FRET assay for the detection of DNA cleavage. *The Journal of Physical Chemistry. B* 110:20745-20748.

Ray PC. 2010. Size and shape dependent second order nonlinear optical properties of nanomaterials and their application in biological and chemical sensing. *Chemical Reviews* 110: 5332-5365.

Rembaum A, Dreyer WJ. 1980. Immunomicrospheres: reagents for cell labeling and separation. *Science* 208:364-368.

Rodriguez JA, Dvorak J, Jirsak T, Liu G, Hrbek J, Aray Y, Gonzalez C. 2003. Coverage effects and the nature of the metal-sulfur bond in S/Au(111): High-resolution photoemission and density-functional studies. *Journal of the American Chemical Society* 125:276-285.

Roeb E, Matern S. 2001. Matrix metalloproteinases: Promoters of tumor invasion and metastasis - A review with focus on gastrointestinal tumors. *Zeitschrift für Gastroenterologie* 39:807-813.

Rojo J, Díaz V, de la Fuente JM, Segura I, Barrientos AG, Riese HH, Bernad A, Penadés S. 2004. Gold glyconanoparticles as new tools in antiadhesive therapy. *Chembiochem* 5:291-297.

Romanic AM, White RF, Arleth AJ, Ohlstein EH, Barone FC. 1998. Matrix metalloproteinase expression increases after cerebral focal ischemia in rats: inhibition of matrix metalloproteinase-9 reduces infarct size. *Stroke* 29:1020-1030.

Rosi NL, Mirkin CA. 2005. Nanostructures in biodiagnostics. *Chemical Reviews* 105:1547-1562.

Roy R, Yang J, Moses MA. 2009. Matrix metalloproteinases as novel biomarkers and potential therapeutic targets in human cancer. *Journal of Clinical Oncology* 27:5287-5297.

Ryu JH, Lee A, Na JH, Lee S, Ahn HJ, Park JW, Ahn CH, Kim BS, Kwon IC, Choi K, Youn I, Kim K. 2010. Optimization of matrix metalloproteinase fluorogenic probes for osteoarthritis imaging. *Amino Acids* doi:10.1007/soo726-010-0769-y.

Sadik OA, Aluoch AO, Zhou A. 2009. Status of biomolecular recognition using electrochemical techniques. *Biosensors and Bioelectronics* 24:2749-2765.

Salem AK, Searson PC, Leong KW. 2003. Multifunctional nanorods for gene delivery. *Nature Materials* 2:668-671.

Sapsford KE, Berti L, Medintz IL. 2006. Materials for fluorescence resonance energy transfer analysis: Beyond traditional donor-acceptor combinations. *Angewandte Chemie* 45:4562-4589.

Saraiva SM, de Oliveira JF. 2002. Control of particle size in the preparation of colloidal gold. *Journal of Dispersion Science and Technology* 23:837-844.

Sardar R, Funston AM, Mulvaney P, Murray RW. 2009. Gold nanoparticles: past, presesnt,

adn future. *Langmuir* 25:1340-13851.

Sato K, Hosokawa K, Maeda M. 2003. Rapid aggregation of gold nanoparticles induced by non-cross-linking DNA hybridization. *Journal of the American Chemical Society* 125:8102-8103

Schmid G. 1992. Large clusters and colloids-metals in the embryonic state. *Chemical Review* 92:1709-1727.

Schneider C, Hanisch M, Wedel B, Jusufi A, Ballauff M. 2011. Experimental study of electrostatically stablilized colloidal particles: colloidal stability and charge reversal. *Journal of Colloid and Interface Science* 358:62-67.

Schultz DA. 2003. Plasmon resonant particles for biological detection. *Current Opinion in Biotechnology* 14:13-22

Segets D, Marczak R, Schäfer S, Paula C, Gnichwitz JF, Hirsch A, Peukert W. 2011. Experimental and theoretical studies of the colloidal stability of nanoparticles: a general interpretation based on stability maps. *ACS Nano* doi:10.1021/nn200465b

Sela-Passwell N, Rosenblum G, Shoham T, Sagi I. 2010. Structural and functional bases for allosteric control of MMP activities: can it pave the path for selective inhibition. *Biochimica et Biophysica Acta* 1803:29-38.

Sellers A, Cartwright E, Murphy G, Reynolds JJ. 1977. Evidence that latent collagenases are enzyme-inhibitor complexes. *The Biochemical Journal* 163:303-307.

Sellers A, Reynolds JJ, Meikle MC. 1978. Neutral metallo-proteinases of rabbit bone. Separation in latent forms of distinct enzymes that when activated degrade collagen, gelatin and proteoglycans. *The Biochemical Journal* 171:493-496.

Seltzer JL, Akers KT, Weingarten H, Grant GA, McCourt DW, Eisen AZ. 1990. Cleavage specificity of human skin type IV collagenase (gelatinase). *The Journal of Biological Chemistry* 265:20409-20413.

Shaw DJ. 1980. Introduction to colloid and surface chemistry. *London: Butterworths*, 3rd edition.

Shiomi T, Lemaítre V, Armiento JD, Okada Y. 2010. Matrix metalloproteinases, a disintegrin and metalloproteinases, and a disintegrin and metalloproteinases with thrombospondin motifs in non-neoplastic diseases. *Pathology International* 60:477-496.

Slocik JM, Zabinski JS Jr, Phillips DM, Naik RR. 2008. Colorimetric response of peptide-functionalized gold nanoparticles to metal ions. *Small* 4:548-551.

Snoek-van Beurden PAM, Von den Hoff JW. 2005. Zymographic techniques for the analysis of matrix metalloproteinases and their inhibitors. *BioTechiques* 38:73-83.

Song S, Qin Y, He Y, Huang Q, Fan C, Chen HY. 2010. Functional nanoprobes for ultrasensitive detection of biomolecules. *Cheical Society Reviews* 39:4234-4243.

Sönnichsen C, Franzl T, Wilk T, Plessen G von, and Feldmann J. 2002. Plasmon resonances in large noble-metal clusters. *New Journal of Physics* 4:931-938.

Sood R, Taheri S, Candelario-Jalil E, Estrada EY, Rosenberg GA. 2008. Early beneficial effect of matrix metalloproteinase inhibition on blood-brian barrier permeability as

measured by magnetic resonance imaging countered by impaired long-term recovery after stroke in rat brain. *Journal of Cerebral Blood Flow and Metabolism* 28:431-438.

Sousa F, Mandal S, Garrovo C, Astolfo A, Bonifacio A, Latawiec D, Menk RH, Arfelli F, Huewel S, Legname G, Galla HJ, Krol S. 2010. Functionalized gold nanoparticles: a detailed *in vivo* multimodal microscopic brain distribution study. *Nanoscale* 2:2826-2834.

Sperling RA, Rivera Gil P, Zhang F, Zanella M, Parak WJ. 2008. Biological applications of gold nanoparticles. *Chemical Society Reviews* 37:1896-1908.

Sperling RA, Parak WJ. 2010. Surface modification, functionalization and bioconjugation of colloidal inorganic nanoparticles. *Philosophical Transactions of the Royal Society A* 368:1333-1383.

Springman EB, Angleton EL, Birkedal-Hansen H, Van Wart HE. 1990. Multiple modes of activation of latent human fibroblast collagenase: evidence for the role of a Cys73 active-site zinc complex in latency and a "cysteine switch" mechanism for activation. *Proceedings of the National Academy of Sciences of the United States of America* 87:364-368.

Stefanidakis M, Koivunen E. 2006. Cell-surface association between matrix metalloproteinases and integrins: role of the complexes in leukocyte migration and cancer progression. *Blood* 108:1441-1450.

Stricklin GP, Jeffrey JJ, Roswit WT, Eisen AZ. 1983. Human skin fibroblast procollagenase: mechanisms of activation by organomercurials and trypsin. *Biochemistry* 22:61-68.

Su KH, Wei QH, Zhang X, Mock JJ, Smith DR, Schultz S. 2003. Interparticle coupling effects on plasmon resonances of nanogold particles. *Nano Letters* 3:1087-1090.

Sullivan MMO, Green JJ, Przybycien TM. 2003. Development of a novel gene delivery scaffold utilizing colloidal gold-polyethylenimine conjugates for DNA condensation. *Gene Therapy* 10:1882-1890.

Sun Y and Xia Y. 2003. Gold and silver nanoparticles: a class of chromophores with colors tunable in the range from 400 to 750 nm. *The Analyst* 128:686-691.

Sumii T, Lo EH. 2002. Involvement of matrix metalloproteinase in thrombolysis-associated hemorrhagic transformation after embolic focal ischemia in rats. *Stroke* 33:831-836.

Suzuki K, Hosokawa K, Maeda M. 2009. Controlling the number and positions of oligonucleotides on gold nanoparticle surfaces. *Journal of the American Chemical Society* 131:7518-7519.

Suzuki Y, Nagai N, Umemura K, Collen D, Lijnen HR. 2007. Stromelysin-1 (MMP-3) is critical for intracranial bleeding after t-PA treatment of stroke in mice. *Journal of Thrombosis and Haemostasis* 5:1732-1739.

Swierczewska M, Lee S, Chen X. 2011. The design and application of fluorophore-gold nanoparticle activatable probes. *Physical Chemistry Chemical Physics* 13:9929-9941.

Tallant C, Marrero A, Gomis-Rüth FX. 2010. Matrix metalloproteinases: fold and function of their catalytic domains. *Biochimica et Biophysica Acta* 1803:20-28.

Templeton AC, Wuelfing MP, Murray RW. 2000. Murry, monolayer protected cluster

molecules. *Accounts of Chemical Research* 33:27-36.

Tischer BK, Schumacher D, Beer M, Beyer J, Teifke JP, Osterrieder K, Wink K, Zelnik V, Fehler F, Osterrieder N. 2002. A DNA vaccine containing an infectious Marek's disease virus genome can confer protection against tumorigenic Marek's disease in chickens. *The Journal of General Virology* 83:2367-2376.

Tsai CS, Yu TB, Chen CT. 2005. Gold nanoparticle-based competitive colorimetric assay for detection of protein-protein interactions. *Chemical Communications* 14:4273-4275.

Tu XK, Yang WZ, Shi SS, Chen CM, Wang CH. 2009. 5-lipoxygenase inhibitor zileuton attenuates ischemic brain damage: involvement of matrix metalloproteinase 9. *Neurological Research* 31:848-852.

Turkevich J, Stevenson PC, Hillier J. 1951. A study of the nucleation and growth processes in the synthesis of colloidal gold. *Special Discussions of the Faraday Society* 11:55-75.

Turkevich J. 1985. Colloidal gold. Part 1. *Gold Bulletin* 18:86-91.

Uehara N, Ookube K, Shimizu T. 2010. Colorimetric assay of glutathione based on the spontaneous disassembly of aggregated gold nanocompositeds conjugated with water-soluble polymer. *Langmuir* 26:6818-6825.

Van Wart HE, Birkedal-Hansen H. 1990. The cysteine switch: a principle of regulation of metalloproteinase activity with potential applicability to the entire matrix metalloproteinase gene family. *Proceedings of the National Academy of Sciences of the United States of America* 87:5578-5582.

Velusamy V, Arshak K, Korostynska O, Oliwa K, Adley C. 2010. An overview of foodborne pathogen detection: In the perspective of biosensors. *Biotechnology Advances* 28:232-254.

Vikesland PJ and Wigginton KR. 2010. Nanomaterial enabled biosensors for pathogen monitoring- a review. *Environmental Science and Technology* 44: 3656-3669.

Vo-Dinh T and Cullum B. 2000. Biosensors and biochips: advances in biological and medical diagnostics. *Fresenius' Journal of Analytical Chemistry* 366:540-551.

Wallon UM, Overall CM. 1997. The hemopexin-like domain (C domain) of human gelatinase A (matrix metalloproteinase-2) requires Ca^{2+} for fibronectin and heparin binding. Binding properties of recombinant gelatinase A C domain to extracellular matrix and basement membrane components. *The Journal of Biological Chemistry* 272:7473-7481.

Wang J, Zhou HS. 2008. Aptamer-based Au nanoparticles-enhanced surface plasmon resonance detection of small molecules. *Analytical Chemistry* 80:7174-7178.

Wang M, Gu X, Zhang G, Zhang D, Zhu D. 2009. Continuous colorimetric assay for acetylcholinesterase and inhibitor screening with gold nanoparticles. *Langmuir* 25:2504-2507.

Wang M, Thanou M. 2010. Targeting nanoparticles to cancer. *Pharmacological Research* 62:90-99.

Wang X, Liu LH, RamströM O, Yan M. 2009. Engineering nanomaterial surfaces for biomedical applications. *Experimental Biology and Medicine* 234:1128-1139.

Wang X, Geng J, Miyoshi D, Ren J, Sugimoto N, Qu X. 2010. A rapid and sensitive

"add-mix-measure" assay for multiple proteinases based on one gold nanoparticle-peptide-fluorophore conjugate. *Biosensors and Bioelectronics* 26:743-747.

Wang Y, Li D, Ren W, Liu Z, Dong S, Wang E. 2008. Ultrasensitive colorimetric detection of protein by aptamer-Au nanoparticles conjugates based on a dot-blot assay. *Chemical Communications (Cambridge, England)* 22:2520-2522.

Wang Z, Lévy R, Fernig DG, Brust M. 2006. Kinase-catalyzed modification of gold nanoparticles: a new approach to colorimetric kinase activity screening. *Journal of the American Chemical Society* 128:2214-2215.

Weiss SJ, Peppin G, Ortiz X, Ragsdale C, Test ST. 1985. Oxidative autoactivation of latent collagenase by human neutrophils. *Science* 227:747-749.

Whyman R. 1996. Gold nanoparticles. A renaissance in gold chemistry. *Gold Bulletin* 29:11-15.

Xiao Y, Ju HX, Chen HY. 1999. Hydrogen peroxide sensor based on horseradish peroxidase-labeled Au colloids immobilized on gold electrode surface by cysteamine monolayer. *Analytica Chimica Acta* 391:73-82.

Xiao Y, Patolsky F, Katz E, Hainfeld JF, Willner I. 2003. "Plugging into enzymes": Nanowiring of redox enzymes by a gold nanoparticle. *Science* 299:1877-1881.

Xu X, Han MS, Mirkin CA. 2007. A gold-nanoparticle-based real-time colorimetric screening method for endonuclease activity and inhibition. *Angewandte Chemie* 46:3468-3470.

Yamada A, Uegaki A, Nakamura T, Ogawa K. 2000. ONO-4817, an orally active matrix metalloproteinase inhibitor, prevents lipopolysaccharide-induced proteoglycan release from the joint cartilage in guinea pigs. *Inflammation Research* 49:144-146.

Yang Q, Wang S, Fan P, Wang L, Di Y, Lin K, Xiao FS. 2005. pH-Responsive Carrier System Based on Carboxylic Acid Modified Mesoporous Silica and Polyelectrolyte for Drug Delivery. *Chemistry of Materials* 17:5999-6003.

Yi DK, Sun IC, Ryu JH, Koo H, Park CW, Youn IC, Choi K, Kwon IC, Kim K, Ahn CH. 2010. Matrix metalloproteinase sensitive gold nanorod for simultaneous bioimaging and photothermal therapy of cancer. *Bioconjugate Chemistry* 21:2173-2177.

You CC, Miranda OR, Gider B, Ghosh PS, Kim IB, Erdogan B, Krovi SA, Bunz UHF, Rotello VM. 2007. Detection and identification of proteins using nanoparticles-fluorescent polymer 'chemical nose' sensors. *Nature Nanotechnology* 2:318-323.

Zeta-Meter, Inc. 1993. "Everything you want to know about coagulation & flocculation". http://www.mtec.or.th/labs/powder/docs/coagulation.pdf

Zhang Q, Huang Y, Zhao R, Liu G, Chen Y. 2008. Determining binding sites of drugs on human serum albumin using FIA-QCM. *Biosensors and Bioelectronics* 24:48-54.

Zhang SC, Kern M. 2009. The role of host-derived dentinal matrix metalloproteinases in reducing dentin bounding of resin adhesives. *International Journal of Oral Science* 1:163-176.

Zhao BQ, Wang S, Kim HYm Storrie H, Rosen BR, Mooney D, Wang X, Lo EH. 2006. Role of matrix metalloproteinases in delayed cortical responses after stroke. *Nature Medicine*

12:441-445.

Zhao W, Brook MA, Li Y. 2008. Design of gold nanoparticle-based colorimetric biosensing assays. *Chembiochem* 9:2363-2371.

Zhao W, Chiuman W, Lam JC, Brook MA, Li Y. 2007. Simple and rapid colorimetric enzyme sensing assays using non-crosslinking gold nanoparticle aggregation. *Chemical Communications (Cambridge, England)* 36:3729-3371.

Zhao W, Chiuman W, Lam JC, McManus SA, Chen W, Cui Y, Pelton R, Brook MA, Li Y. 2008. DNA aptamer folding on gold nanoparticles: from colloid chemistry to biosensors. *Journal of the American Chemical Society* 130:3610-3618.